CONTROL OF PEPTIDE SECONDARY STRUCTURE: PHOTOMODULATION OF PEPTIDE α-HELICITY IN THE APOPTOSIS SIGNALLING PATHWAY

by

Nicholas John Taylor

A thesis submitted to

The University of Cardiff

For the degree of

DOCTOR OF PHILOSOPHY

School of Chemistry

The University of Cardiff

December 2008

UMI Number: U584618

UMI®

Dissertation Publishing

ProQuest®

Department of Chemistry
Head of School Professor KJ Cavell

Memo

CARDIFF
UNIVERSITY
PRIFYSGOL
CAERDYDD
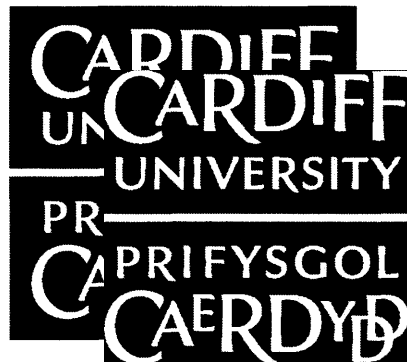
To: Science Library   From: School of Chemistry

Subject: Error in Nicholas Taylor's thesis   Date: 15th July 2009

To Whom It May Concern:

Nicholas Taylor's Thesis

This is to confirm that the declaration statement to confirm the Bar on Access to the
thesis has been signed in error. There is no Bar on Access so the thesis can be
made available in your library.

Professor K. J. Cavell
Head, School of Chemistry

**NOTICE OF SUBMISSION OF THESIS FORM:
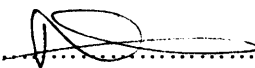POSTGRADUATE RESEARCH**

CARDIFF
UNIVERSITY

PRIFYSGOL
CAERDYⱣ

APPENDIX 1:
Specimen layout for Thesis Summary and Declaration/Statements page to be included in a Thesis

DECLARATION

This work has not previously been accepted in substance for any degree and is not concurrently submitted in candidature for any degree.
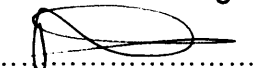
Signed .... (candidate)   Date ...18/12/2008...........

STATEMENT 1

This thesis is being submitted in partial fulfillment of the requirements for the degree of ....PhD............(insert MCh, MD, MPhil, PhD etc, as appropriate)

Signed .... (candidate)   Date ...18/12/2008...........
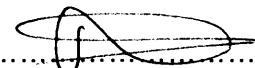
STATEMENT 2

This thesis is the result of my own independent work/investigation, except where otherwise stated. Other sources are acknowledged by explicit references.

Signed .... (candidate)   Date ...18/12/2008.........

STATEMENT 3

I hereby give consent for my thesis, if accepted, to be available for photocopying and for inter-library loan, and for the title and summary to be made available to outside organisations.

Signed .... (candidate)   Date ...18/12/2008.........

STATEMENT 4: PREVIOUSLY APPROVED BAR ON ACCESS

I hereby give consent for my thesis, if accepted, to be available for photocopying and for inter-library loans **after expiry of a bar on access previously approved by the Graduate Development Committee.**

Signed .... (candidate)   Date ...18/12/2008.........

Abstract

Short peptides have been designed and synthesised based on the *N*-terminus of the p53 tumour suppressor. The crosslinking of these peptides with a thiol-reactive azobenzene crosslinker, optimised for water solubility, builds on previous research that has demonstrated the effective use of this chemical crosslinker in the regulation of a helical peptide structure. Both the crosslinked and uncrosslinked peptides were reported to bind Hdm-2 with high affinity when compared to the wild-type peptide and the isomeric conformation of the attached crosslinker was reported to influence Hdm-2 binding. Although the extent of binding affinity change through crosslinker conformational switching was not as high as intended, this low degree of structural control contributed to the hypothesis that the strength of the peptide interactions with Hdm-2 is enough to overcome the conformational constraints imposed by the crosslinker and that the extent of secondary structure change upon photoswitching may be enhanced by engineering peptides to bind Hdm-2 though with a reduced affinity. The synthesis of Hdm-2 mutants designed to possess a reduced affinity for p53 further supported this proposal. The design of Hdm-2 binding peptides based on a polyalanine scaffold was explored, since polyalanine forms a stable α-helix. The substitution of alanine residues in the appropriate positions respective to one-another with key p53 residues critical to Hdm-2 binding in addition to cysteine residues to enable the attachment of the azobenzene crosslinker led to the development of peptides with Hdm-2 binding affinities comparable to wild-type p53.

Dedicated to

William G Johns

Acknowledgements

I wish to express my gratitude to Ruedi Allemann for giving me the opportunity to join his research group and for introducing me to chemical biology. His enthusiasm and attention to detail has made me the researcher I am today. Many thanks to Mahmoud Akhtar for his help, advice and for the proof reading of this thesis, his contribution to the group is greatly appreciated by everyone.

For his patience when I was a new starter I wish to thank Andy Nicoll, thanks also to Richard Swanwick for sparking my interest in molecular biology. I would like to thank Joel Loveridge for his guidance throughout my final year, for proof reading this thesis and for showing me how to make the best out of the trickiest situations. Thanks to my good friends Rhiannon Evans and Neil Young, for all the laughs and support when surprisingly public transport let me down.

A special thanks to my parents for their endless support. They always believed in me and have taught me to question everything. Whether they like it or not, I am the person I am today because of them.

List of Contents

Appendices

References   **180**

List of Figures

List of Tables

List of Schemes

Abbreviations

General

bHLH	Basic helix-loop-helix motif
S_N2	Bimolecular nucleophilic substitution reaction
DD	Death domain
DED	Death effector domain
IAP	Inhibitor of apoptosis
LB	Luria-Bertani media
MWCO	Molecular weight cut off
PT	Permeability transition of mitochondrial membrane
ROS	Reactive oxygen species

Chemicals

FAM	5,6-carboxyfluorescein
dATP	Deoxyadenosine triphosphate
dCTP	Deoxycytosine triphosphate
dGTP	Deoxyguanine triphosphate
dNTP	Deoxyribonucleotide triphosphate
dTTP	Deoxythymidine triphosphate
DIC	*N,N*-Diisopropylcarbodiimide
DMF	*N,N*-Dimethylformamide
EDTA	Ethylenediaminetetraacetic acid
GSH	Glutathione

HoBt	*N*-hydroxybenzotriazole
IPTG	Isopropyl-β-*D*-thiogalactopyranoside
NAD(P)H	Nicotinamide adenine dinucleotide (phosphate)
Pap	Phenylazophenylalanine
PMSF	Phenylmethylsulphonyl fluoride
SDS	Sodium dodecyl sulphate
TFA	Trifluoroacetic acid
TFE	2,2,2-trifluoroethanol
TAE	Tris-acetate EDTA buffer
TCEP	Tris(2-chloroethyl) phosphate

Amino Acids (Abbreviated using standard one and three letter codes)

Boc	t-Butoxycarbonyl
tBu	t-Butyl
Cl-Trp	6-Chlorotryptophan
Fmoc	9-Fluorenylmethoxycarbonyl

Macromolecules

AIF	Apoptosis inducing factor
Apaf-1	Apoptosis protease activating factor
aPP	Avian pancreatic polypeptide
Bcl-2	B-cell lymphoma-2
CED	*C. elegans* death gene
DISC	Death inducing signalling complex

DNase   Deoxyribonuclease

DNA   Deoxyribose nucleic acid

FasL   Fas ligand

GST   Glutathione-*S*-transferase

Hdm-2   Human double minute-2 protein

ICE   Interleukin converting enzyme

mRNA   Messenger ribonucleic acid

Mdm-2   Murine double minute-2 protein

tRNA   Transfer ribonucleic acid

TNFR   Tumour necrosis factor receptor

p53   Tumour suppressor protein 53

Techniques

CD   Circular dichroism

ELISA   Enzyme-linked immunosorbent assay

FPLC   Fast protein liquid chromatography

HPLC   High pressure liquid chromatography

ITC   Isothermal titration calorimetry

MALDI-TOF   Matrix assisted laser desorption/ionisation time of flight

NMR   Nuclear magnetic resonance

PCR   Polymerase chain reaction

SDS-PAGE   Sodium dodecyl sulphate polyacrylamide gel electrophoresis

SPPS   Solid phase peptide synthesis

UV   Ultra-violet

CHAPTER 1:

INTRODUCTION

1.1 Programmed Cell Death – The Significance of Apoptosis

The term *programmed cell death* was introduced by Lockshin *et al.* when proposing the occurrence of specific cell death during the development and maintenance of multicellular biological systems.[1] It was proposed that localised cell destruction occurs as a result of a highly regulated sequence of steps leading to physiological cell death.

Apoptosis was first described by Kerr *et al.* to explain the morphological process which characterised the programmed self-destruction of cells.[2] The word *Apoptosis* is of Greek origin meaning *to fall or drop off*, an analogy to the falling of leaves and petals from trees and flowers. This analogy refers to the life cycle of living organisms, and the importance of controlled cell death in growth, development and in the continuation of this cycle. It is said that mitosis produces approximately 100,000 cells every second in the adult human body, and that a similar number die by apoptosis.[3] Programmed cell death has widespread biological significance in numerous processes in living organisms such as development and morphogenesis, it has been intensely studied in the nematode *Caenorhabditis elegans* and found to be critical in the formation of independently mobile limbs and digits by the specific death of the interdigital mesenchymal tissue of a developing foetus.[4] Certain aspects of homeostasis, notably of the immune system lymphocytes, are regulated by apoptosis in addition to the highly important process of deleting damaged and dangerous cells such as those having sustained DNA damage and those subject to trauma or infection.[5]

Cells undergoing apoptosis display distinct morphological changes (Figure 1.1).[6] The cell shows deformation and shrinkage, losing contact with adjacent cells. Proteolytic enzymes become activated, resulting in the chromatin condensating and marginating at the nuclear membrane, a process known as *pyknosis*. The plasma membrane undergoes *budding* yielding *apoptotic bodies* where it seals to form a separate membrane around solid materials arising from the fragmentation (*karyorrhexis*) of the cytosol, chromatin and organelles. These tightly packed membrane-enclosed structures later undergo phagocytosis by macrophages, resulting in the complete digestion and removal of the cell without initiating an inflammatory response.

APOPTOSIS
(cell shrinks, chromatin condenses)

"budding"

Apoptotic bodies are phagozytosed - no inflammation

Viable Cell

NECROSIS
(cell swells)

Cell becomes leaky blebbing

Cellular and nuclear lysis causes inflammation
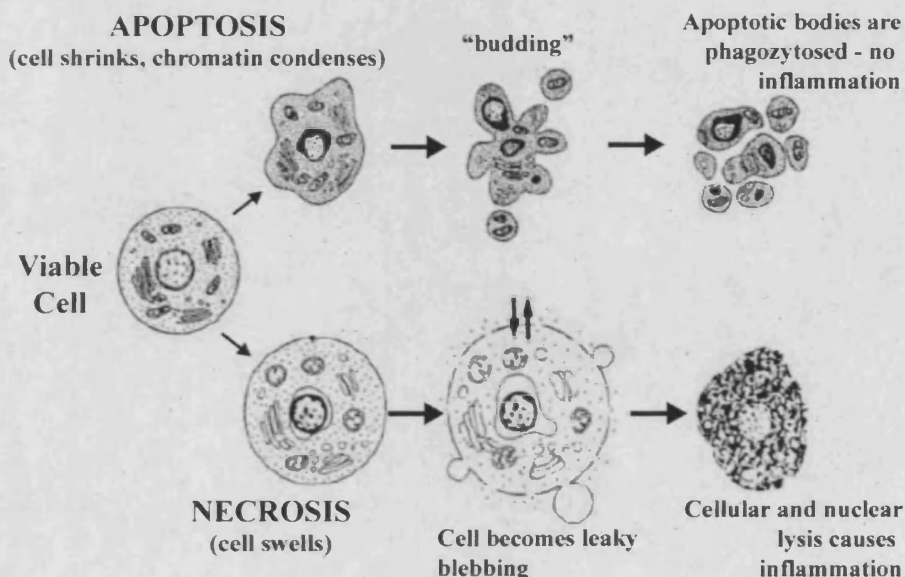
Figure 1.1: *Apoptosis and necrosis in cells can be identified by distinct differences in cellular morphology.*

Apoptosis demonstrates a highly regulated, precisely controlled method for removing damaged or infected cells whilst minimising localised effects. This is in stark contrast to necrotic cell death following rapid loss of cellular homeostasis (Figure 1.1), which is characterised by the swelling and subsequent failure of the cell membrane and

rupture of the cell and leakage of its contents to the surrounding tissue.[7] Uncontrolled exposure of the surrounding cells to previously shielded cellular contents, including proteolytic enzymes, result in DNA and protein fragmentation, eliciting a localised immune response resulting in inflammation and damage to adjacent cells.

Many diseases arise as a consequence of disruption of apoptosis signalling pathways. Cancer, for example, can occur due to inhibited apoptosis resulting in cell accumulation and tumour growth. Excessive apoptosis has been linked to neurodegenerative diseases such as Alzheimer's and Parkinson's disease.[8] It has been proposed that malfunctions in apoptosis signalling pathways arise due to malfunctions within genes coding for factors critical for the initiation, mediation or execution of apoptosis. An example of this is the receptor Fas, in which mutation prevents the binding of its ligands (FasL) and subsequently inhibits apoptosis as observed in malignant lymphomas and solid tumours.[9] Also, the oncogene coding for the p53 tumour suppressor undergoes modifications resulting in mutant variants of p53, the most common cause of many malignant tumours. These mutations are generally found to be concentrated within the regions of p53 essential for sequence-specific DNA binding.[9]

In cancer research, specific attention is being paid to the role of defective apoptosis pathways in tumourigenesis and the identification of such mutations. It has been found that defective cells acquire resistance to apoptosis through the untimely activation of oncogenes leading to the expression of anti-apoptotic proteins, and conversely by the deactivation of pro-apoptotic factors which under normal conditions function as tumour suppressors.[10]

1.2 The Biological Mechanisms of Apoptosis

The apoptosis signalling pathway is highly regulated in order to prevent the destruction of healthy tissues, this is achieved by the incorporation of an intricate network of signalling processes comprising of many evenly distributed *checkpoints*. The process of apoptosis commences with the *initiation phase*, requiring a pro-apoptotic stimulus that after a variable period of time, depending on both the type of cell and stimulus, results in the activation of the cells molecular signalling cascade. DNA fragmentation at inter-nucleosomal regions is initiated by endogenous deoxyribonucleases (DNases), which become selectively activated upon the proteolytic cleavage of certain members of the caspase family, notably caspase-3.[11] Caspases are *cysteine-dependent aspartate proteases*, the activation of which has been suggested as essential for the induction of apoptotic cell death.[12-15] Caspases were first implicated in programmed cell death when the *C. elegans* death gene 3 (CED-3) was related to mammalian *interleukin-1β-converting enzyme* (ICE), otherwise known as caspase-1. Critical for activity, caspases contain a cysteine residue within a highly conserved pentapeptide active site and utilise aspartate side-chains within a specific proximity for cleavage. Recognition of a tetrapeptide within its substrate's active site results in its cleavage at the carbonyl side of specific aspartic acid (Asp) residues.[15] Caspases are initially present as inactive pro-enzymes (*zymogens*) known as procaspases (MW; 30,000-50,000). These carry a prodomain at the *N*-terminus in addition to a large (MW; 20,000) and small (MW; 10,000) subunit with activation

occurring auto-catalytically, known as a *caspase cascade*, arising from the existence of Asp cleavage sites between the prodomains and subunits of caspases.

Crystallographic studies suggest that active caspases exist as heterotetramers arising from proteolytic cleavage between the large and small prodomains, yielding both the large and small subunit, a further pair of which produces an active caspase with the restoration of full enzymatic activity and yielding both large and small subunits.[16] This enables the processing of one caspase to be followed by the activation of another once the activation of an initiator caspase has taken place.[15] These initiator caspases, for example caspase-2, -8, -9 and –10, contain long prodomains to allow for interaction with other proteins, ensuring that initiator caspases can remain within close proximity to one another, thus enabling the caspase cascade. Initiator caspases have both direct and indirect influences upon the activation of downstream or *effector* caspases such as caspase-3, -6 and 7, which are characterised by their relatively short prodomains, the activation of which results in the initiation and execution of the apoptotic degradation phase.

It is the direct and indirect action of the activated effector caspases, which is responsible for the characteristic cellular morphology seen in classical caspase-dependant apoptosis. Activated cells in the *effector phase* are said to be *committed* and subsequent experiments involving cytosolic extracts from these cells has been shown to induce apoptotic changes in the nuclei of *non-committed* cells.[17,18] Caspase-dependant apoptosis is optimised in such a way as to ensure that the signals required for the initiation of phagocytosis are clearly displayed prior to the release of the cellular constituents, thus minimising localised damage to surrounding tissues as

characterised by necrotic cell death. Initiator caspase activation occurs in two different pathways. *Extrinsic apoptosis* arises from the ligation of cell surface death receptors, leading to formation of a complex known as a *death inducing signalling complex* (DISC), and intrinsic apoptosis occurs *via* signals from within the cell releasing apoptogenic factors from within the mitochondria.

Extrinsic apoptosis is initiated by the ligation of *tumour necrosis factor receptor* (TNFR) family members to the DISC, which then permits the ligation of death receptors including the cell surface protein Fas (also known as CD95 and Apo-1) resulting in caspase activation (Figure 1.2).[19] In this pathway caspase-8 is the most influential, becoming recruited as inactive procaspase-8 *via* binding sites on the large subunit known as *death effector domains* (DED's) which bind to the highly conserved cytoplasmic *death domains* (DD's) of the DISC. Here, numerous procaspase-8 molecules are within close proximity to one another and are thought to become activated by autoproteolysis.[16]
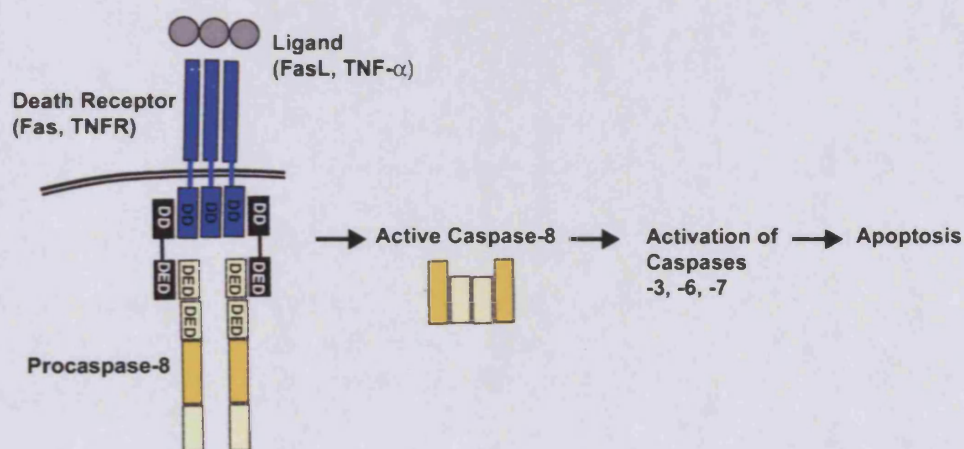
Figure 1.2: *Autoproteolytic activation of caspase 8 at the DISC by binding of the death effector domains (DED's) of procaspase-8 to the death domains (DD's) of the DISC.*

Cells with the ability to induce apoptosis by direct caspase-dependent pathways such as the extrinsic apoptosis pathway are classified as *type I* cells and can be characterised by the large amount of active caspase-8 and -3 present compared to the concentrations found within *type II* cells.[20,21] In the case of *type II* cells, the extrinsic signalling process is not strong enough to result directly in cell death due to reduced DISC formation but requires amplification *via* the mitochondria-dependant apoptosis pathway.[22]

The mitochondrial pathway, or *intrinsic apoptosis*, incorporates the influences of cytotoxic agents, abnormal oncogene expression and the activities of the p53 tumour suppressor protein upon apoptosis signals. The mitochondrial pathway is also the target of some proteins associated with the *B-cell lymphoma-2* family (Bcl-2), in particular Bid which provides the link between the extrinsic and intrinsic apoptosis pathways. Bid is translocated into the mitochondria as its truncated form (tBid) arising from its cleavage by caspase 8. Once within the mitochondrion tBid interacts with other pro-apoptotic Bcl-2 family members such as Bax and Bak leading to a key checkpoint in the intrinsic/mitochondrial apoptosis pathway. This checkpoint is the release of the protein cytochrome C (the only water-soluble constituent of the mitochondrial electron transport chain), amongst other caspase activating factors such as *apoptosis inducing factor* (AIF), into the cytosol from the mitochondrial trans-membrane space. AIF is a 57,000 Da flavoprotein, which also induces the caspase independent formation of large chromatin fragments (50 kb), in contrast to the caspase activated DNases, which yield oligosomal DNA fragments.[23,24] AIF induced caspase independent apoptosis can be identified by a lesser degree of compaction of the chromatin and nuclear fragmentation.[11]

In the mitochondrial pathway, the initiation of apoptosis begins with the activation of procaspase-9 by a complex consisting of cytochrome C, dATP (deoxyadenosine triphosphate) and also the CED-4 homologue called *apoptosis protease activating factor* (Apaf-1). The mechanism of release of cytochrome C from the mitochondrion during apoptosis has been a highly debated topic since the mitochondrion maintains its structural integrity throughout. Methods suggested include the mitochondrial membrane permeability transition and subsequent opening of its associated pores and also the opening of selective release channels and swelling of the mitochondrial matrix causing a permeability transition arising from a rupturing of the mitochondrial membrane.[25-27] The release of cytochrome C leads to the interruption of electron transportation within the mitochondria, which leads to an increase in the concentration of reactive oxygen species (*ROS*). This results in the oxidation of NAD(P)H, loss of ATP and oxidation/depletion of glutathione (*GSH*). These are all common observations preceding apoptosis, leading Loeffler *et al.* to propose that inhibition of caspases and nucleases often results only in changes to the biochemical and morphological characteristics of cell death whilst ultimately failing to prevent apoptosis from occurring.[28,29]

A key checkpoint is the release of additional proteins such as DIABLO and Smac from the mitochondria, the role of which is the removal of caspase-inhibitory factors. These are proteins, the function of which is to bind to and act as antagonists of inhibitors of apoptosis (IAP's) and are necessary prior to the full activation of the execution caspases. Upon the release of cytochrome C into the cytosol, the formation of a multi-protein complex known as the *apoptosome* is triggered, which in addition

to cytochrome C contains Apaf-1 which functions to catalyse the ATP-dependent auto-activation and dimerisation of caspase-9 (Figure 1.3):[30]
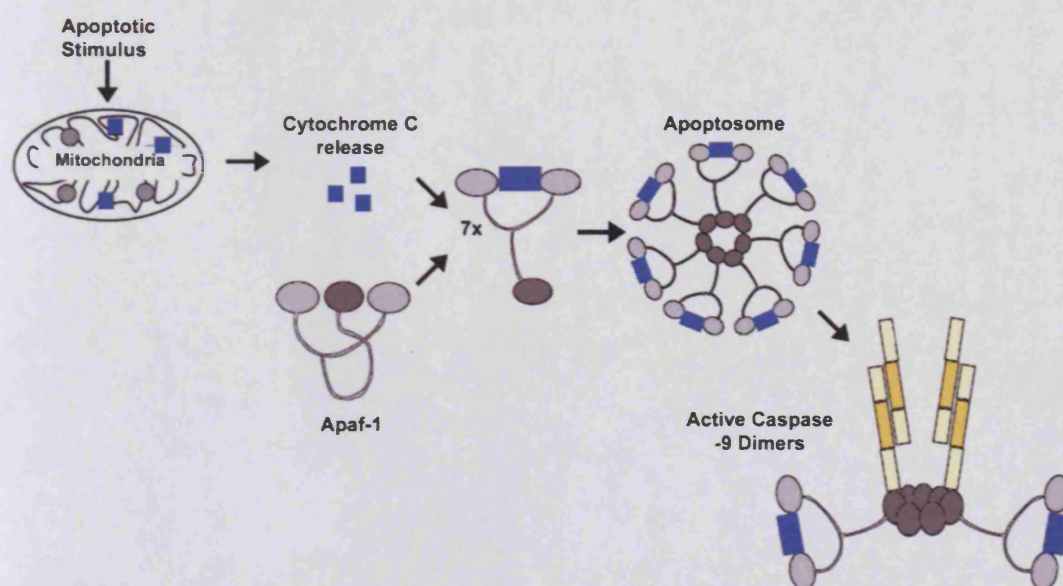
Figure 1.3: *Intrinsic apoptosis resulting from cytochrome C release from the mitochondria, formation of the apoptosome and activation of procaspase-9.*[31]

Upon activation of such initiator caspases and apoptosome formation, cell death results *via* the CD95 signalling pathway by the proteolytic activation of effector caspases such as caspases-3, -6 and -7. Also known as *executioner* caspases these cleave numerous structural and regulatory proteins such as lamins (fibrous proteins with a structural function in the nucleus) and also cytokeratins (which form filaments within the cytoskeleton).

Biochemical studies have demonstrated that apoptosis and necrosis may share some pathways in the early stages of cell death. Anti-apoptotic proteins of the Bcl-2 (BH3) family such as Bcl-2 and Bcl-x_L inhibit the release of cytochrome C from the

mitochondrion preventing both apoptotic and non-apoptotic cell death, whereas pro-apoptotic members such as Bax, Bak, Bid and Bim induce both cell death pathways,[32-35] maintaining an equally strong presence. These pro-apoptotic proteins translocate into the mitochondria, the extent of which is dependant on various death stimuli (Figure 1.4), and ultimately it is the ratio between the pro- and anti-apoptotic members of the Bcl-2 family which determines whether the cell lives or dies.[23,36,37]
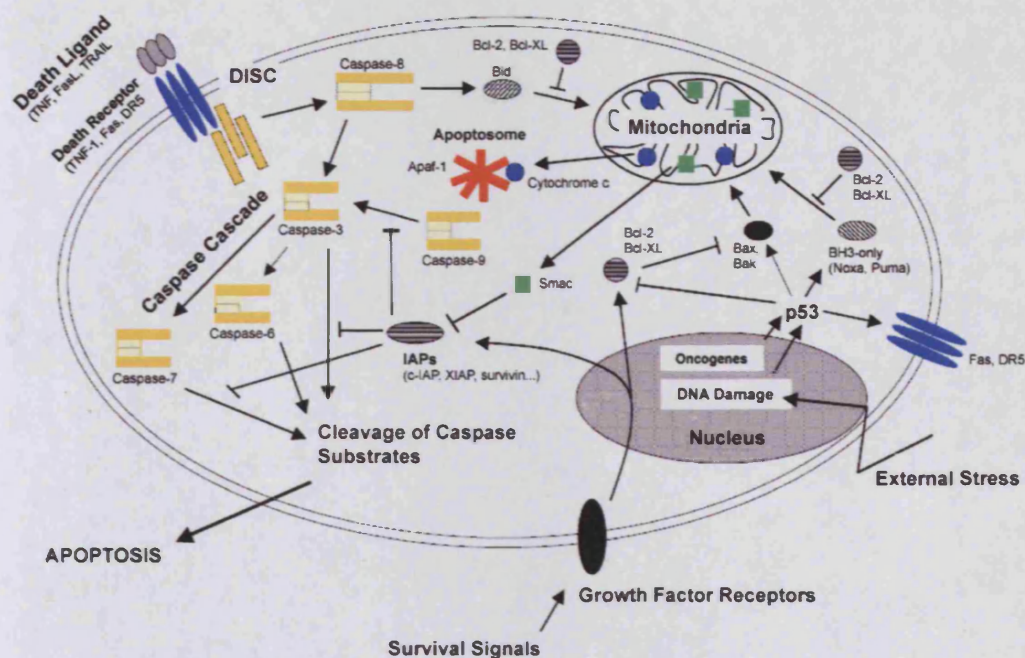
Figure 1.4: *The intrinsic and extrinsic apoptotic signalling pathways result in caspase activation through protein-protein mediated interactions.*[11]

In addition to amplifying and mediating extra-cellular apoptotic pathways the mitochondria possess a central role in the management and propagation of intra-cellular death signals resulting from cell damage or starvation, DNA damage and oxidative stress in addition to cell death signals stimulated by cytotoxic/chemotherapeutic agents. Most apoptosis-inducing conditions incorporate

the disruption of the mitochondrial inner transmembrane potential in addition to an increase in the inner mitochondrial membrane permeability to solutes with a molecular mass less than 1500 Da, the so called permeability transition (PT). The result of these changes is the influx of water into the mitochondrial matrix leading to osmotic mitochondrial swelling and rupturing of the outer mitochondrial membrane. These morphological changes result in the release of pro-apoptotic proteins from the mitochondrial intermembrane space into the cytoplasm.

1.3 Regulatory Mechanisms in Apoptosis Signalling

The initiation of apoptosis in response to extrinsic and intrinsic death signals implies that all cells are capable of undergoing programmed cell death and that such cellular responses remain inactive until activated by such signals. Ameisen has proposed that all cells are intrinsically programmed to self-destruct, and that this would inevitably occur were it not for continual repression by survival signals which enhance or maintain the functioning of anti-apoptotic molecules, thereby suppressing the activity of pro-apoptotic factors.[38] Consequently, cellular agents with opposing pro- and anti-apoptotic functions have been identified, and it is the control and release of these agents that determine the precision and timing of the cell's demise.

The 25,000 Da oncoprotein Bcl-2 (see chapter 1.2) was the first oncogene discovered to be involved in the inhibition rather than promotion of cell death, and was the first known component of the apoptosis signalling pathway to be identified to play a role

in tumourigenesis.[39] Vaux *et al.* investigated the effect of Bcl-2 on haemopoietic cells in addition to its interaction with c-myc, a transcription factor involved in cell proliferation, commonly found to be up-regulated in many cancers. Bcl-2 was found to contribute to neoplasia and was therefore concluded to function within the antiapoptotic signalling pathway.[39] Hockenbery and co-workers determined that Bcl-2 was located intra-cellularly, localising in the mitochondria. Their research concluded that the over-expression of Bcl-2 in pro-β-lymphocyte cells was found to block cell death *via* the intrinsic apoptosis pathway, whereas deregulation of Bcl-2 expression in the same cells lines was found to extend cell survival.[40] Consequently, Bcl-2 have been found to be over-expressed in a variety of diseases, for example non-Hodgkins lymphomas, propagating the survival of cancerous cells through the inhibition of apoptosis.

Further discoveries of homologues of Bcl-2, all containing conserved sequence motifs known as Bcl-2 homology domains (BH1 to BH4) led to the proposition of a division existing in the Bcl-2 family between anti-apoptotic members such as Bcl-2 and Bcl-x_L (Bcl-2 survival factors) and proapoptotic members such as Bak and Bax in addition to the BH3 death proteins, so called due to their pro-apoptotic function arising from the presence of a conserved homology known as the BH3 domain.[41,42] The balance between pro- and anti-apoptotic members is thought to enable the Bcl-2 family to function as a checkpoint within the intrinsic apoptosis signalling pathway, indeed *Bcl-2 knockout mice* engineered to possess an inactivated gene coding for Bcl-2, have been shown to die after only a few weeks displaying symptoms of lymphocyte, neuronal and intestinal apoptosis.[9] Further investigation by Antonsson *et al.* has shown that the interaction of pro-apoptotic BH3 homologues of the Bcl-2 family

displaces downstream pro-apoptotic factors such as Bak and Bax, previously in an inactive state due to their interaction with mitochondrial membrane bound antiapoptotic factors such as Bcl-2. The displaced pro-apoptotic factors are free to associate with the mitochondrial membrane, disrupting its permeability and resulting in the release of apoptogenic factors into the cytosol facilitating the propagation of intrinsic apoptosis (Figure 1.5).[43]
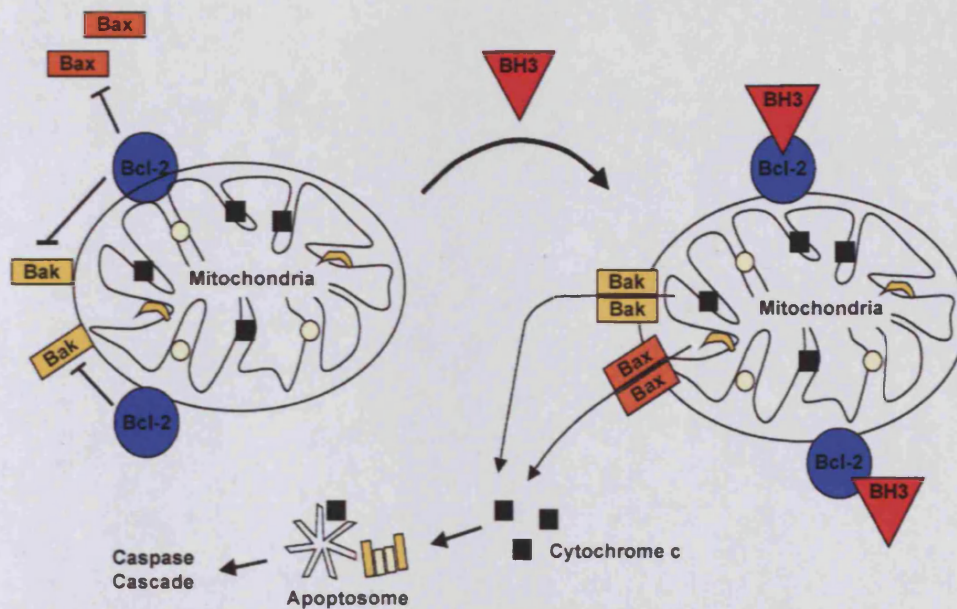
Figure 1.5: *The role of the Bcl-2 family proteins in mediating the release of apoptogenic factors in the intrinsic apoptosis pathway.*[11]

1.4 The Role of the p53 Tumour Suppressor in Regulating Apoptosis Signalling

The 393 amino acid tumour suppressor protein p53 functions as a promoter of apoptosis within cells and is hence referred to as a tumour suppressor. Within cells, p53 can evoke several responses such as cell-cycle arrest, senescence, differentiation and apoptosis depending upon the stimuli. The most intensely studied apoptosis

related tumour suppressor, p53 is found to have become de-activated in over 50% of human cancers. Additionally, mutations in p53 have been linked to chemoresistance, for example in metastatic breast cancer where its mutation results in a significantly reduced response to the drug tamoxifen.[9] The p53 tumour suppressor becomes activated in cells in response to both internal and external stimuli such as DNA damage and hypoxia, and has been referred to as "*the guardian of the genome*" due to its central role as a checkpoint in numerous pathways responsible for maintaining the genomic integrity of the cell.[44] p53 functions as a transcription factor resulting in the expression of a variety of p53 target proteins such as Fas, a cell surface protein involved in the initiation of extrinsic apoptosis by inhibition of cell survival signalling processes, and Apaf-1, a component in a complex leading to the activation of pro-caspase-9 in the mitochondrial apoptosis pathway.[10] Chemotherapy treatments involving the use of methotrexate and cisplatin have been shown to stimulate the expression of the ligand FasL, which ligates to Fas resulting in the activation of caspase-8 and the commencement of apoptosis *via* the extrinsic death-receptor pathway.[21] The exact mechanism is however thought to be more complex, since cells deficient in Fas and so unable to undergo FasL binding and therefore extrinsic apoptosis have been shown to undergo apoptosis upon exposure to these same anticancer drugs.

Not only does p53 stimulate protein expression it also acts as a repressor of the expression of antiapoptotic factors such as Bcl-x$_L$ of the Bcl-2 family proteins, for example p53 has been shown to actively repress the Bcl-2 promoter by binding to its TATA sequence.[45] Mihara *et al.* proposed that the intrinsic mitochondrial apoptosis pathway involves the translocation of activated p53 from the nucleus to the

mitochondria where it interacts with the DNA binding domain of Bcl-x$_L$.[46] This results in the formation of a complex inducing mitochondrial permeabilisation leading to the release of cytochrome c, which is not observed with many examples of mutated p53.

The p53 tumour suppressor must be tightly regulated since in non-stressed, undamaged cells its presence, particularly in an active state, would unnecessarily induce apoptosis within an otherwise healthy cell. As a result p53 is present at extremely low concentrations where it is retained in the cytoplasm in a deactivated, *metastable* state unable to penetrate the nucleus.[47] Upon activation p53 translocates to the nucleus where apoptosis is induced through the transcription of pro-apoptotic genes. Malfunctions of p53 and its associated pathways occur in many ways, such as lesions preventing p53 activation or by mutation of downstream mediators of p53. Mutations involving p53 itself are predominantly single-point mutations as opposed to the deletions and frame-shifts commonly seen in other tumour suppressor proteins.[10] Therefore, the cell retains its ability to express p53, albeit in a mutated form, which is often, more stable than the wild-type protein and thus present within the cell at more elevated concentrations.

A variety of analytical techniques have been employed to evaluate the structure-function relationship of p53 with respect to its quaternary structure, including X-ray crystallography and NMR.[48] p53 is a homotetramer with the 393 amino acid sequence divided into two principal domains, a DNA binding domain (residues 94-294) and a tetramerisation domain (residues 323-360) which are linked by disordered sequences.[48] The majority of p53 mutations associated with the disruption of the

apoptosis-signalling pathway are found to occur in the DNA binding domain, which consists of two loops stabilised by a zinc ion and a loop-sheet-helix motif.[49]

The 491 amino acid oncoprotein Human double minute-2 (Hdm-2) plays a central role in the regulation of p53 levels in cells, since Hdm-2 can bind to and inhibit the activity of p53 (K_d 340 ± 10 nM).[50] One of the many functions of Hdm-2 is as an E3 ubiquitin ligase, mediating the ubiquitination of p53 at specific Lys residues of the p53 *C*-terminus, where it is subsequently targeted for degradation by the proteasome. The activity of Hdm2 is controlled by *Akt kinase* in response to anti-apoptotic factors, which phosphorylates Hdm2 enabling its translocation from the cytosol to the nucleus in an active form, where it functions as an inhibitor of p53. However, in a further twist to the complex mechanism that is the regulation of both p53 and Hdm2, Akt is inhibited by the phosphatase PTEN, the expression of which is induced by p53.

Hdm-2 binding is facilitated by the *N*-terminal transactivation domain (residues 1-67) which in the unbound state is largely disordered.[48] This domain is the site of interaction of p53 with transcription factors and is subjected to extensive post-translational modifications such as phosphorylation which regulates its transcriptional activity.[51,52] A proline-rich region (residues 69-94) within p53 has been associated with regulation of stability, this has been supported by the work of Sakamuro *et al.* who demonstrated that upon deletion of this region, p53 showed an increased susceptibility to degradation by Mdm-2.[53] The *C*-terminus of p53 (residues 360-393) is known as the regulatory domain, and has been linked to the negative regulation of p53, involved in the induction of apoptotic programmed cell death.[10,54]

This intricate mechanism, a negative feedback loop, is highly efficient at minimising p53 levels in healthy cells. So called Mdm-2 *knockout mice*, engineered to be in possession of an inactivated gene coding for the mouse equivalent of Hdm-2, Mdm-2 (Mouse double minute-2), die early during development.[55] Crossing mice that are heterozygous for the deletion alleles for Mdm2 and p53 results in the 'normal' development of such Mdm-2 and p53 knockout mice, thus demonstrating the importance of both p53 and Mdm-2 in the regulation of one another.

As previously described, the p53 tumour suppressor becomes inhibited by the 90 kDa oncoprotein Mdm-2, leading to suppression of apoptosis and as a result cell accumulation and tumour growth. The role of p53 in malfunctioning apoptosis signalling pathways is supported by its involvement in both uncontrolled cell proliferation and premature activation of cell death through interlinked cellular pathways where p53 is a central checkpoint. These cellular pathways result in the activation of a transcription factor, *E2F-1*, a function of which is the stimulation of the tumour suppressor *ARF* (p14-*ARF* in humans) which promotes apoptosis by preferentially binding to Hdm2 leading to the stabilisation and activation of p53.[56]

Consequently, it has been found that Mdm-2 over-expression is a common characteristic of certain cancers, for example more than a third of soft-tissue sarcomas, and is also a contributing factor in less common cancers such as leukaemia and breast cancer.[57-60] In cases where Mdm-2 over-expression has been found to occur, the cell is typically found to contain wild-type p53, implying an alternative mechanism to that previously discussed, whereby over-expressed Mdm-2 provides an alternative to the mutational deactivation of p53 in apoptosis inhibition (Figure 1.6).

[59,60] This is supported by previously mentioned work involving Mdm-2 knockout mice, which has been shown to enhance the tumourigenic potential of cells.[55]
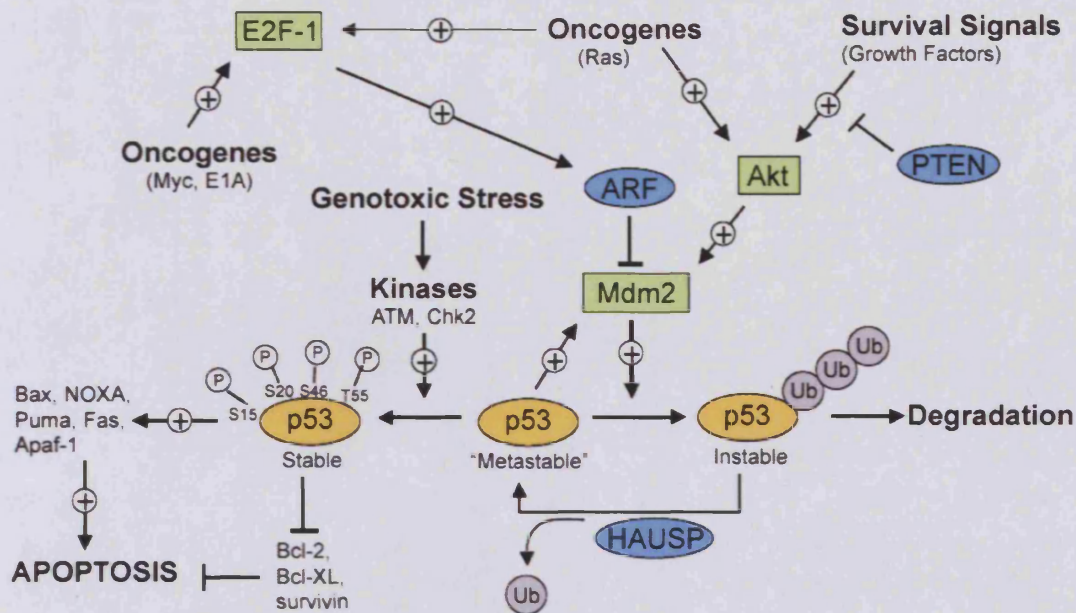
Figure 1.6: *The p53 network incorporating the p53 – Mdm-2 negative feedback loop.*[11]

1.5   The Mechanism of the p53/Hdm2 Interaction

There are four principal domains within the structure of Mdm-2, a *C*-terminal RING domain (residues 430-480) which requires two zinc ions for structural stabilisation and is associated with the function of Mdm-2 as a ubiquitin ligase.[61] Mdm-2 also contains a central acidic domain (residues 230-300), this is required for both regulating p53 ubiquitination in addition to Mdm-2 translocation within the cell. The phosphorylation of specific residues within this region has been reported to be important for the regulation of Mdm-2 function.[62,63] A combination of deletion and

mutation analysis have revealed that it is the 109 amino acid *N*-terminal domain of Mdm-2 which is responsible for binding to the transactivation domain of p53.[64-67] Chen and co-workers synthesised Hdm-2 deletion mutants corresponding to various fragments of Hdm-2 and conducted an immunoprecipitation assay with p53 as a GST fusion protein, it was reported that Hdm-2 residues 19-102 were critical for an interaction with p53.[67] This has been further refined by proteolytic digestion, which has elucidated that it is the highly conserved 12,000 Da *structural domain* at the *N*-terminus of Mdm-2 residues 17-125 that is important.[68] Within the p53 *N*-terminal transactivation domain it is a sequence of 11 amino acids comprising of residues 17-27, which are critical for p53-Mdm-2 binding.
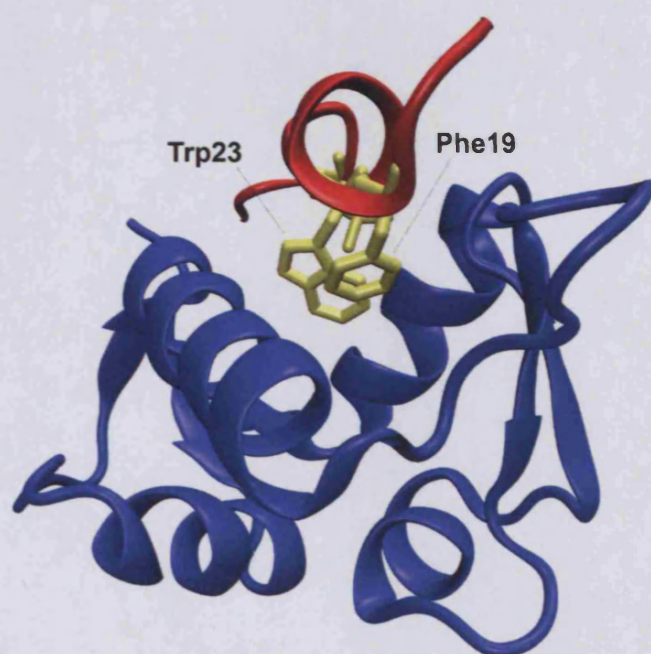
Figure 1.7: *Structure of the p53 N-terminal transactivation domain (red) adopting a helical structure and binding to Mdm-2 (blue) via key interactions of p53 residues (yellow) Phe19, Trp23 and Leu26 projected into the hydrophobic binding cleft of Mdm-2.[68]*

The tertiary structure of the *N*-terminal domain of Mdm-2 is arranged in such a way as to form a deep hydrophobic cleft of approximately 25 Å in length, 10 Å width and 10 Å in depth, narrowing towards the bottom. The cleft is comprised of two α-helices for the sides, two shorter α-helices for the bottom, and is enclosed at the ends by a pair of anti-parallel 3-stranded β-sheets. The *N*-terminal transactivation domain of p53 has been shown in NMR studies to be unstructured in the absence of Mdm-2, however, it adopts an amphipathic α-helix of approximately 2.5 helical turns in length along Residues 18-26 when bound within the Mdm-2 hydrophobic cleft (Figure 1.7).[68]

The p53 α-helix presents a hydrophobic face that binds within the hydrophobic cleft of Mdm-2, facilitated by the interaction of specific amino acids on the surfaces of both proteins. Schon *et al.* demonstrated that upon binding to p53, the tertiary structure of Mdm-2 undergoes a significant rearrangement, and further NMR studies of 'free' *apo*-Mdm-2 have revealed that an unstructured segment of the *N*-terminus of Mdm-2 occludes the narrowed p53 binding cleft and is displaced upon p53 binding.[69-71]

Critical to the interaction between these two proteins are three hydrophobic amino acids along one face of the p53 α-helix namely, Phe19, Trp23, and Leu26 which are inserted deeply into the hydrophobic Mdm-2 cleft (Figure 1.7). These residues were identified by a range of techniques including the screening of peptide libraries and site-directed mutagenesis of wild-type p53.[64,65,72] Substitution of Leu26 for Ala in a designed p53 peptide resulted in a 100-fold reduction in Hdm-2 binding, and that similar substitution of either Phe19 or Trp23 resulted in the total loss of Hdm-2 binding.[73-75]

The structural examination of the binding interface between p53 and Mdm-2 reveals key information about the mechanism of inhibition of the activity of p53 as a tumour suppressor by Mdm-2. The binding of these same hydrophobic amino acids that are critical for the p53-Mdm-2 interaction facilitates the translocation of p53 in an active state from the cytoplasm to the nucleus where apoptosis is initiated. This translocation is facilitated by the binding of these p53 residues to the TATA box binding protein associated proteins (TAF's).[76] Upon p53 binding to Mdm-2 however, these residues are shielded from the TAF's, preventing the activation and translocation of p53 to the nucleus and breaking the chain of events in the apoptosis signalling pathway that lead to programmed cell death.

Supporting evidence for the involvement of the p53 transactivation domain in apoptosis signalling is provided by the occurrence of a highly conserved sequence of amino acids in mammals referred to as the *Box1* region (Figure 1.8).[73] The initial six amino acids of the *Box1* region (residues 13-18), although highly conserved, contain no residues that are critical for Mdm-2 binding. This has been suggested to have sufficient helical propensity to permit the formation of the p53 α-helix upon binding to Mdm-2 whilst also maintaining being flexible enough to divert the following residues in the p53 sequence away from the Mdm-2 hydrophobic cleft. It was found that mutation of Phe19 to Ala completely blocked the interaction of p53 with Mdm-2 and its subsequent degradation.[64] This supported a previous study which showed a peptide containing alanine substitutions of both Leu14 and Phe19 which exhibited no p53-Mdm-2 binding.[64,73,74]

Box I

	1	13	26
mouse	MEESQSDISLEL	**PLSQETFSGLWKLLP**	PEDLLP
human	MEEPQSDPSVEP	**PLSQETFSDLWKLLP**	ENNVLSPLP
rat	MEDSQSDMSIEL	**PLSQETFSCLWKLLP**	PDDLLPTTA
hamster	MEEPQSDLSIEL	**PLSQETFSDLWKLLP**	PNNVLSTLP
rabbit	MEESQSLPSLEP	**PLSQETFSDLWKLLP**	ENNLLTTSL
monkey	MEEPQSDPSIEP	**PLSQETFSDLWKLLP**	ENNVLSPLP
cow	MEESQAELNVEP	**PLSQETFSDLWNLLP**	ENNLLSSEL
sheep	MEESQAELGVEP	**PLSQETFSDLWNLLP**	ENNLLSSEL

Figure 1.8: *N-terminal amino acid sequence of p53 from various mammals, showing the highly conserved BoxI region.*

Residues within the *BoxI* region of p53 have been shown to become phosphorylated at specific serine residues in positions 15 and 20 by checkpoint kinases Chk1 and Chk2. This occurs in response to a variety of factors that result in DNA damage such as UV and ionising radiation and has been shown to contribute towards the stabilisation of p53 with an insignificant effect upon p53-Mdm-2 binding (270 nM and 360 nM respectively).[70] Additionally, the phosphorylation of p53 at Ser20 initiates its phosphorylation at Thr18, which has the most significant effect upon p53-Mdm-2 binding, rendering p53 in the active state by inhibiting its interaction with Mdm-2 *via* disruption of the stability of the p53 amphipathic α-helix.[77] Examination of the rate constants for the interaction of synthesised p53 peptides with Mdm-2 residues 2-125 showed that p53 phosphorylated at Thr18 possessed a k_{on} rate comparable to the wild-type peptide, however a significantly faster k_{off} rate results in a weaker K_d (3150 ± 280 nM), leading to apoptosis through the prevention of Mdm-2 mediated degradation of p53.[70]

Schon and co-workers also investigated the effect of removing the surplus terminal residues of p53,[70] and found that the optimum binding between Mdm-2 and a p53-based peptide was achieved using a peptide 10 amino acids in length corresponding to p53 residues 17-26 (K_D = 46 nM ± 7 nM). The removal of Glu17 from the p53 peptide reduced the binding affinity of the peptide for Mdm-2 (K_D = 70 nM) although still much improved upon the original 15 amino acid peptide (K_D = 280 nM).[68]
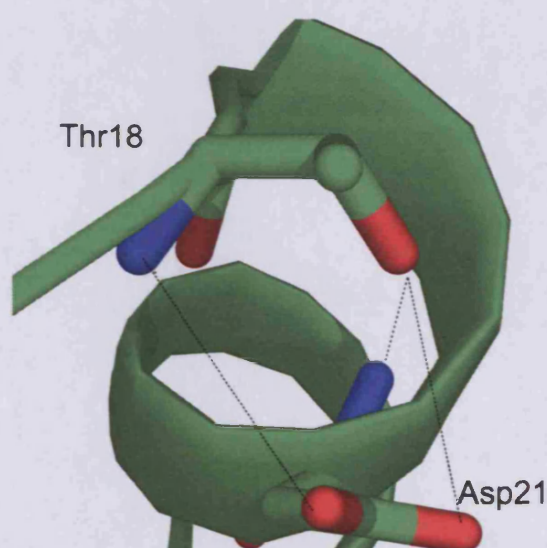
Figure 1.9: *Helix stabilising interactions; p53 Thr18 side-chain hydroxyl group hydrogen bonding with the backbone amide and side-chain carboxyl groups of Asp21, in addition to hydrogen bonding between the Asp21 carboxyl group and Thr18 backbone amide.*

As previously mentioned, the phosphorylation of p53 at specific serine and threonine residues is a key step in the regulation of the p53-Mdm-2 interaction whereby the affinity of p53 for Mdm-2 is reduced upon its phosphorylation. The work of Schon and co-workers demonstrated a K_D of 3150 nM (± 280 nM) for a 15 amino acid peptide corresponding to p53 residues 15-29 phosphorylated at Thr18.[70] Further investigation by Lai *et al.* supports the hypothesis that Thr18 phosphorylation results in disruption of inter-molecular interactions between p53 and Hdm-2, in addition to

proposing that intra-molecular hydrogen bonds within the p53 α-helix formed between the side-chain hydroxyl group of Thr18 and the backbone amine and side-chain carboxyl groups of Asp21 (Figure 1.9) are not able to form when Thr18 is phosphorylated, resulting in α-helix destabilisation.[75] Sakaguchi *et al.* further suggested that the p53 α-helix disruption is further enhanced by charge-charge repulsions between the phosphorylated Thr18 side-chain and the carboxyl group of Asp21 due to their proximity when in the α-helical conformation.

Fluorescence anisotropy measurements have been employed to measure the binding affinity of a range of short p53 peptides incorporating variations in peptide length and phosphate incorporation with Hdm-2 residues 1-126.[75] The results demonstrated that phosphorylation of p53 at Thr18 had a significant effect upon the affinity of p53 peptides for Hdm2, with a 20-fold increase in the dissociation constant (K_d) from 0.7 to 11 μM. It is thought that the phosphorylation of p53 regulates sub-cellular localisation and its transcriptional activity, with studies showing that the phosphorylation of p53 at the *N*-terminus leads to increased transcriptional activity through increased p53 stability, whereas p53 phosphorylation at the *C*-terminus results in enhanced DNA binding.[78] Oren has proposed that other modifications in addition to phosphorylation are responsible for the disruption of the p53-Mdm2 interaction resulting in the inhibition of p53 binding, such as the acetylation of p53, which has been shown to result in an increase in p53 DNA binding.[79]

Studies investigating the variation in the p53 peptide length showed no significant changes in K_d when the *N*-terminal peptide length was reduced from amino acids 1-35 to residues 10-29 indicating that the subtracted residues play no part in the p53-Hdm2

interaction.[75] However, a nine amino acid peptide (p53 residues 18-26) showed a ten-fold increase in affinity for Hdm-2 (K_d 70 nM), whereas the additional deletion of Thr18 (p53 residues 19-26) resulted in an increase in the K_d by an order of magnitude (K_d 800 nM). It has been proposed that the shorter p53 peptides bind faster due to a smaller loss of entropy, and further investigation into the conformational change that Mdm-2 undergoes upon p53 binding has revealed that the long and short peptides (15 and 10 amino acids respectively) caused a similar magnitude of conformational change within the p53 binding cleft of Mdm-2; however there was a significant difference in the long-range conformational effects.[71,75] In the work published by Schon *et al.* these longer-range conformational changes were found to occur predominantly in the β-sheets capping the ends of the Mdm-2 hydrophobic cleft. In accordance with proposals within the previous work,[70,75] it was suggested that the reduced binding affinity of the longer p53-based peptides occurs due to a loss in binding energy whilst overcoming the unfavourable energetics of the induced conformational change in the Mdm-2 domain.

Previous research involving the quantification of the binding interaction between p53 and Mdm-2 has used fluorescence anisotropy.[50,75,77] By exciting a sample with polarised light at a wavelength dependant upon the fluorophore present, an emission is observed as polarised light which gradually becomes depolarised in a manner that is dependant upon several factors including the rotational diffusion caused by the movement or *tumbling* of the fluorophore in solution. The anisotropy intensity is directly related to the polarisation, being the ratio of the polarised light component to the total intensity of the emission. This relationship is ideal for studying interactions between small macromolecules. By taking measurements of the fluorescence

anisotropy corresponding to a specific fluorophore upon a ligand it is possible to monitor the behaviour of this molecule when in the presence of its target protein, for example p53 and Hdm-2.

A small molecule will tumble in solution freely, resulting in a prompt reduction in the polarisation of the emitted light, and thus a low reading for the anisotropy intensity. As the molecule binds it will form part of a larger complex that tumbles in solution at a reduced rate due to its increased size. This reduction in the rate of tumbling means that the polarisation of the emitted light becomes scrambled at a much slower rate resulting in a larger reading for the anisotropy intensity. It is important to note that anisotropy data is most accurate when observing a fluorophore upon the smallest component of a complex since the overall increase in size and hence the net change in rotational diffusion of the emitted polarised light will be greatest. In the case of the p53-Hdm-2 interaction, by observing the changes in the fluorescence anisotropy of a fluorophore attached to a p53-based peptide it is possible to calculate the dissociation constant (K_D) for the binding interaction between the two molecules. Since there is a finite quantity of ligand (peptide) present amongst an increasing quantity of protein, the anisotropy intensities will increase until the ligand is completely bound at which point the anisotropy will remain constant, indicating that saturation of the ligand with the target protein has occurred.

When considering the placement of the fluorophore upon the p53-based peptide a location in which a definitive structural change occurs is ideally suited. For this reason Lai *et al.* chose to attach a fluorophore to the side-chain of the lysine corresponding to p53 residue 24 within their peptide based on the *N*-terminal residues

1-35 of p53.[75] At this point the disordered peptide becomes a highly ordered α-helix fixing the position of the side-chain and therefore the fluorophore within the complex, thus a small change in the binding of the complex results in a definite change in anisotropy of the fluorophore.

1.6   Small Molecule Inhibitors of the p53-Hdm2 Interaction

In apoptosis, protein-protein interactions are heavily involved in the regulation of both intrinsic and extrinsic apoptosis. For example, the oligomerisation of death receptors leads to the activation of caspase-8 and the activation of caspase-9 *via* the formation of the apoptosome from the association between cytochrome c and Apaf-1. Apoptosis research has been undertaken using small molecules such as synthetic peptides, natural products and designed compounds that modulate protein-protein interactions by binding to specific protein surfaces. The central role of p53 as a key checkpoint in programmed cell death highlights the importance of finding ways to inhibit complex formation between p53 and Mdm-2, and has been proposed as a novel strategy for tumour therapy.[74]

Studies have shown that the activation of p53 can occur by the disruption of the p53-Mdm-2 interaction and suppression of Mdm-2 expression leading to a reduction in tumour growth.[80] The confined nature of the Mdm-2 hydrophobic p53 binding cleft and the critical involvement of only a small number of amino acids on the same face of the p53 α-helix support the use of small molecules to disrupt p53-Mdm-2 binding

by preferentially binding Mdm-2. Based on the understanding of the p53-Mdm-2 interaction the ideal inhibitor should lead to the blockage of p53 nuclear export and degradation through the stabilisation and accumulation of p53 in addition to stimulating the expression of Mdm-2 and activation of downstream p53-regulated genes. The activation of p53 by DNA damaging treatments such as chemotherapy or radiotherapy may be limited in cells retaining the ability to express Mdm-2 and in particular, cases of Mdm-2 over-expression. Therefore, the therapeutic effectiveness of p53 activation in response to DNA damaging treatments is enhanced by the inactivation of the p53-Mdm-2 negative feedback loop.

The crystal structure of the p53-Mdm-2 binding interface revealed the interaction between the p53 *N*-terminal transactivation domain and the hydrophobic cleft formed by the Mdm-2 *N*-terminal domain to be augmented by two intramolecular hydrogen bonds. These were identified as occurring between the backbone amide of Phe19 from p53 with the Gln72 side chain of Mdm-2, in addition to the indole group of p53 Trp23 and the backbone carbonyl of Mdm-2 Leu54.[68] Various strategies have been applied in the design of synthetic mimics of the p53 binding interface, Holak *et al.* synthesised a number of chalcone derivatives, which, although showing activity through binding to Mdm-2, had high IC_{50} values ranging from 50 to more than 250 μM and further synthesis of molecules designed with additional refinement based on data from the p53-Mdm-2 crystal structure yielded similar results (Figure 1.9).[68,81]
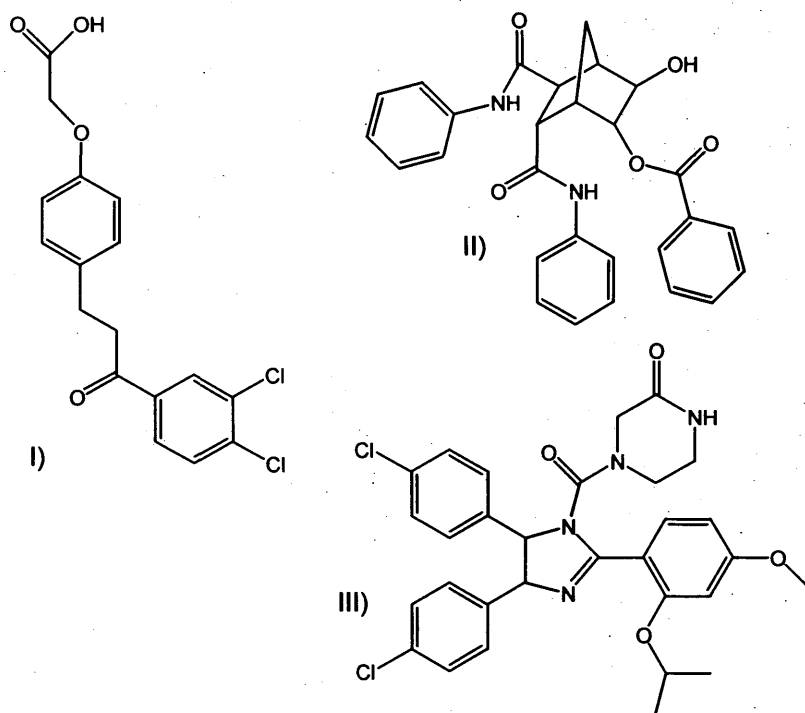
Figure 1.10: *Small molecule inhibitors of the p53-Mdm-2 interaction, I) chalcone derivative of Holak et al.[81] II) polycyclic compound originating from rational design using the p53-Mdm-2 crystal structure[68] and III) Nutlin-1 synthesised by Vassilev et al.[80]*

A combination of rational drug design and computational drug screening has advanced the discovery of non-peptidic small-molecule inhibitors of protein-protein interactions, and are considered the preferred treatment option due to a higher permeability to cells when compared to peptide-based drugs. Vassilev *et al.* used library screening to identify lead structures resulting in the discovery of a group of compounds termed *Nutlins*, which are *cis*-imidazoline analogues that have been optimised for improved specificity and binding, resulting in IC_{50} values in the range of 100 to 300 nM (Figure 1.10).[80]
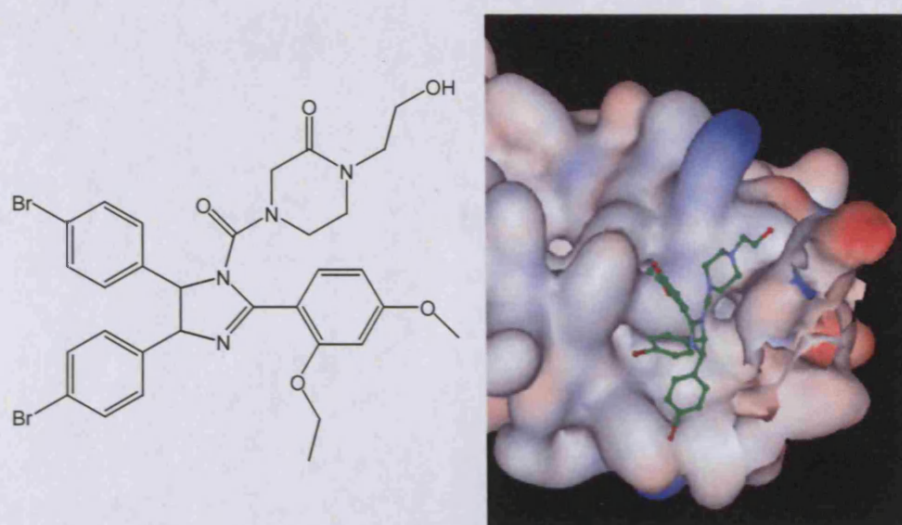
Figure 1.11: *Nutlin-2 (left) functions as an inhibitor of the p53-Mdm-2 interaction by the projection of a bromophenyl ring deep into the hydrophobic cleft of Mdm-2 (right).*[80]

It was reported by Vassilev *et al.* that the imidazoline scaffold exhibited a similar structure to the backbone of an α-helix and the design of the Nutlin compounds drew inspiration from previous work involving the substitution of p53 Trp23 with 6-chlorotryptophan, which resulted in substantially improved binding leading to the incorporation of halogen substituted aromatic rings within the Nutlin structures.[82] X-ray analysis was used to evaluate the crystal structure of Mdm-2 with Nutlin-2, this showed that one of the bromophenyl rings of Nutlin-2 is oriented directly within the p53 Trp23 binding site, whilst the other acts as a substitute for Leu26 (Figure 1.11). Also present is an ethyl ether side-chain that takes the position of Phe19, while the imidazoline scaffold effectively acts as a substitute for the p53 helical backbone. These small molecules showed p53-dependant activity in multiple cellular models demonstrating a link between an anti-tumour mechanism and the activation of the p53 pathway.

The screening of combinatorial libraries has resulted in molecules that lead to the reactivation of mutant p53 through binding to DNA, however these interactions are potentially non-specific and may also yield mutagenic effects despite being demonstrated to restore wild type p53 function.[83] Antisense oligonucleotides have been engineered through rational gene-based drug design to block protein expression, and have shown both *in vitro* and *in vivo* activity using prostrate cancer cell lines in the inhibition of Mdm-2 expression, which has led to increased p53 levels.[84] Also, a combination of both the antisense oligonucleotide and a conventional cancer chemotherapeutic agent results in significant inhibition of tumour growth as opposed to the action of either substance alone. This research highlights the importance of Mdm-2 regulation in apoptosis signalling in a p53-independent manner in addition to its role with p53, thus demonstrating how the suppression of Mdm-2 expression leads to the accumulation of activated p53, enhancing the effectiveness of DNA damaging drugs.

Recently attempts have been made to mimic the side-chain components of α-helices through the de novo design of scaffolds that present side-chain functionality with similar distance and angular constraints to that found along one face of an α-helix. Scaffolds investigated included oligo-amide, terephthalamide and terphenyl (Figure 1.12).[85-87] Hamilton *et al.* investigated the use of terphenyl groups as scaffolds for mimicking the face of an α-helix by the appropriate placement of functional groups along a terphenyl scaffold in the design of molecules which bind Bcl-x$_L$, assessment of their binding affinities using fluorescence polarisation showed the most potent binding to be 114 nM, with lower affinities for the less hydrophobic terphenyl derivatives.[88]
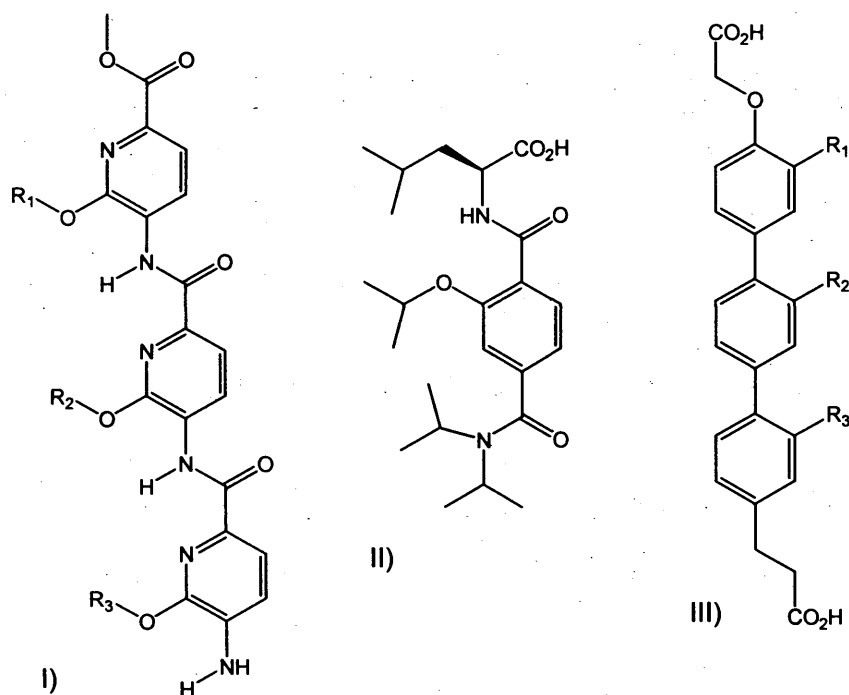
Figure 1.12: *Non-peptidic scaffolds used as mimics for α-helices I) oligo-amide,[87] II) terephthalamide[86] and III) terphenyl.[85]*

This work demonstrated the potential for the design of scaffolds mimicking helical structures in addition to highlighting the significance of the role of hydrophobic interactions in the binding of ligands to Bcl-x$_L$. Further work resulted in the development of inhibitors of the p53-Hdm-2 interaction through the development of a library of terphenyl compounds created by the substitution of the *ortho* positions of the terphenyl scaffold, projecting groups in a manner similar to the *i,i*+4 and *i,i*+7 residues of an α-helix, the most potent of which disrupted the p53-Hdm-2 interaction with a k_i of 182 nM.[89] Like the work of Schepartz *et al.* the versatility of the approach of Hamilton *et al.* was demonstrated by the subsequent development of mimics of the BH3 region of Bak and Bad with dissociation constants in the region of 114 nM to 2.09 μM when tested against a protein target that was also used to prove the effectiveness of polyamide foldamers utilising a trispyridylamide scaffold.[85,87,90]

1.7 Proteomic Applications in the Design of Inhibitors Targeting the p53-Hdm2 Interaction

The therapeutic potential for the use of synthetic proteins in addition to designed, short, stable peptides for the disruption of specific protein-protein interactions, in particular the activation of p53 in the absence of stress signals or DNA damage was highlighted by Bottger *et al.*[91] who designed a synthetic Mdm-2 binding protein. This was achieved by constructing a modified *Escherichia coli* thioredoxin gene incorporating a sequence coding for a 12-amino acid peptide (previously identified by phage selection) between Gly33 and Pro34 of the thioredoxin active site loop.[74] The location of the peptide insert ensures the deactivation of thioredoxin whilst providing a stable scaffold that is readily expressed in both prokaryotes and eukaryotes. Interestingly, the Mdm-2 binding peptide identified by phage display was found to incorporate the key p53 amino acids required for Mdm-2 binding Phe, Trp and Leu with the same spacings as found in wild-type p53.

The synthetic protein designed by Bottger *et al.* (Figure 1.13) was found to interact with Mdm-2 with the same strength as the wild-type p53 protein, and cells that were injected with the plasmid encompassing the gene for the synthetic protein were found to accumulate high levels of activated p53 leading to cellular growth arrest.[91] This is supported by the work of Wasylyk *et al.* who investigated the effectiveness of the disruption of the p53-Mdm-2 interaction at stimulating p53-dependant cell death. This was highlighted as an important area of interest since Mdm-2 over-expression was reported to lower cellular p53 concentrations which were thought to potentially be

below the threshold required to initiate apoptosis.[92] Although this hypothesis was proved incorrect, the peptides synthesised by Wasylyk *et al.* were Glutathione-*S*-Transferase (GST) fusions; at this point little evidence existed to support the efficacy of short independent peptides in the cellular environment, an area of particular interest since the inhibition properties of peptides fused to GST and thioredoxin may be reduced due to steric inhibition by the bulky fusion proteins.

Wild Type TIP   PPLSQETFSDLWKLLPENG
Super TIP   PPLSMPRFMDYWEGLNENG
Super TIP-Ala   PPLSMPRAMDYAEGANENG

Figure 1.13: *Thioredoxin insert amino acid sequences incorporated by Bottger and co-workers[91], the control (Wild Type TIP) was comparable to the p53 protein as was the sequence selected by phage display (Super TIP). Substitution of critical amino acid residues (bold) eliminated Mdm-2 binding (Super TIP-Ala).*

The design of short p53 peptide mimetics that activate p53-dependant transcription in cells in which this has become blocked or deactivated by defective apoptosis signalling pathways provides a novel target for the re-activation of p53, in particular circumstances in which the wild-type p53 protein has become inactivated due to over-active degradation arising from the over-expression of Mdm-2. Chene *et al.* demonstrated the use of peptidic small molecule inhibitors to disrupt protein-protein interactions *in vivo* with a synthetic 8-mer peptide incorporating four non-natural amino acids, which had already showed potential as an inhibitor of the p53-Mdm-2 interaction *in vitro*.[93] The peptide was found to activate the p53-pathway in tumour cells expressing wild-type p53 with an IC_{50} of 5 nM, which is 60 times more potent

than the synthetic protein reported by Bottger *et al.*[91] The peptide synthesised by

Chene and co-workers induced p53 accumulation in colon cancer cells however, due

to the poor cellular penetration of peptides a high concentration was required for

effective use.[93]

Hara *et al.* reviewed inhibitors of the p53-Mdm-2 interaction and concluded that the

most effective inhibitors of p53 binding were hydrophobic, oligomeric molecules in

which the hydrophobic side-chains are positioned in the same conformational

arrangement as found with the wild-type p53 α-helix.[94] Peptoids were investigated as

potential small-molecule inhibitors of the p53-Mdm-2 interaction, and have high

potential as alternatives to peptide-based inhibitors, since peptoid monomers are

essentially *N*-substituted glycines incorporating a wide range of side-chains and are

therefore less susceptible to proteolytic digestion due to the substitution of the amino

acid α-carbon atom for nitrogen.[95]

The handedness of a peptide backbone is determined by the chirality of the α-carbon

atom, which for all naturally occurring amino acids is identical. The backbone

conformation is driven by the local conformational properties of the differing amino

acids within the peptide sequence in addition to the side-chain interactions. Peptoid

backbones may adopt forced conformations by the incorporation of chiral side-chains

upon the α-nitrogen atom, these give steric bias to the peptoid and can result in the

peptoid backbone adopting dihedral angles which promote an α-helical

conformation.[96] Consequently, favourable binding can be engineered due to the

reduced entropy arising from the presence of a pre-formed α-helical scaffold. Hara *et*

al. synthesised peptoid derivatives based on a *N*-terminal p53 peptide incorporating

novel side-groups that showed competition for Hdm-2 binding with wild-type p53 in the lower micromolar range.[94] Sadowsky *et al.* further investigated the importance of having a well-defined secondary structure as a tool for designing inhibitors of protein-protein interactions by examining the use of foldamers, oligomers with a well-defined secondary structures.[97] Their research focussed on the development of foldamers that were intended to bind tightly to selective protein surfaces, in this instance ligands for Bcl-x_L based on the Bak BH3 domain. A combination of peptides were evaluated consisting of β-amino acids (β-peptides) and also sequences of alternating α- and β-amino acids (α-β-peptides), with both structures showing binding activity. Sadowsky *et al.* proposed that since α-peptides have a regular and flexible structure, this allows for localised distortion, whereas foldamers typically contain conformational restraints, which act to reduce this flexibility thus reducing the affinity of the foldamer ligand for the its target. The needs of different protein-epitopes for a variety of foldamer scaffolds were highlighted from this work. It was suggested that further research be conducted into creating greater variation in foldamer side-chain projection in order to achieve the desired localised distortions at the binding interface.[97]

1.8 Secondary Structure Considerations in The Regulation of Protein-Protein Interactions – The α-Helix

Protein-protein interactions are highly coordinated events facilitated by the specific geometry of functional groups within the amino acid side-chains and backbones of protein sequences. Consequently these interactions often occur between highly ordered structural motifs such as α-helices and β-sheets, as a result random coil

segments of proteins must be modulated by entropy and enthalpy compensation to facilitate the adoption of an ordered structure. When considering the interaction between proteins, the α-helix is a widely used structural motif employed to facilitate such an interaction. Examples of the versatility of a helical structure can be found extensively in nature, for example the DNA double helix, collagen triple helices and bacterial flagella.

The residues in a right handed α-helix backbone adopt Phi (φ, C'-N-C$^{\alpha}$-C') and Psi (ψ, C$^{\alpha}$-C'-N-C$^{\alpha}$) dihedral angles of approximately -60° and -45° respectively. Within an α-helix the Phi and Psi angles of successive amino acids must be the same for each residue in order to obtain the cooperativity between residues required to facilitate helix formation. Examination of dihedral angles in relation to the occurrence of structural motifs in proteins led to the development of the Ramachandran plot.[98] This presents a schematic representation of Phi dihedral angles plotted against Psi for each residue in a polypeptide sequence. Using computational models to discount sterically disallowed conformations, α-helices and β-sheets were found to occupy specific regions of the plot. Using this information, these plots are useful when examining the amino acid sequences of proteins, enabling the prediction of secondary structure motifs within the folded structure. The sheer variation of amino acids within a sequence give rise to a vast number of proteins each with their own individual structure and consequently their own specific function. Indeed the correct sequence is required to enable key interactions between residues in order to facilitate both the protein folding and activity, a single mutation of the most apparently insignificant residue can render a protein unstructured or more likely lead to the formation of aggregates and insoluble particulates.
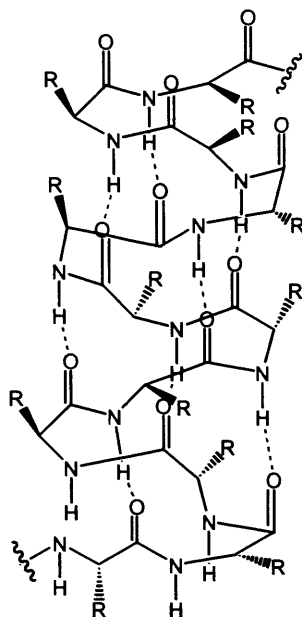
Figure 1.14: *The α-helix is stabilised by a network of hydrogen bonds (green) between carbonyl oxygen atoms (hydrogen bond acceptor, blue) and the amino acid backbone amides (hydrogen bond donor, red).*

The α-helix is stabilised by hydrogen bonds between the carbonyl (CO) and amide (NH) groups situated along the peptide backbone. The carbonyl group of one amino acid (*i*) extends almost parallel to the axis of the helix towards the *C*-terminus and is pointed directly at the *N*-terminal facing amide group of the peptide bond four amino acids ahead in the sequence (*i*+4) forming a hydrogen bond. Along an α-helix the side-groups of each amino acid are oriented approximately perpendicular to the helix axis, projecting away from the helix slightly towards the *N*-terminus (Figure 1.14). The amino acids in an α-helix are spaced in such a way as to complete a single helical turn every 3.6 residues occupying a length along the helical axis of 5.4 Å, thus each amino acid constitutes a 100° turn of the helix, with a translation of 1.5 Å along the helical axis.

The formation of α-helices is driven by enthalpically favoured packing interactions in addition to a gain in entropy due to desolvation arising from the exclusion of water during the formation of the helical core. The loss of water occurs due to the high density of residue packing within an α-helix, making the core a highly hydrophobic environment.[99] The formation of the α-helix from a random conformation first requires the initiation of the helical structure by the first four amino acids of the helix, which although an entropically disfavoured process once commenced this propagates the remaining favourable residues to form a helix. Typically, α-helices are short structures comprising of approximately ten residues in length giving a three turn helical motif. This is because of the increased loss in entropy for the protein due to the high degree of organisation required to maintain a stable helical structure. Scholtz *et al.* proposed that α-helices comprising of less than 15 amino acids are unstable in the absence of supporting forces, since folding leads to a loss in entropy.[100] The fewer residues involved in the α-helix results in a shorter helical backbone and therefore a reduction in the number of stabilising hydrogen bonding interactions available to overcome the unfavourable reduction in entropy.

The ability of specific residues to participate in α-helix formation is dependant upon the intrinsic helical propensity of each individual amino acid, whereby residues that actively participate in α-helix formation do so with minimal entropic and steric cost to the overall structural integrity. Proline is a good example of a molecule which is unlikely to be found within conventional α-helical structures due to it having no ability to form a helix backbone stabilising amide hydrogen bond in addition to its side-chain presenting steric interferences with the backbone Phi dihedral angle. Proline residues are however often located close to the nucleation site of an α-helix,

this is due to its high structural rigidity and is illustrated by the presence of a proline

residue within the sequence of the p53 *N*-terminal transactivation domain which forms

an α-helix upon interaction with Mdm-2. Glycine is another residue which is

considered helix disrupting due to its side-chain permitting a high degree of

conformational flexibility therefore its incorporation within an α-helix would be at a

high entropic cost and so is considered unfavourable, glycine residues are commonly

found upon termination of an α-helix. Contrary to glycine yet differing structurally by

the presence of a methyl group upon the α-carbon atom is alanine, which is highly

favoured within α-helices due to increased rigidity arising the presence of the methyl

group and also has a minimal steric interference with the helix backbone.

Chou and Fasman pioneered a technique for the prediction of protein secondary

structure by collating data on the frequency of occurance of amino acid residues in α-

helices, β-sheets and turns using X-ray crystallographic data from known protein

structures.[101-103] Using this data probability parameters were derived from the

frequency of appearance of amino acid residues in each secondary structural motif,

thereby enabling the calculation of the probability of the occurance of an α-helix, β-

sheet or turn motif within a given amino acid sequence. This method has yielded data

acknowledged to be 50-60 % accurate showing how alanine, glutamic acid, leucine

and methionine are typically found to be most abundant within α-helices and are

therefore considered helix forming residues. This is contrary to proline and glycine, as

previously described, which are found commonly after termination of the helical

motif.[103]

The GOR method of secondary structure prediction, so called since it was developed by Garnier, Osguthorpe and Robson, built upon the work of Chou and Fasman by the inclusion of Bayesian inference, a statistical inference whereby data is collated and the experimental results consistently updated and re-evaluated as a result.[104] This method was expanded to take into account the probability of specific residues being found within a given structural motif based not just on residue specific data, but also by evaluating the additional occurance of neighbouring residues, therefore providing increased sensitivity in particular for prediction of α-helices and β-sheets for residues with only minimal differences in helical propensities.[104]

The relative helical propensities of individual amino acids was calculated by Degrado *et al.* relative to glycine by substituting each of the naturally occurring amino acids into a guest site within a peptide which forms a non-covalent α-helical dimer which is in equilibrium with a randomly coiled monomeric state. The equilibrium constants for the monomer-dimer equilibrium were determined to assess the free energy differences arising from the incorporation of each amino acid (Table 1.1).[105]

Upon the α-helix resides an overall dipole due to the cumulative effect of dipoles arising from the carbonyl groups of the peptide bonds and their parallel orientation along the helical axis. The helix dipole charge has been found to be stabilised by the presence of a positively charged residue at the *C*-terminus and a negatively charged residue at the *N*-terminus resulting in neutralisation of the dipole charge. The helix dipole causes the destabilisation of the helical structure as a result of entropic effects, and its elimination through the positioning of complimentary charged residues has been noted to be widely employed in nature.[106] This technique has been adopted in the

design of stable α-helices and has become known as helix capping. For example, residues that act as hydrogen bond acceptors such as Asp and Glu provide stabilisation to the α-helix when situated at the *N*-terminus. Similarly, amino acids such as Arg and Lys which have side-chain amine groups, provide stability to the *C*-terminus by acting as hydrogen bond donors to the backbone carbonyl groups, however this is less common and can disrupt the helical structure.[99]

Table 1.1: *Relative helical tendencies of all natural amino acids measured from the free energy change (ΔΔG) calculated from the equilibrium constant of a specifically designed helix-loop-helix dimer peptide.*[105]

Amino Acid	Relative Stabilisation of α-Helical Conformation (kcal mol^{-1})
Ala	-0.77
Arg	-0.68
Lys	-0.65
Leu	-0.62
Met	-0.50
Trp	-0.45
Phe	-0.41
Ser	-0.35
Gln	-0.33
Glu	-0.27
Cys	-0.23
Ile	-0.23
Tyr	-0.17
Asp	-0.15
Val	-0.14
Thr	-0.11
Asn	-0.07
His	-0.06
Gly	0.00
Pro	~3

1.9 Strategies For Engineering α-Helix Stabilisation and The Design of Helical Mimics of Ligands Involved in Protein-Protein Interactions

A variety of strategies have been employed to stabilise α-helices, although most have been based upon novel concepts some very successful applications have taken inspiration from nature. Fairlie *et al.* noted that in nature the coordination of histidine to metal ions has been utilised in stabilising helical motifs, examples of this practice include haemoglobin and plastocyanin.[107] This has been seen to occur in zinc finger transcription factors where the formation of an α-helix that binds to the major groove of DNA is facilitated by the coordination of a metal ion to two histidines *via* their imidazole N1 nitrogens.[107] In order to use metal ions to stabilise short α-helical peptides the metal ion is required to ideally stabilise two amino acid side-chains with the appropriate spacing. Fairlie *et al.* investigated the use of metal-ion clips involving the chelation of histidine residues at various intervals, with particular attention to improving α-helix stability in water *via* overlapping His-M-His bridges.[107] Their results showed that the coordination of the metal ion (M) to the histidine residues exhibited a preference to an *i,i*+3 spacing, however greater thermodynamic stability was gained in an *i,i*+4 conformation enabling the correct geometry between residues to facilitate multiple intra-molecular hydrogen bonds.

Nicoll *et al.* synthesised a helical switch, the activity of which was induced by metal binding, this was referred to as a metal-induced *N*-terminal stabilised peptide (MINTS), and was based on a previously designed *N*-terminally stabilising peptide known as NTSP originating from the reverse sequence of apamin.[108-110] Apamin is a

neurotoxic peptide consisting of 18 amino acids half of which are found in an α-helical conformation stabilised by two disulphide bridges.[111,112] The design of MINTS involved the insertion of two histidine residues $i,i+4$ to one-another in order to enable metal co-ordination, and was found to have a high-affinity for copper with the peptide adopting an α-helical conformation from random upon co-ordination to a metal ion.[111] The development of MINTS shows promise for the application of histidine residues within designed protein sequences to regulate functionality through the co-ordination of metal ions by inducing a helical conformation.

Natural oxaloacetate decarboxylases are large proteins, the activity of which requires the co-ordination of a Mn^{2+} ion within the active site.[113] A key step in the industrial synthesis of phenylalanine is the decarboxylation of oxaloacetate, therefore for environmental reasons it was highlighted that a metal free oxaloacetate decarboxylases enzyme would be desirable.[114] It was a series of artificial oxaloacetate decarboxylases which first demonstrated the importance of secondary structure with respect to the function of a de-novo designed peptide. Two 14-residue peptides were synthesised, termed Oxalidie-1 and Oxaldie-2 these differed only by Oxaldie-2 being *N*-terminally acetylated in order to observe the effect of stabilising the helix dipole. CD experiments showed the helical contents to be 18 % and 33 % respectively, however catalysis experiments showed the efficiency of Oxalide-1 to be three times greater than Oxaldie-2 (0.47 and 0.15 M^{-1} s^{-1} respectively) and the activity was found to be concentration dependant.[115]

This study highlighted the possibility for the synthesis of short peptides with catalytic activity; however small peptides are predominantly found as disordered structures

when in the absence of supporting protein structures/interactions due to the thermodynamically unfavourable folding process. As shown previously (Table 1.1) some amino acids provide an increased helix propensity when included within peptide sequences yielding known helical structures that provide structural clues as to how to incorporate such amino acids into synthetic peptides with a view to obtaining a desired conformation. A shortcut to this goal has been to take a known short, stable helical motif as a scaffold and substitute residues that have no detrimental effect upon structural integrity with key residues at specific locations required to facilitate a desired interaction. Further work concerning the development of oxaloacetate decarboxylases focussed on developing peptides upon a structural support, in the case of the synthesis of Oxaldie-3, the chosen scaffold was avian pancreatic polypeptide (aPP), a peptide hormone produced in nature in the pancreas of turkeys, where it functions as a regulator of weight. aPP is a 36 amino acid helix-loop-helix homodimer, with two antiparallel monomers stabilised by a hydrophobic core of aliphatic and aromatic residues (Figure 1.15).[116]
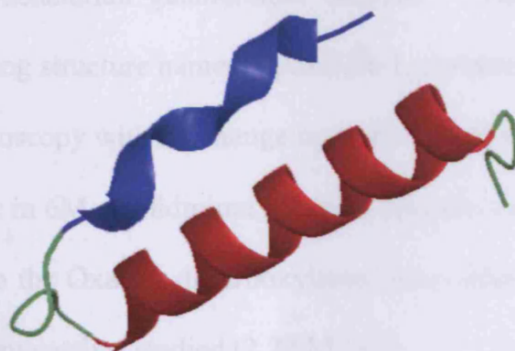
Figure 1.15: *The 36 amino acid protein avian pancreatic polypeptide consisting of an α-helix (red) stabilised by a type II polyproline helix (blue).*

CD studies of Oxaldie-3 showed a helical content of 52 %, this was similar to the 58 % helicity obtained from the evaluation of the crystal structure of aPP.[117] The catalytic efficiency of Oxaldie-3 was reported to be one order of magnitude greater than for Oxaldie-2 and was found to be concentration independent.[116] In order to evaluate the effect of increasing the tertiary structure stability on Oxaldie catalysis, a further structure was synthesised, Oxaldie-4, based on the scaffold bovine pancreatic polypeptide (bPP).[118,119] Thermal denaturation and NMR experiments showed that Oxaldie-4 was more stable than its predecessor Oxaldie-3, in addition to remaining fully folded in solution, these findings were attributed to Oxaldie-4 demonstrating a catalytic efficiency twice that of Oxaldie-3 (3.5 M^{-1} s^{-1}).[116]

A further miniaturisation step was achieved in the development of oxaloacetate decarboxylases by the use of the disulphide stabilised motif apamin, a peptide found in bee venom containing short helices stabilised by a single disulphide bridge in an *i,i+7* conformation. The presence of the two disulphide bonds provides additional stabilisation to apamin at both high temperatures and also in the presence of 6 M concentrations of the denaturant guanidinium chloride.[109] This same stability was observed for the resulting structure named Apoxaldie-1, maintaining a stable structure observed by CD spectroscopy with no change up to 80 °C and the majority of helicity still present at 95 °C or in 6M guanidinium chloride. Despite a three-fold reduction in size when compared to the Oxaldie decarboxylases, Apoxaldie-1 was reported to be the second most efficient catalyst studied (2.22 M^{-1} s^{-1}).

The ability of nature to produce stable α-helical structures which can be adapted for use as scaffolds has also been readily exploited by Schepartz *et al.* who also used aPP

to produce a stable α-helix which bound DNA tightly and with high specificity and was further proof-of-principle for the technique which has been termed as '*protein grafting*'.[120] This technique was further adapted by Schepartz and co-workers to produce ligands based on the highly conserved BH3 domain (Bcl-2 homology domain) of the oncoprotein Bak which bound Bcl-2 and Bcl-X_L using aPP as a scaffold to project specific residues in a stable conformation within the binding sites of Bcl-2 and Bcl-X_L.[90]

Schepartz *et al.* further refined the use of aPP as a helical scaffold, developing a DNA binding motif based upon Q50K engrailed homeodomain, a DNA binding protein, which resulted in both high affinity and selectivity for DNA previously seen in proteins only containing a complete functional epitope.[121] The versatility of this technique was further enhanced with the synthesis of an inhibitor of the p53-Hdm-2 interaction with dissociation constants in the low-nanomolar region, again based upon the aPP scaffold incorporating the functionally selective amino acids required by p53 for Hdm-2 binding.[122]

Gellmann *et al.* demonstrated how β-peptides could be synthesised to give differing secondary structures to their corresponding naturally occurring amino acid counterparts.[123] β-Amino acids differ from natural α-amino acids by the presence of an additional carbon atom and therefore show resistance to metabolism and proteolysis. The use of β-peptides to form stable α-helices was also investigated by Schepartz *et al.* and was used to construct an α-helical β-peptide based upon a stable helical β-decapeptide that exhibited nanomolar binding affinity for Hdm-2.[124] Helix stabilisation has been investigated using a variety of other methods including the use

of non-natural amino acids, for example the work of Chene and co-workers as mentioned previously in section 1.7.[93,125] Cheng *et al.* reported the use of fluorinated amino acids to enhance secondary structure stabilisation in many applications, referring to the '*fluoro-stabilisation effect*', whereby protein stability is enhanced by replacing hydrocarbon residues with fluorocarbon residues. Hydrophobics have been strongly associated with the fluoro-stabilisation effect since it was reported by Marsh *et al.* that the difference in hydrophobicity when substituting leucine with hexafluoroleucine in a peptide that adopts a four-helix bundle structure results in a similar change in the peptide stability.[126] Cheng and co-workers evaluated the helical propensity of three highly fluorinated amino acids using an alanine based peptide incorporating the fluorinated residue of interest within the central region of the peptide sequence. Circular dichroism studies were used to evaluate the helical content of the peptides where it was reported that the helical propensities were reduced for the fluorinated residues, proposing that the observed increase in α-helix stability arises due to the increased hydrophobicity of the fluorinated side-chain.[127]

The introduction of side-chain constraints such as disulphides, hydrazones and lactams for forcing helical conformations has been thoroughly examined (Figure 1.16).[128-130] Doig *et al.* investigated the use of salt bridges in stabilising α-helices, stating that they are found in approximately 60% of protein structures, 20% of which are present in α-helices in an *i,i*+3 or *i,i*+4 spacing. It was also noted that the role of salt bridges in enhancing protein stability is supported by their increased occurrence in thermophillic proteins.[131]
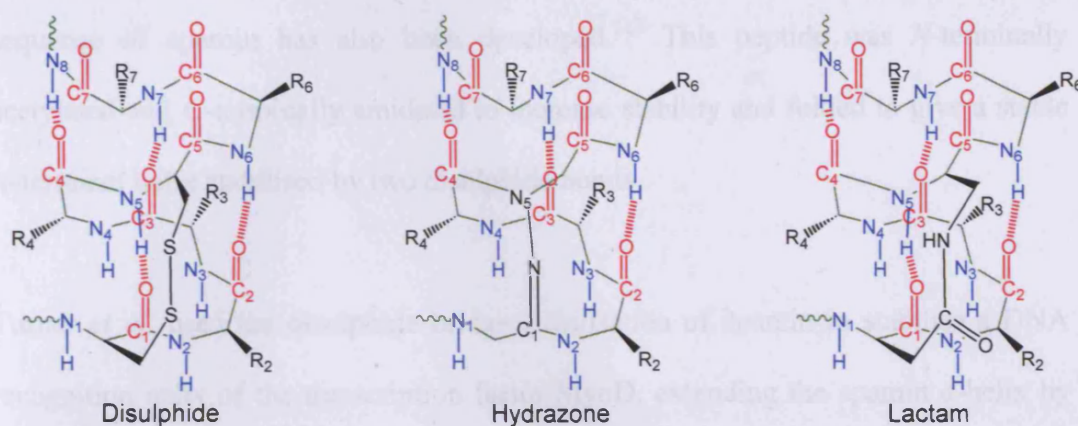
Figure 1.16: *Side-chain constraints within an α-helix (black) shown amongst helix backbone (green) and supporting hydrogen bonds (red).*

1.10 Manipulating Peptide Secondary Structure Through The Incorporation of Reversible Conformational Constraints

The introduction of conformational constraints within a peptide as a means to manipulate secondary structure is a thoroughly researched field. The most fundamental constraint incorporated within amino acid sequences and frequently used in nature as a means of stabilising all manner of proteins is the disulphide bridge, for which the relative positions of cysteine residues have been found to be highly conserved. The use of disulphide bonds in the provision of additional stability has previously been highlighted through the successful development of a miniaturised oxaloacetate decarboxylase termed Apoxaldie, utilising a scaffold based on apamin (Section 1.9). Schulz *et al.* also took advantage of the disulphide bridge framework of apamin.[130] The versatility of disulphide bonds is such that they can be formed under mild conditions, in a variety of solvents and in the presence of a variety of functional groups. An *N*-terminally stabilised α-helical peptide optimised from the reversed

sequence of apamin has also been developed.[112] This peptide was *N*-terminally acetylated and *C*-terminally amidated to increase stability and folded to give a stable *N*-terminal helix stabilised by two disulphide bonds.

Turner *et al.* used the disulphide bridge stabilisation of apamin to stabilise a DNA recognition helix of the transcription factor MyoD, extending the apamin α-helix by the fusion of the *N*-terminus of the basic helix-loop-helix (bHLH) domain of MyoD to produce ApaMyoD.[132] This was found to bind DNA more avidly than the parent protein and circular dichroism (CD) spectroscopy showed a significantly higher proportion of α-helix, hence the increased affinity for DNA and improved thermal stability. All these changes could be attributed directly to the presence of the disulphide linkage within the apamin scaffold, since the reduced form of ApaMyoD displayed properties directly comparable to the parent protein. The work of Turner *et al.* reinforced the importance of structural constraints with respect to the regulation of protein activity through its secondary structure.

The use of disulphides and their reversible nature under oxidising and reducing conditions enhances the possibilities for the use of structural constraints and has prompted a search for chemical crosslinkers that may be attached to peptide chains at the appropriate spacing in which to initiate the formation of a specific structural motif. This has led to the desire to posses control over the functionality of these crosslinkers and the use of certain functional groups has been employed at the centre of such crosslinkers that elicit a reversible response depending upon the stimuli applied.
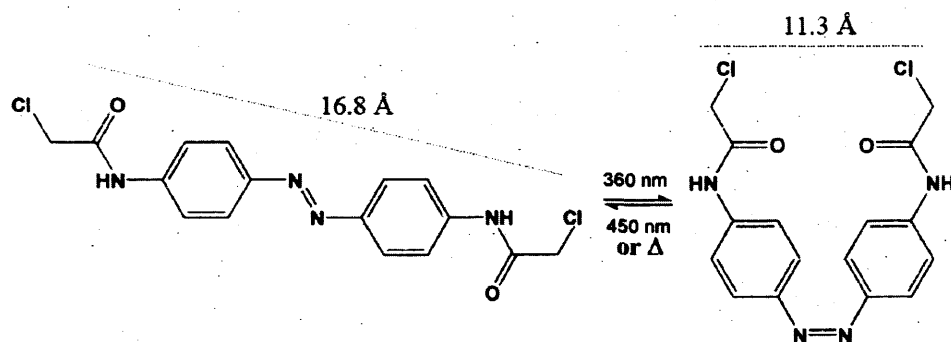
Scheme 1.1: *Photoisomerisation of azobenzene, the end-to-end distances for the chloroacetamido groups are given for the cis and trans isomers*

The sensitivity of proteins and their respective interactions within their environment means that there are few conditions that can be varied and are applicable to the use of chemical crosslinkers both *in vitro* and *in vivo*, with the notable exception of disulphide bonds as previously discussed. However, the sensitivity of specific chromophores to light and the non-invasive nature of such an environmental change have led to the development of molecules for use as chemical crosslinkers that undergo reversible changes upon exposure to specific wavelengths of light. The most versatile and hence widely researched example of such crosslinkers are those which incorporate an azobenzene, undergoing reversible *trans* to *cis* isomerisation upon exposure to UV light (Scheme 1.1). The azobenzene chromophore undergoes fast (picosecond) isomerisation with a low rate of photo-degradation (bleaching), high quantum yields and a long lifetime for the excited *cis* azobenzene state.[133]

Moroder *et al.* examined the use of azobenzene crosslinkers in the construction of cyclic bis-cysteinyl peptides based on the active site of thioredoxin reductase in addition to the incorporation of further structural constraints by the presence of a disulphide bridge.[134] An azobenzene moiety was used to cyclise the molecule,

however it was reported that the presence of disulphide bridges led to multiple conformers of both the *cis* and *trans* isomers. This was resolved by the addition of methylene spacers between the azobenzene moiety and the peptide, permitting the folding of the peptide into lower energy conformations. Differences in the redox potentials of the peptide-linker system when comparing the *cis* and *trans* isomers were observed and compared against the subsequent change in folding as observed by CD spectroscopy measurements. Moroder *et al.* later adapted this linker for use within an integrin binding ligand, successfully manipulating the binding affinity of the ligand for the integrin by the application of specific wavelengths of UV light.[135]

Moroder and co-workers later optimised a β-hairpin structure based upon a tryptophan zipper motif.[136] Unstable and difficult to characterise spectroscopically, β-hairpins are heavily involved in both protein-protein and protein-DNA interactions, β-hairpins occur where two anti-parallel strands of β-sheet are linked by a small loop. The incorporation of an azobenzene motif enabled control over the formation or disruption of the β-hairpin structure (Structure 1.1) and was confirmed by NMR spectroscopy, and the degree of secondary structure change caused by the disruption induced by the temperature dependant relaxation of the azobenzene crosslinker from *cis* to *trans* conformations enabled studies to be undertaken using CD measurements into the rate of folding of the β-hairpin into its stable secondary structure upon reversion of the azobenzene functional group from *cis* to *trans*.
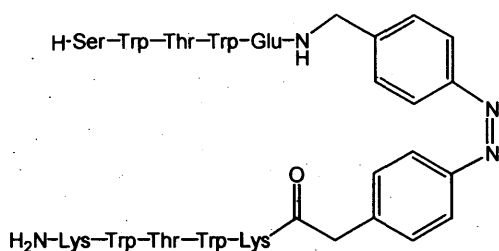
Structure 1.1: *A photo-controlled β-hairpin structure designed by Moroder et al.*[136]

The incorporation of photo-inducible crosslinkers into β-hairpin structures was further adapted by Hilvert *et al.* who incorporated an azobenzene containing amino acid derivative within an open-chain β-hairpin peptide sequence 12 amino acids in length, the sequence segment ^{D}Pro-Gly was identified as the nucleation site for the β-turn and so was replaced with the azobenzene-containing mimetic (Figure 1.17).

Arg-Trp-Gln-Tyr-Val-^{D}Pro-Gly-Lys-Phe-Tyr-Val-Gln-NH$_2$

Arg-Trp-Gln-Tyr-Val-X-Lys-Phe-Tyr-Val-Gln-NH$_2$
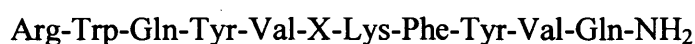
Figure 1.17: *Peptide sequences for a β-turn peptide (top) and the modified photo-switchable azobenzene containing (X, bottom) β-turn motif designed by Hilvert et al.*[137]

A reversible change in peptide conformation upon the switching of the azobenzene *trans/cis* configuration was observed, supporting the data from molecular dynamic simulations carried out by the same researchers.[137] Hilvert and co-workers later extended their research into investigating helical polypeptides, using the previously mentioned aPP since it contains a stable, well-researched secondary structure.[138] Their work on photo-controllable β-hairpins was incorporated through the substitution of three residues from a β-turn with an azobenzene containing synthetic amino acid

moiety. Hilvert and co-workers used CD spectroscopy to show the modified peptide

to exhibit similar helicity to wild-type aPP, they concluded that although they were

able to produce an analogue of aPP in which the secondary structure, and therefore

dimerisation could be manipulated by the switching of the *cis/trans* conformation

repeated isomerisation of the structure led to its precipitation.[138]

Woolley and co-workers have carried out further research into the development of

reversible crosslinkers that can be used to both stabilise and destabilise α-helix

formation. This was initially achieved by the incorporation of an azobenzene

containing amino acid, phenylazophenylalanine (Pap) within the ribonuclease A

sequence. The rate of RNA hydrolysis was observed, and was found to be influenced

by the isomerisation of the Pap side-chain.[139] Woolley and co-workers conducted

further research into the development of azobenzene containing crosslinkers through

the exploitation of the change in length of the crosslinker through photoisomerisation.

The initial crosslinker used iodoacetamide functional groups bonded to each end of

the azobenzene motif, these were attached to a short peptide *via* reaction with the thiol

side-chains of cysteine residues engineered within the sequence at an *i,i*+7 spacing.

CD spectroscopy showed a four-fold increase in α-helicity from 12 % to 48 % for the

crosslinked peptide in the *cis* conformation when compared to the helix destabilising

trans conformation. Further work by Kumita *et al.* used enhanced molecular

modelling techniques to identify alternative spacings of the cysteine residues and

therefore the appropriate spacing for the crosslinker influences the subsequent end-to-

end distance between chloroacetamide groups of the crosslinker. It was found that for

stabilisation of a helical structure in the *cis* isomer cysteines were required to be

distributed *i,i*+4 or *i,i*+7 obtaining 70-90 % *cis* in the light-adapted state, whereas for

the *trans* isomer a spacing of *i,i*+11 is required whereby > 99 % *trans* is obtained in

the dark-adapted state.[140,141] Further work by Flint *et al.* supported the findings of

Kumita and co-workers, peptides were synthesised incorporating cysteine residues in

both *i,i*+4 and *i,i*+11 spacings. The crosslinking of these peptides and subsequent

analysis by CD spectroscopy revealed a degree of photocontrol for both peptides.[141]

Kumita and co-workers designed a coiled-coil peptide, a common structural moiety

found in nature; based on the coiled-coil leucine zipper peptide GCN-4-P1. This

structure consists of two parallel amphipathic α-helices that wrap around one another

to yield a homodimeric left-handed supercoil. A coiled-coil structure was chosen

because the formation of two helices that then combine to give a more helical

quaternary structure makes CD spectroscopy an ideal tool to monitor the changes in

helicity which can be related directly to interactions between the two peptides and it

was found that the helicity and therefore ability for the coiled-coil structure to

dimerize was influenced by the isomerisation of the crosslinker.[140] Although some

degree of photocontrol was achieved, the choice of location for the *i,i*+7 spaced

cysteine residues were found to significantly affect the functionality of the peptide.

A potential drawback in the use of the azobenzene crosslinker designed by Woolley *et*

al. is the poor aqueous solubility of the molecule, illustrated in the published method

for crosslinking describing the use of a water and dimethylsulphoxide co-solvent.

Further work by Zhang *et al.* led to the development of a water-soluble crosslinker

through the addition of sulphonate groups to the *meta* positions within the azobenzene

ring system.[142] The iodoacetamide groups were also substituted for chloroacetamide

groups in order to improve the light stability of the linker (Scheme 1.2).[142,143]
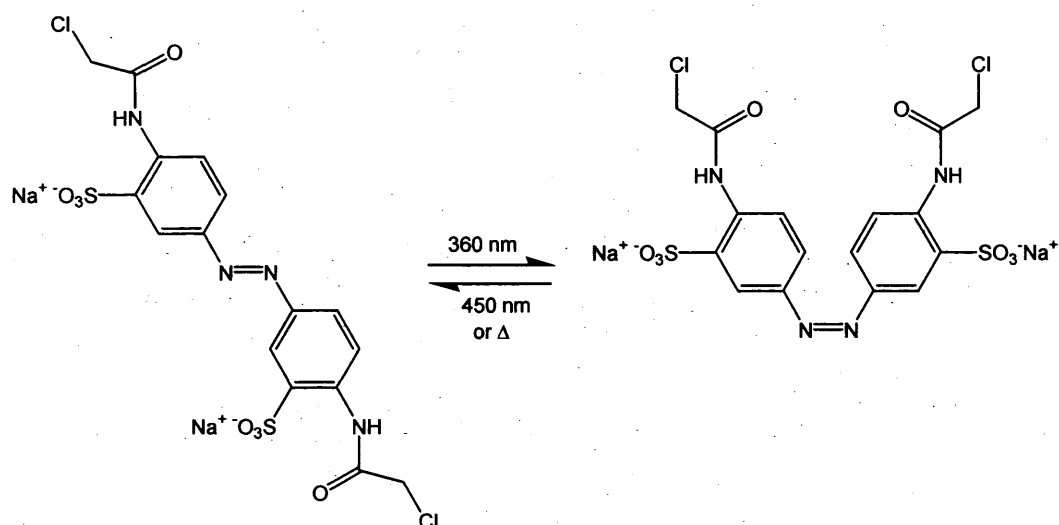
Scheme 1.2: *Azobenzene crosslinker designed and optimised by Zhang et al.[142]*

In order to assess whether the reversibility of the conformational change provided by the attachment of the engineered water-soluble azobenzene crosslinker would be maintained when the conformational change is associated with a change in biological activity such as binding to another molecule Woolley *et al.* studied the bZIP DNA binding domain of the yeast transcriptional activator GCN4.[144] An *i,i*+7 spaced cysteine containing peptide was synthesised and crosslinked, the helical propensity and therefore the dimerisation and DNA binding affinity was reported to be increased for the light induced (*cis*) crosslinked structure, whereas the dark adapted (*trans*) crosslinked peptide showed reduced helicity and DNA binding when compared to wild-type GCN4-bZIP.[144]

The azobenzene crosslinker designed by Zhang and co-workers for optimised light and water stability was also used by Guerrero *et al.* to design an 18 residue DNA binding peptide based on the recognition helix of the Q50K engrailed homeodomain. This peptide, referred to as HDH-3 incorporated cysteine residues within an *i,i*+11 spacing at locations shown in molecular modelling to not interfere with DNA binding.

CD spectroscopy showed the uncrosslinked peptide to be unstructured, however upon addition of the crosslinker the *trans* isomer displayed a significant increase in α-helicity that was reduced upon irradiation of the crosslinker to the *cis* isomer. The CD data was supported by fluorescence anisotropy DNA binding assays which for the dark-adapted *trans* isomer a K_D of 7.5 nM (± 1.3) was reported, this was reduced significantly to 140 nM (± 11) upon irradiation with 360 nm UV light (Figure 1.18).[145]
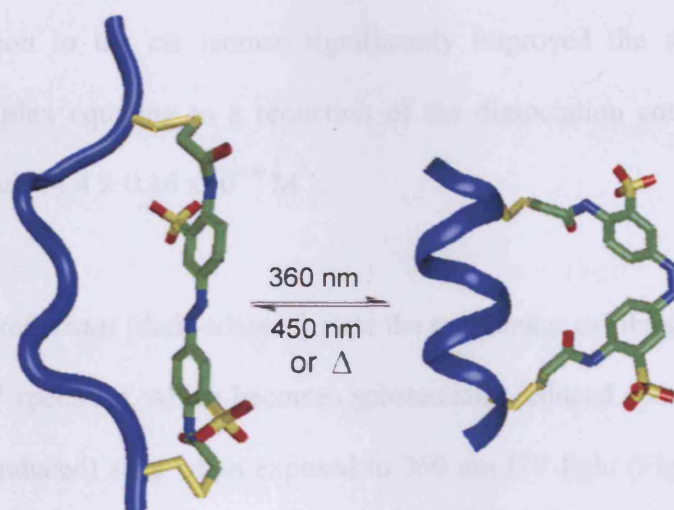
Figure 1.18: *Photocontrol of peptide helicity for an i,i+7 spaced azobenzene crosslinker incorporated within a short peptide based on the p53 N-terminus.*[145]

Guerrero *et al.* further tested the use of azobenzene crosslinkers in the regulation of peptide secondary structure through the design of photoMyoD, a peptide derived from MyoD, a muscle-specific transcription factor that relies on the basic helix-loop helix (bHLH) domain for DNA binding which is mediated through its *N*-terminal recognition α-helix contacting the major groove of DNA. An 18 residue peptide based on this helical motif was synthesised incorporating cysteine residues in an *i,i+7*

spacing, this peptide photoMyoD, was identified by CD spectroscopy to be predominantly random coil, containing approximately 10 % α-helix. Upon crosslinking, the secondary structure of the *trans* isomer was reported to be comparable to the uncrosslinked peptide and irradiation of crosslinked photoMyoD was reported to give 19 % α-helicity for the *cis* isomer. Fluorescence anisotropy measurements of the dissociation constants for the interaction of photoMyoD with DNA showed little difference between the uncrosslinked and the *trans* isomer of the crosslinked peptide (8.8 ± 2.2 x10^{-15} M^2 and 1.5 ± 0.38 x10^{-14} M^2 respectively), however irradiation to the *cis* isomer significantly improved the stability of the photoMyoD complex equating to a reduction of the dissociation constant by three orders of magnitude (4.4 ± 0.16 x10^{-18} M^2).

When in the relaxed, *trans* (dark-adapted) state the crosslinker exhibits a maximum at 360 nm in its UV spectrum, which becomes substantially reduced upon isomerisation to the *cis* (light-induced) state when exposed to 360 nm UV light (Figure 1.19). It is important to note that since the isomerisation of the crosslinker from the *trans* to *cis* isomer only produces a maximum yield of 60-70 % the presence of the remaining *trans* isomer means that the crosslinker solution will always exhibit some absorbance at 360 nm.[141] Contrary to the moderate quantum yield arising from the light induced isomerisation of the crosslinker from *trans* to *cis*, its subsequent relaxation into the dark-adapted state from *cis* to *trans* results in an approximate 100 % yield of the *trans* isomer, hence a full recovery of its maximum at 360 nm in the UV spectrum, thus enabling the relaxation of the crosslinker molecule to be monitored by UV spectroscopy.
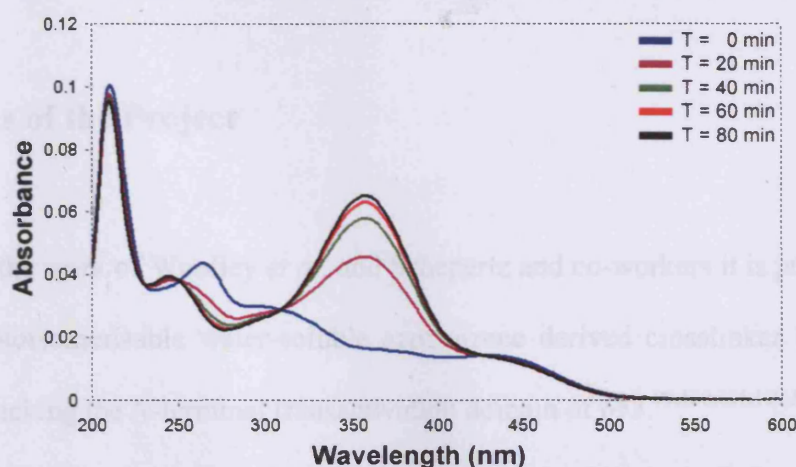
Figure 1.19: *The UV maxima at 360 nm for the crosslinker is reduced upon isomerisation to the cis isomer. This recovers in a time and temperature dependant manner (shown crosslinker at 20 °C)*

We propose that the relaxation times of the crosslinker when attached to a variety of p53-based peptides will be greater than the relaxation time for the free crosslinker due to its restraint at both ends to the peptide cysteine residues. Direct comparison of the relaxation times for the crosslinked peptides will reveal information relating to the stability of the constrained peptide secondary structure influenced by the crosslinker conformation. This is proposed since a more stable induced secondary structure would be more resistant to relaxation of the crosslinker, resulting in increased relaxation times.

1.11 Aims of the Project

Based upon the work of Woolley *et al.* and Schepartz and co-workers it is proposed to attach a photoisomerisable water-soluble azobenzene derived crosslinker to a short peptide mimicking the *N*-terminal transactivation domain of p53.[90,120,121,139,140,142-144] It is believed that the potency of such molecules may be controlled *via* photo-isomerisation of the crosslinker through the manipulation of the peptide secondary structure, since Mdm-2 binding of p53 requires the adoption of an α-helical motif. This will be achieved through the design and synthesis of short peptides based on the *N*-terminal transactivation domain of p53 which incorporate cysteine residues at desired spacings for the attachment of the crosslinker.

The interaction of optimised p53-based peptides with Hdm-2 is to be measured using fluorescence anisotropy and the differences in the binding affinities of the uncrosslinked, light induced and dark-adapted peptides are to be compared against structural information relating to these peptides acquired from circular dichroism spectroscopy. Additionally, the rate of relaxation of the crosslinked peptide from the light induced, *cis* state to the dark-adapted, *trans* state will be investigated, and it is proposed that this rate of relaxation is related to the stability of the induced α-helix. For example, a more stable α-helix arising from a light induced crosslinker conformation is proposed to result in an increased relaxation time for the crosslinker to revert back into the dark-adapted state.

The purpose of this research is to build upon the work of Guerrero *et al.* who developed a DNA binding peptide in an *i,i*+11 spacing resulting in a stabilised α-helix in the dark-adapted, *trans* isomer.[145] The application of this to the development of photo-switchable p53-based peptides that bind Hdm-2 with high affinity in a reversible manner shows potential for therapeutic use in patients in which the apoptosis pathway is inhibited as a result of over-expression of Hdm-2 inhibiting free p53. The introduction of high affinity Hdm-2 binding peptides are proposed to compete with cellular p53 and ensure the saturation of p53 binding sites upon Hdm-2, whilst the use of the azobenzene crosslinker provides a means of regulating their specificity, since the control of the conformation of the azobenzene chromophore might allow switching between an active and inactive conformation of the peptide.

CHAPTER 2:

MATERIALS & METHODS

2.1 Materials

All chemicals, solvents and biological buffers were purchased from Fisher, Sigma-Aldrich or Fluka. Amino acids and reagents for peptide synthesis were purchased from Novabiochem or AGTC Bioproducts Ltd. Molecular biology reagents were purchased from New England Biolabs, GE Healthcare or QIAGEN.

2.1.1 Preparation of Reagents and Buffers

50 x TAE (Tris-acetate/EDTA) Electrophoresis Buffer

Tris base (242.0 g) was dissolved in deionised water (500 ml) containing glacial acetic acid (57 ml). 100 ml ethylenediaminetetraacetic acid (EDTA) solution (0.5 M, pH 8.0) was added and the resulting solution diluted to 1 L with deionised water.

10 x SDS Running Buffer

Glycine (72.0 g), Tris base (15.4 g) and sodium dodecyl sulphate (SDS, 5.0 g) were dissolved in deionised water (250 ml). The resulting solution was diluted to 500 ml with the same solvent.

SDS Gel loading Buffer

To 0.5 M Tris-HCl (pH 6.8, 1.25 ml) was added, deionised water (3.55 ml), glycerol (2.5 ml), 10 % w/v SDS (2.0 ml) and 0.5 % w/v bromophenol blue (0.2 ml). Prior to use 950 µl of this mixture was added to 50 µl 2-mercaptoethanol.

Stain Buffer for SDS-PAGE

Coomassie brilliant blue G (0.25 g) was dissolved in a solution consisting of deionised water (45 ml), ethanol (45 ml) and glacial acetic acid (10.0 ml).

Destain Buffer for SDS-PAGE

Isopropanol (100 ml) was added to a solution consisting of deionised water (780 ml) and glacial acetic acid (120 ml).

Gel-loading Buffer for Agarose Gel Electrophoresis

Bromophenol blue (0.25 % (w/v), 2.5 μl) was added to a solution consisting of deionised water (697.5 μl) and glycerol (30 % (v/v), 300 μl). This solution was stored at -20 °C prior to use.

0.12 M Ethanolic Sodium Acetate Solution

Anhydrous sodium acetate (0.2 g) was added to a solution containing deionised water (1.0 ml) and ethanol (15.0 ml). The resulting solution was made up to 20 ml with ethanol.

0.1 M CaCl$_2$ Solution

CaCl$_2$ (5.88 g) was dissolved in deionised water (400 ml), prior to sterilisation by autoclaving (20 min, 15 lb in^{-2}) on a liquid cycle.

80 mM MgCl₂, 20 mM CaCl₂ Solution

MgCl$_2$ (6.50 g) and CaCl$_2$ (1.17 g) were dissolved in deionised water (400 ml), prior to sterilisation by autoclaving (20 min, 15 lb in^{-2}) on a liquid cycle.

0.5 M EDTA Solution

EDTA (14.61 g) was dissolved in deionised water (50 ml), and the pH adjusted to 8.0 using NaOH (5 M). The resulting solution was diluted to 100 ml with deionised water.

10 % Ethidium Bromide Solution

Ethidium bromide (0.5 g) was dissolved in deionised water (50 ml) by stirring at room temperature overnight protected from light. The resulting solution was stored at 4 °C prior to use.

10 % (w/v) SDS Solution

SDS (10.0 g) was dissolved in deionised water (90 ml) and diluted to 100 ml with the same solvent.

0.5 % (w/v) Bromophenol Blue Solution

Bromophenol blue (50 mg) was dissolved in deionised water (10 ml).

10 % (w/v) Ammonium Persulphate Solution

Prepared on day of use. Ammonium persulphate (100 mg) was dissolved in deionised water (1 ml).

10 x Phosphate Buffered Saline Solution (PBS)

NaCl (40.9 g), KCl (1.05 g), Na_2HPO_4 (7.05 g) and KH_2PO_4 (1.2 g) were dissolved in deionised water (400 ml) and diluted to 500 ml with the same solvent.

Deoxyribonucleotide triphosphate (dNTP) Mix

An aqueous solution (pH 7.5) was made consisting of 0.2 mM of each; dATP, dCTP, dGTP and dTTP.

Hdm-2 Lysis Buffer

50 mM Tris-HCl (pH 8.0)

500 mM NaCl

10 mM 2-mercaptoethanol

1 mM EDTA

1 mM phenylmethylsulphonyl fluoride (PMSF)

0.1 % (w/v) Triton X-100

Hdm-2 Buffer A

50 mM Tris-HCl (pH 8.0)

500 mM NaCl

10 mM 2-mercaptoethanol

1 mM EDTA

Hdm-2 Buffer B

This buffer was prepared as per Hdm-2 Buffer A with the inclusion of 10 mM reduced

glutathione

Fluorescence Anisotropy Buffer

100 mM Potassium phosphate buffer (pH 7.0)

5 mM dithiothreitol

150 mM NaCl

Circular Dichroism Buffer

5 mM Potassium phosphate buffer (pH 7.0)

0.5 mM dithiothreitol

For solutions containing 2,2,2-trifluoroethanol (TFE) the appropriate volume of

deionised water was substituted for the desired concentration (v/v) of TFE.

p53 Lysis Buffer

50 mM Tris-HCl (pH 8.0)

2 mM EDTA

100 mM NaCl

1 mM PMSF

p53 Buffer A

This buffer was prepared as per p53 Lysis buffer with the inclusion of 0.5 % (w/v) Triton X-100.

p53 Buffer B

5 M guanidine chloride

50 mM Tris-HCl (pH 8.0)

0.005 % (w/v) Tween 80

p53 Buffer C

1 M guanidine chloride

50 mM Tris-HCl (pH 8.0)

0.005 % (w/v) Tween 80

2 mM Reduced glutathione

0.02 mM Oxidised glutathione

p53 Buffer D

50 mM Tris-HCl (pH 8.0)

150 mM NaCl

0.005 % (w/v) Tween 80

p53 Buffer E

0.15 M NaCl

50 mM Tris-HCl (pH 8.0)

p53 Buffer F

0.5 M NaCl

50 mM Tris-HCl (pH 8.0)

2.1.2   Culture Media

Preparation of Luria-Bertani (LB) Medium

Tryptone (10.0 g), NaCl (10.0 g) and yeast extract (5.0 g) were added to deionised

water (950 ml) and the pH of the resulting solution adjusted to 7 with NaOH (5 M).

The solution was made up to a final volume of 1 L, prior to sterilisation by

autoclaving (20 min, 15 lb in^{-2}) on a liquid cycle.[146]

2.1.3   Preparation of Antibiotic Solutions

50 mg ml^{-1} Ampicillin Stock Solution

Ampicillin sodium salt (500 mg) was dissolved in sterile deionised water (10 ml) and

the resulting solution filter-sterilised using a 0.22 μm syringe filter, prior to dividing

into 200 μl aliquots which were stored at −20 °C.

34 mg ml^{-1} Chloramphenicol Stock Solution

Chloramphenicol (34 mg) was dissolved in ethanol (1.0 ml), and stored at −20 °C

prior to use.

2.1.4   Agar Plates

LB Agar Plates

Tryptone (2.10 g), NaCl (2.10 g), yeast extract (1.06 g) and agar (3.16 g) were dissolved in deionised water (200 ml), prior to sterilisation by autoclaving (20 min, 15 lb in^{-2}) on a liquid cycle. The resulting mixture was cooled to *ca.* 30 °C prior to dividing between sterile petri dishes, where it was cooled and stored inverted at 4 °C.

Ampicillin-Agar Plates

Prepared as described for standard LB agar plates. Upon cooling (*ca.* 30 °C) a 200 μl aliquot of ampicillin stock solution was added (resulting ampicillin concentration 0.1 mg ml^{-1}) and gently mixed, prior to dividing between sterile petri dishes, where it was cooled and stored inverted at 4 °C.

Chloramphenicol-Agar Plates

Prepared as described for standard LB agar plates. Prior to use 15 μl of chloramphenicol stock solution (34 mg ml^{-1}) was spread across the plate surface and dried at 37 °C for 10 min.

2.2 Methods

2.2.1 Crosslinker Synthesis

The synthesis of the water-soluble azobenzene crosslinker (3,3'-bis-(sulfo)-4,4'-bis-(chloroacetamido)-azobenzene) was carried out as described by Zhang *et al.* (Scheme 2.1) with ^{1}H and ^{13}C NMR employed to characterise the products at the end of each step as detailed in Scheme 3.2 and Appendix 1.[142]

2.2.2 Peptide Synthesis and Purification

Peptide Synthesis

Peptides were synthesised using the CEM Liberty microwave assisted peptide synthesiser using standard Fmoc protocols as detailed further in Section 3.1.[147] The 9-fluorenylmethoxycarbonyl (Fmoc) chloride and side-chain protected amino acids (Asn, Cys, Gln (trt); Asp, Glu (OtBu); Tyr, Ser, Thr (tBu); Lys, Trp (Boc)) were coupled in accordance with the desired sequence, starting from the carboxy terminus using a Rink Amide MBHA resin on a 0.1 mmol scale.

N-Terminal Fluorophore Labelling of Peptides

The peptide containing resin was added to a mixture of 5,6-carboxyfluorescein (FAM, 25 mg), *N*-hydroxybenzotriazole (HOBt, 10 mg) and *N,N'*-diisopropylcarbodiimide (DIC, 13 µl) in *N,N*-dimethylformamide (DMF, 3.0 ml). The resulting mixture was

shaken gently (protected from light) for 2 hours prior to the washing of the resin with

DMF using a sintered glass funnel.

Peptide Cleavage

The resulting peptides underwent a cleavage and deprotection with trifluoroacetic acid

(TFA):water: phenol:triisopropylsilane (88:5:5:2; v/v) per gram of resin for 2 hours,

protected from light at room temperature. The resin was removed by filtration and the

filtrate concentrated *in vacuo* and precipitated by washing with ice-cold diethyl ether

(3 x 5 ml) and allowed to stand at –20 °C for 2 hours. The crude peptide mixture was

dissolved in a water:acetonitrile solution (3:1) followed by lyophilisation.

Peptide Purification

Peptides were eluted from a LUNA 10μ C_{18} column (250 x 100 mm) with a linear

gradient from 0-60 % acetonitrile in water (0.05 % TFA) over 60 min with a flow rate

of 4.0 ml min^{-1}. Peptide fractions were identified by *matrix-assisted laser

desorption/ionisation time of flight* (MALDI-TOF) mass spectrometry, and the solvent

removed from the appropriate fractions *in vacuo* followed by lyophilisation and

storage protected from light at –20 °C. The experimentally determined peptide masses

were found to be in good agreement with the calculated masses. The purity of the

purified peptides was demonstrated to be greater than 98 % by reversed-phase high

performance liquid chromatography (HPLC) using an analytical LUNA 10μ C_{18}

column (250 x 4.6 mm).

Crosslinking of Peptides

The uncrosslinked peptide (*ca.* 0.5 mg) was dissolved in 50 mM Tris-base (pH 8.3, 3.0 ml) containing 2 mM tris(2-chloroethyl)phosphate (TCEP), and incubated with stirring at 4 °C (30 min) to ensure cysteine residues were in the reduced state. The water-soluble azobenzene crosslinker, 3,3'-bis-(sulfo)-4,4'-bis-(chloroacetamido)-azobenzene (2 mM) was dissolved in 50 mM Tris base (pH 8.3, 1.0 ml) and slowly added to the peptide solution in three aliquots of 333.3 µl at 20 min intervals. The reaction was allowed to proceed overnight protected from light with stirring at 4 °C.

Purification of Crosslinked Peptides

Crosslinked peptides were purified according to the standard procedure for peptide purification.

Photoisomerisation of Crosslinked Peptides

The photoisomerisation of the dark-adapted peptides was achieved by the irradiation of samples at 4 °C using a 250 W metal halide UV light point source (UV-P 280) coupled to a 360 nm band pass filter. Photoisomerisation by UV irradiation was conducted for 3 min, and was calculated as sufficient due to the absence of changes in the UV-Vis spectra of the samples.

2.2.3 Molecular Biology

Preparation of Competent Cells

A sample of a competent cell stock was plated onto agar and incubated at 37 °C overnight. A single bacterial colony was incubated in 5 ml LB media overnight at 37 °C with shaking. 100 µl of the resulting culture was transferred to 5 ml of LB media and incubated with shaking at 37 °C until an OD_{600nm} of *ca.* 0.4 was achieved and the cells recovered by centrifugation (4 °C, 4000 rpm, 10 min). The cell pellet was resuspended in 1.5 ml ice-cold $MgCl_2$ (80 mM), $CaCl_2$ (20 mM) solution and the cells recovered by centrifugation (4 °C, 4000 rpm, 10 min). The cell pellet was then resuspended in 0.2 ml $CaCl_2$ solution (0.1 M) followed by the addition of 0.2 ml sterile glycerol prior to dividing into 100 µl aliquots and stored at –80 °C.

DNA Plasmid Extraction and Purification

Plasmid DNA was purified using a QIAGEN plasmid purification kit according to the manufacturers protocols.[148-150]

Transformation of Competent Cells with DNA Plasmids

Competent cells (100 µl) were thawed on ice prior to the addition of the DNA plasmid (1-2 µl). After 20 min, the cells were heat shocked for 90 sec at 42 °C and returned to ice for 3 min, followed by the addition of 1.0 ml of media and incubation with shaking at 37 °C for 1 hour. The culture was then spread onto an agar plate containing the appropriate concentration of antibiotic where required and incubated overnight with shaking at 37 °C. Plates containing transformed cells were stored at 4 °C.

Agarose Gel Electrophoresis

A 5 % (w/v) agarose solution was made by dissolving agarose (0.5 g) in TAE buffer (50 ml) by microwave heating. This solution was poured into a Mini-Sub Cell (Bio-Rad), and covered in TAE buffer, prior the loading of the DNA samples (0.25 % bromophenol blue, 30 % glycerol). Gels were run at 60 mA (*ca.* 45 min) and soaked in deionised water (200 ml) containing 200 µl of ethidium bromide solution (10 mg ml⁻¹) prior to visualisation by the fluorescence of the intercalated ethidium bromide.

Digestion of DNA with Restriction Enzymes

Restriction endonucleases (New England Biolabs) were used to digest DNA following the manufacturers recommended protocols, incubated with shaking at 37 °C for 1 hour. Agarose gel electrophoresis was used to analyse the digestion products.

Polymerase Chain Reaction (PCR)

All oligonucleotide primers were synthesised and purified by Operon Biotechnologies. Reactions were performed in a Biometra T Personal Thermal Cycler, and were prepared in a 0.5 ml PCR tube comprising of *Pfu* DNA polymerase (5 U), 2 ng DNA template, 0.5 mM of each primer, dNTP mix (10 mM), 1 x PCR buffer, KCl (500 mM) and MgCl₂ (2 mM). Sterile deionised water was added to give a final volume of 50 µl, and mineral oil (30 µl) was used to form an upper surface to prevent evaporation of the reaction mixture during thermal cycling.

Table 2.1 – *Primer sequences for the mutation of Hdm-2 Ile61 to Ala.*

Primer	Oligonucleotide	Melting Temp (°C)
Hdm-2$_{1-125}$ Wild-Type	5'-CTTGGCCAGTATA**TT**ATGACTA AACGATTATATGATGAG-3'	-
Hdm-2$_{1-125}$ Ala61 Fwd	5'-CTTGGCCAGTAT**GCG**ATGACTA AACGATTATATGATGAG-3'	68.9
Hdm-2$_{1-125}$ Ala61 Rev	5'-GAACCGGTCATA**CGC**TACTGAT TTGCTAATATACTACTC-3'	68.9

Table 2.2 – *Primer sequences for the mutations induced in wild-type Hdm-2$_{1-125}$ position 72.*

Primer	Oligonucleotide	Melting Temp (°C)
Hdm-2$_{1-125}$ Wild-Type	5'-CGATTATATGATGAGAAGCAA**C**AACATA TTGTATATTGTTCAAATG-3'	-
Hdm-2$_{1-125}$ Asn72 Fwd	5'-CGATTATATGATGAGAAGCAA**AAC**CATA TTGTATATTGTTCAAATG-3'	65.6
Hdm-2$_{1-125}$ Asn72 Rev	5'-GCTAATATACTACTCTTCGT**TTT**GGTAT AACATATAACAAGTTTAC-3'	65.6
Hdm-2$_{1-125}$ Met72 Fwd	5'-CGATTATATGATGAGAAGCAA**ATG**CATA TTGTATATTGTTCAAATG-3'	65.6
Hdm-2$_{1-125}$ Met72 Rev	5'-GCTAATATACTACTCTTCGT**TTAC**GTAT AACATATAACAAGTTTAC-3'	65.6
Hdm-2$_{1-125}$ Leu72 Fwd	5'-CGATTATATGATGAGAAGCAA**CTG**CATA TTGTATATTGTTCAAATG-3'	66.5
Hdm-2$_{1-125}$ Leu72 Rev	5'-GCTAATATACTACTCTTCGT**TGAC**GTAT AACATATAACAAGTTTAC-3'	66.5

The melting temperatures of the primers were considered when determining the cycling temperatures. A typical cycle commenced with denaturation (1 min at 95 °C),

followed by annealing (1 min at 55 °C) and extension (30 sec 70 °C). The thermal

cycling was repeated 30 times.

Agarose gel electrophoresis was used to confirm the amplification of the desired DNA

fragment.

Site Directed Mutagenesis

The procedure for PCR was followed using the appropriate primers (Tables 2.1-2.2).

Plasmid DNA was digested with the addition of *Dpn*I restriction endonuclease using

previously described conditions. Agarose gel electrophoresis was used to determine

the presence of the desired DNA fragment, which was transformed into JM109

competent *E. coli* and incubated on LB agar overnight at 37 °C.

DNA plasmids were extracted and purified following the previously described

protocol, and successful mutagenesis was confirmed by DNA sequencing.

Preparation of Glycerol Stocks

A sample from an overnight culture (0.8 ml) was aseptically mixed with sterile

glycerol (0.2 ml) and stored at –80 °C.

Ethanol Precipitation of Nucleic Acids

0.12 M ethanolic sodium acetate (1.0 ml) was added to sample DNA and stored at –20

°C for 1 hour. The solution was centrifuged (13,000 rpm, 10 min) and the supernatant

decanted. The precipitate was dried at 42 °C prior to storage at –80 °C.

2.2.4 Gene Expression and Protein Purification

Over-Expression of Recombinant Proteins

A single transformed bacterial colony was incubated in 5 ml of LB broth containing ampicillin (0.1 mg ml^{-1}) overnight with shaking at 37 °C. The overnight culture was transferred to 500 ml of LB media containing ampicillin (0.1 mg ml^{-1}) and incubated with shaking at 37 °C until an OD$_{600nm}$ of *ca.* 0.6 was achieved. Isopropyl-beta-D-thiogalactopyranoside (IPTG, 0.8 mM) was added to induce protein expression for a further 4 hours after which, cells were centrifuged (5,000 rpm, 10 min) to remove the supernatant and stored at –20 °C.

Cell Lysis

Pellets from a large-scale expression were thawed on ice and resuspended by vortexing in the appropriate lysis buffer. The suspension was sonicated for 5 min (30 sec on, 30 sec off) on ice using a Sonicator W-37 (Heat Systems Ultrasonics Inc.). The resulting lysate was centrifuged (14,000 rpm, 20 min) and the protein-containing supernatant decanted, the pellet was retained for use as a reference when analysing the supernatant by SDS-PAGE.

Purification of the desired protein was commenced within 2 hours, however the solution was stored at 4 °C prior to use.

Affinity Chromatography

Crude protein was loaded using a Watson Marlow 101U/R peristaltic pump onto a drip-column prepared using glutathione sepharose 4B resin with a 5 ml bed volume. Washed columns were stored in 20 % ethanol solution at 4 °C.

Thrombin Cleavage of Hdm-2

Concentrated GST-Hdm-2 was incubated in a water bath overnight (30 °C) with 60 U thrombin protease.

Size-Exclusion Chromatography

Concentrated protein was loaded onto a Superdex G75 10/300 GL gel filtration column attached to an AKTA FPLC using the appropriate buffer. The fractions containing pure protein were pooled and stored at 4 °C.

DEAE Ion-Exchange Chromatography

Dialysed protein solution was loaded onto a DEAE Biogel A ion exchange column attached to an AKTA FPLC using the appropriate buffer. The fractions containing pure protein were pooled and stored at 4 °C.

SDS Polyacrylamide Gel Electrophoresis

SDS gels were produced in accordance with the Bio-Rad Mini-PROTEAN™ 3 Cell protocols.[151] Protein samples were mixed with SDS-Gel loading buffer and heated (80 °C, 4 min) before loading onto 15 % gels, which were run for 45-60 min (200 V) in

SDS running buffer. To visualise the bands, gels were stained with SDS-PAGE stain buffer and destained with SDS-PAGE destain buffer.

Dialysis of Protein Solutions

To remove undesired buffer components, samples were dialysed using Medicell International Ltd. dialysis membranes (3,500 molecular weight cut off (MWCO)) into 2 l of the appropriate buffer with stirring at 4 °C. The dialysis buffer was changed at *ca.* 9 hour intervals a total of three times.

Protein Concentration

Concentration of proteins was carried out using an Amicon ultrafiltration system fitted with a Millipore ultrafiltration membrane (~3,000 MWCO) with a N_2 pressure of 3 bar at 4 °C.

2.3   Analytical Techniques

2.3.1   MALDI-TOF Mass Spectrometry of Peptides

MALDI-TOF mass spectra were obtained using a Waters Micro MX mass spectrometer. Peptides were ionised on a thin film of one part peptide solution to one part α-cyano-4-hydroxy cinnamic acid.

2.3.2 Circular Dichroism (CD) Spectroscopy

CD experiments were performed using an Applied Photophysics Chirascan CD spectrometer. Scans were performed (190-320 nm) on samples in CD buffer at 20 °C using a 1 mm pathlength cuvette. The mean residue ellipticity $[\Theta]_r$ was calculated according to Equation 2.1.

$$[\Theta]_r = \Theta / (10 \times n \times c \times l) \qquad \textit{Equation 2.1}$$

Where n is the number of backbone amide bonds, c is the molar (M) concentration of the sample solution and l is the cuvette pathlength (cm). Mean residue ellipticity is expressed with the units $deg\ cm^2\ dmol^{-1}$.

$$100\ \%\ \alpha\text{-helix } [\Theta]_{r\ 222} = [-40,000\ (n-4)] / n \qquad \textit{Equation 2.2}$$

The percentage α-helix content of the peptides was calculated using the value for 100 % α-helix derived from Equation 2.2.[152]

2.3.3 Estimation of DNA and Oligonucleotide Concentration

The concentration of nucleic acids was determined spectrophotometrically using a Shimadzu Biospec-mini spectrophotometer. The optical density of a sample solution was measured at 260 nm (OD_{260}). A solution of double stranded DNA *ca.* 50 µg ml^{-1} gives an OD_{260} of 1.0 with single stranded DNA (40 µg ml^{-1}) and oligonucleotides (20 µg ml^{-1}).

The ratio of absorbancies measured at 260 and 280 nm (OD_{260}/OD_{280}) was used as an indicator of the purity of the nucleic acid sample. A ratio value *ca.* 1.8 indicates a DNA sample is pure; this becomes reduced as the level of contaminant proteins and lipids is increased.

2.3.4 DNA Sequencing

DNA sequencing was performed by Cogenics Ltd, using an Applied Biosystems 3730xl DNA analyser.

2.3.5 Peptide and Protein Concentration Determination

The concentration of purified Hdm-2$_{1-125}$ in addition to the uncrosslinked and crosslinked peptides was determined spectrophotometrically using a Jasco V-660 UV-Vis spectrophotometer at 20 °C.

$$A = \varepsilon\, c\, l \qquad\qquad \textit{Equation 2.3}$$

The concentrations (*c*) were calculated according to the Beer-Lambert law (Equation 2.3), using a quartz UV cuvette with a 1 cm pathlength (*l*). The molar extinction coefficient (ε) of Hdm-2$_{1-125}$ (54,055 M^{-1} cm^{-1} ± 1809) was determined from the amino acid analysis data (Appendix A2) and for the peptides was taken as the value for the *N*-terminal attached FAM (83,000 M^{-1} cm^{-1}) from the manufacturer's product specification.

2.3.6   Fluorescence Anisotropy

Fluorescence anisotropy measurements were performed at 20 °C on a Perkin Elmer LS 55 Luminescence spectrophotometer arranged in L format (494 nm excitation; 520 nm emission). Binding assay titrations were performed in the fluorescence anisotropy buffer using a 1 ml quartz fluorescence cuvette. Fixed quantities of Hdm-$2_{1\text{-}125}$ (2.0-4.0 μM) were added successively to 1.0 ml of a peptide solution (10-50 nM). The G factor, the monochromator ratio of sensitivities for horizontally and vertically polarised light, was calculated for each equation as a correction for bias in one of the detectors (Equation 2.4).[153]

$$G = I_\perp \,/\, I_{\parallel} \qquad\qquad \textit{Equation 2.4}$$

Where $I_{\parallel}$ and $I_\perp$ are the intensities of the fluorescent emissions in parallel and perpendicular planes, respectively, to the excitation plane. The values for the G factor were always found to be between 1.11 and 1.13. The fluorescence anisotropy was determined with an integration time of 5 sec (Equation 2.5) for each step in the titration, which was repeated a total of 5 times for each assay.[154]

$$A = (I_{\parallel} - G \times I_\perp) \,/\, (I_{\parallel} + G \times I_\perp) \qquad \textit{Equation 2.5}$$

The fraction of peptide bound for each addition of protein was calculated by determining the end-point of the titration, whereby the anisotropy values remained unchanged despite the continued addition of protein.

2.3.7 Quantification of Crosslinker Relaxation by UV Spectroscopy

Crosslinker relaxation was observed by UV measurements using a Jasco V-660 UV-Vis spectrophotometer with a 1 cm pathlength quartz UV cuvette. Samples were dissolved in CD buffer and experiments were conducted with varying temperatures, using a Julabo F12 temperature controller. By assuming the kinetics of the thermal relaxation of the azobenzene crosslinker (*cis* to *trans*) to be a first-order process, the half-life ($t_{1/2}$) of the *cis* isomer can be calculated (Equation 2.6).

$$t_{1/2} = \ln 2 \, / \, k \qquad\qquad\qquad Equation\ 2.6$$

Where the rate constant for the thermal relaxation process is given as k, calculated by plotting the natural logarithm of the percentage of the *cis* isomer (derived from UV measurements at 360 nm) against time (Figure 2.1).
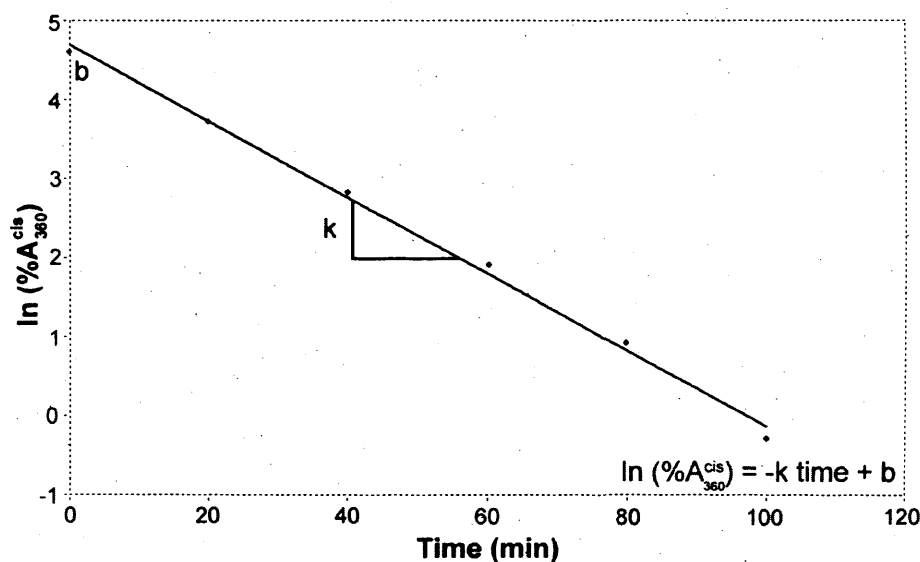
Figure 2.1: *The rate constant for the thermal relaxation of the cis isomer of the azobenzene crosslinker is derived from the plot of the natural logarithm of the percentage cis isomer against time.*

2.3.8 Determination of Dissociation Constants (K_D) From Fluorescence Anisotropy Data

Fluorescence anisotropy experiments were conducted by titrating Hdm-2 (protein) of a known concentration into a 1 cm fluorescence cuvette containing 1 ml of a known concentration of peptide ($[L]_{Total}$, ligand). The change in fluorescence anisotropy was recorded upon each addition of protein and this was considered saturated with respect to protein-ligand binding once the anisotropy values remained constant despite continued addition of protein.

The cumulative volume of the resulting protein-ligand solution (V_2) was recorded upon each protein addition (total added = V_1) and the resulting protein concentration (C_2) calculated accordingly based on the known concentration of the protein solution added (C_1, Equation 2.7). In order to evaluate the saturation point of the titration (100 % peptide bound), the constant anisotropy values at saturation were plotted against protein concentration and the values representative of *m* and *c* from the equation of the resulting straight line used to determine the Y value (Equation 2.8).

$$C_2 = \frac{C_1 \times V_1}{V_2} \qquad\qquad \textit{Equation 2.7}$$

$$Y = m \times C_2 + c \qquad\qquad \textit{Equation 2.8}$$

A fraction (F_1) was generated for each anisotropy value using the initial anisotropy value as 100% free ligand (A_0, Equation 2.9), this was converted to represent the fraction of ligand bound (F_2, Equation 2.10).

$$F_1 = \frac{A - Y}{Y - A_0} \qquad\qquad \textit{Equation 2.9}$$

$$F_2 = F_1 + 1 \qquad\qquad \textit{Equation 2.10}$$

Fraction F_2 was converted to represent a concentration of peptide bound ($[L]_{Bound}$), Equation 2.11. This value was plotted against protein concentration ($[P]$) and a curve fitted from the resulting data points using a one-site binding model (Equation 2.12, where B_{max} = maximum concentration of bound peptide).

$$[L]_{Bound} = F_2 \times [L]_{Total} \qquad\qquad \textit{Equation 2.11}$$

$$[L]_{Bound} = \frac{B_{max} \times [P]}{K_D + [P]} \qquad\qquad \textit{Equation 2.12}$$

2.3.9 Calculation of Error Values From Experimental Data

The error for n repeats were determined according to Equation 2.13, where z represents the value for standard deviation (σ) from the mean. A 68 % confidence limit arises from a value of $z = 1$, increasing to 95 % where $z = 2$.

$$\text{Error} = \frac{\sigma \times z}{\sqrt{n}} \qquad\qquad \textit{Equation 2.13}$$

The errors reported from the fluorescence anisotropy binding data are reported using a value of $z = 1$.

CHAPTER 3:

SYNTHESIS OF p53 PEPTIDES

& EXPRESSION OF RELATED

PROTEINS

3.1 Fundamental Principles of Peptide Synthesis

The biosynthesis of proteins and peptides occurs as a result of a chain of processes commencing with transcription, where in mammalian cells an *m*RNA template is formed from one strand of the DNA double helix. The *m*RNA then migrates to the ribosomes within the cytoplasm of the cell where *t*RNA containing amino acids complementary to the *m*RNA result in the formation of peptide bonds between the adjacent amino acids and the production of a protein. The chemical synthesis of peptides involves a repetitive sequence of reactions undertaken to ensure optimum yield and purity. Unlike the biosynthetic pathway additional care must be taken during peptide bond formation to ensure that bonds are formed between the desirable functional groups, since during biosynthesis reactions are mediated by enzymes which co-ordinate the geometry of the molecules ensuring the formation of the correct bonds. The challenge for the development of synthetic peptides is to ensure the correct reactions are permitted, whilst the amino acid side-chains remain unadulterated throughout the duration of the synthesis. This is achieved by the extensive use of protecting groups to shield specific functional groups from undesirable reactions, in addition to the immobilisation of the peptide chain upon a solid support. By immobilising the peptide upon a *resin*, it is possible to carry out many reactions in one chamber by the sequential washing and filtration of this peptide-bound solid support to remove traces of the previous reactants.

Merrifield first introduced the concept of solid phase peptide synthesis (SPPS) in

1963, with the publication of the synthesis of a tetrapeptide.[155] The basic principle of

SPPS involves the covalent attachment of the *C*-terminus of the first amino acid to a

solid support, essentially a porous bead. The *N*-terminus of this amino acid is also

covalently attached to a protecting group, which then undergoes a deprotection

reaction with a weak base such as piperidine to yield a free amine terminus prior to

the addition of another *N*-terminally protected amino acid. A coupling reaction then

takes place to facilitate peptide bond formation (Scheme 3.1). This process is repeated

using the required amino acids until the desired peptide length is achieved, at which

point the peptide then undergoes a final deprotection and cleavage from the solid

support.
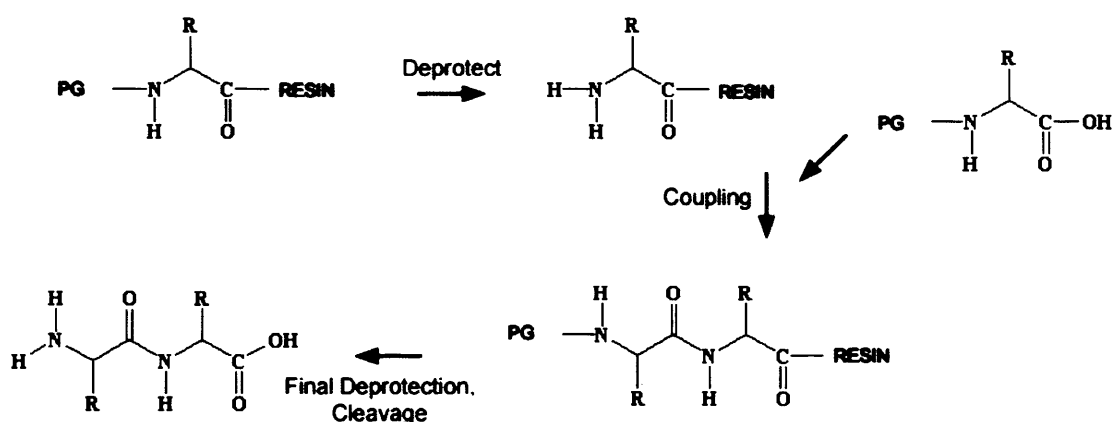
Scheme 3.1: *A solid phase peptide synthesis coupling and deprotection cycle leading to a single peptide bond between two amino acids.*

Some amino acid side-chains have the potential to undergo reactions in place of the

functional groups of the amino acid backbone, for example the carboxyl side-chain of

aspartic acid or the amino side-chain of lysine. These side reactions result in reduced

yields due to increased levels of impurities, so in order to prevent the occurrence of

these impurities additional protecting groups are used in order to prevent the reaction

of free carboxyl groups (t-Butyl protection) and amine side chains (Fmoc and Boc) (Figure 3.1).
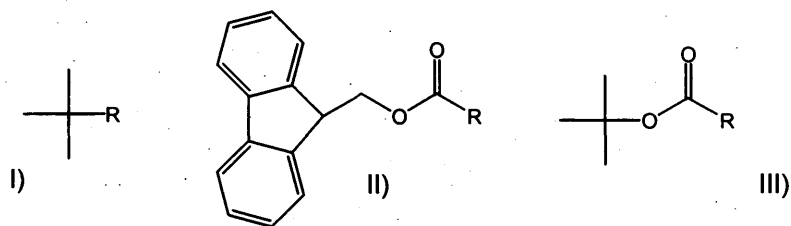
Figure 3.1: *Commonly used protecting groups I) t-Butyl (t-Bu), II) 9-Fluorenylmethoxycarbonyl (Fmoc) and III) t-Butyloxycarbonyl (Boc).*

It is essential that these side-chain protecting groups are unreactive under the basic conditions used to remove the backbone *N*-terminal protecting group so as to remain bonded to the side-chains throughout the repeated deprotection reactions that precede each additional coupling reaction. However, the side-chain protecting groups must also be able to be cleanly removed upon the cleavage of the peptide from its solid support for which a strong acid such as trifluoroacetic acid is conventially used. Upon cleavage, peptides are typically precipitated into cold ether where the precipitate is collected for purification by reversed-phase HPLC using a water and acetonitrile gradient (0-100 % ACN, 60 min). Fractions collected corresponding to peaks on the HPLC chromatogram are subjected to matrix-assisted laser desorption ionisation time of flight (MALDI-TOF) mass spectrometry in order to verify the existence of the correct mass corresponding to the amino acid sequence of the desired peptide.

3.2 Design and Synthesis of p53 Based Peptides

3.2.1 Design and Synthesis of Wild-Type p53 Peptides

The highly conserved Box I region of p53 contains the critical amino acids required to facilitate binding to Hdm-2 (Chapter 1, Section 1.5). Within this region a 15 amino acid sequence has been identified previously as a suitable starting point for the investigation into the functionality of the Hdm-2 binding α-helix of p53.[68] By means of a control and also in order to validate the p53-Hdm-2 binding assay, a 15 amino acid peptide based on p53 *N*-terminal residues 15-29 was synthesised incorporating a fluorophore, 5,6-carboxyfluorescein (FAM). All peptides in this chapter were synthesised on an Fmoc-amide resin, resulting in an amidated *C*-terminus and they were labelled with FAM at the *N*-terminus. These were then purified by reversed phase HPLC, and the desired product identified by MALDI-TOF mass spectrometry. The synthesised wild-type (WT), truncated wild-type (twt) and alanine substituted (P27A) mutant peptides are summarised in Table 3.1.

Table 3.1: *Summary of FAM labelled synthesised p53 derived peptides.*

Peptide	Sequence	Calculated	Actual	% Yield	mg
p53_WT	SQETFSDLWKLLPEN	2164.0	2165.5	3.7	8.0
p53_twt	ETFSDLWKLL	1608.4	1608.7	2.5	4.0
p53_P27A	SQETFSDLWKLLAEN	2138.0	2138.2	4.1	8.8

The 15 amino acid p53_WT peptide is an appropriate length for use as a template for the design and optimisation of an *i,i*+7 and *i,i*+11 crosslinked peptide. As discussed further in chapter 5.1 it has been reported from the crystal structure that the *N*-terminal amino acids of p53 are in an extended conformation which is proposed to enhance helix destabilisation reducing the strength of the p53-Hdm-2 binding interaction due to increased entropy.[68] The work of Schon and co-workers resulted in the identification of a peptide sequence ten amino acids in length corresponding to p53 residues 17-26 in which the K_D was improved by one order of magnitude when compared to the 15 amino acid wild-type peptide.[70] This peptide is a good length for investigating the design of an *i,i*+4 crosslinked p53-based peptide since a peptide of this length, with the crosslinker in an *i,i*+4 conformation is expected to be more stable due to the reduced number of residues in the sequence not within the constraint of the *i,i*+4 cysteine spacing thus reducing entropy. The synthesis of the truncated ten amino acid p53-wild type peptide, p53_twt, described by Schon *et al.* was repeated using an Fmoc amide resin and labelled a the *N*-terminus with FAM (Table 3.1).[70]

The presence of a proline residue at position 27 of the p53 *N*-terminus facilitates the extended conformation proposed to reduce the affinity of p53 for Hdm-2.[68] This is due to the poor helical propensity of proline (Chapter 1.8 Table 1.1) and to resolve this it was decided to substitute this for an alanine residue (P27A mutant) due to its high helical stabilisation and the minimally invasive nature of the methyl side-chain with respect to the Hdm-2 hydrophobic cleft.

3.2.2 Design and Synthesis of Cysteine Containing Modified p53 Peptides for the Attachment of the Azobenzene Crosslinker

When modifying the peptide sequences in order to accommodate the cysteine residues for the attachment of the azobenzene crosslinker, the most appropriate spacings must be considered based upon the desired peptide conformation with respect to each isomer of the crosslinker. In order to favour an α-helical conformation when applied to the azobenzene crosslinker in the light induced conformation, the end-to-end distance between the chloroacetamide groups (11.3 Å, Scheme 3.1) is stabilised by the positioning of the cysteine residues in both an *i,i*+4 and *i,i*+7 spacing. The increased distance between the crosslinker chloroacetamide groups when in the dark-adapted, *trans* isomer (16.8 Å, Scheme 1.1) permits the promotion of an α-helical conformation when attached by cysteine residues in an *i,i*+11 spacing.
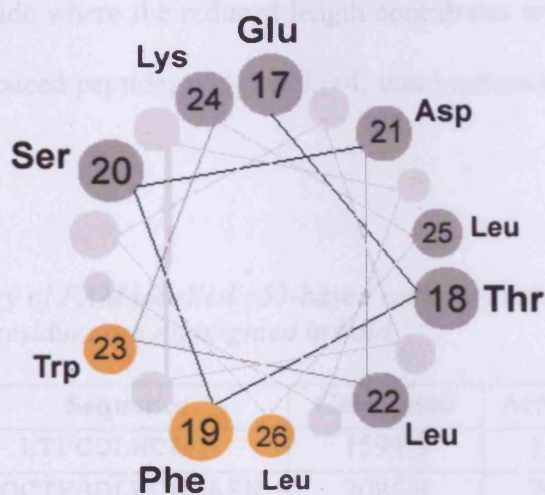
Figure 3.2: *Helical wheel representation of the ten amino acid peptide p53_twt, the residues critical for Hdm-2 binding are shown in orange. Structure numbered according to p53 sequence homology.*

The design of a light-stabilised α-helical p53-based peptide where the azobenzene crosslinker is attached by the incorporation of cysteine residues in an *i,i*+4 spacing is better suited to a shorter length peptide as previously discussed in this section. Consequently, a modified derivative of the peptide p53_twt was evaluated and a helical wheel projection of p53_twt is depicted in Figure 3.2 with the critical residues for Hdm-2 binding (Phe19, Trp23 and Leu26) highlighted in orange. It can be seen that they are concentrated around the same hydrophobic face of the p53 α-helix.

The most appropriate residues to substitute for cysteines in order to allow for the attachment of the crosslinker are Ser20 and Lys24, since other possible locations involve the substitution of Asp21. The deprotonated side-chain carboxyl group of Asp21 acts as a hydrogen bond acceptor from the side-chain hydroxyl of Thr18, this is a helix-stabilising hydrogen bond and therefore needs to be retained, especially in an already shortened peptide where the reduced length contributes to α-helix instability. As a result, the *i,i*+4 spaced peptide, p53_twt_*i,i*+4, was synthesised and is shown in Table 3.2.

Table 3.2: *Summary of FAM labelled p53-based cysteine containing modified peptides. Cysteine residues are highlighted in bold.*

Peptide	Sequence	Calculated	Actual m/z	% Yield
p53_*i,i*+4	ETF**C**DLW**C**LL	1599.5	1599.8	2.5
p53_P27A_*i,i*+7	SQ**C**TFSDLW**C**LLAEN	2086.9	2087.9	3.2
P53_P27A_*i,i*+11	SQ**C**TFSDLWKLLA**C**N	2086.0	2085.3	3.0
P53_D21E_*i,i*+7	SQ**C**TFSELW**C**LLAEN	2101.0	2101.2	2.8
P53_D21E_*i,i*+11	SQ**C**TFSELWKLLA**C**N	2100.0	2099.0	2.2

The incorporation of cysteine residues in an *i,i*+7 spacing also has the potential to stabilise a helical structure when the crosslinker is in the *cis*, light induced state. However, unlike the *i,i*+4 spacing it is proposed that this provides additional stabilisation for a longer peptide chain, due to an increased number of residues constrained between the cysteines. For this reason the 15 amino acid peptide is better suited to an *i,i*+7 spacing for cysteines as opposed to the *i,i*+4 distribution employed for the truncated ten amino acid peptide.

The helical wheel projection for the peptide p53_P27A is shown in Figure 3.3. There are three possibilities for the incorporation of cysteine residues in an *i,i*+7 spacing where the crosslinker remains on the opposing face of the α-helix to the residues critical to Hdm-2 binding, therefore being oriented away from the hydrophobic binding cleft of Hdm-2 to minimise any disruption its presence may cause to the p53-Hdm-2 interaction. Ideally the substitution of Asp21 and Glu28 for cysteines would position the crosslinker exactly opposite the site of the p53-Hdm-2 binding interaction, however as mentioned (Chapter 1.5) Asp21 provides additional stability to the p53 α-helix by the formation of hydrogen bonds involving the Asp21 side-chain carboxyl group and Thr18. It was also noted that this configuration does not contain Phe19 between the cysteine residues and therefore the influence of this residue, already noted to be highly important for helix formation, may not be directly under the control of the crosslinker. The second possible location for the positioning of the cysteine residues in an *i,i*+7 spacing involves the substitution of Thr18 and Leu25. However this is not favoured due to the interaction between Thr18 and Asp21, which as previously mentioned provides an additional hydrogen bond, enhancing the stability of the p53 α-helix.
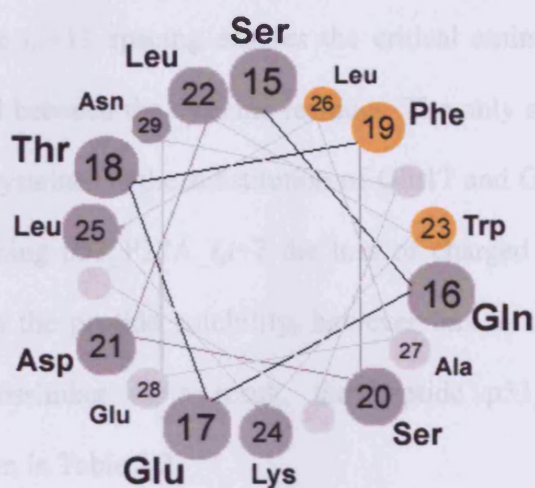
Figure 3.3: *Helical wheel representation of the 15 amino acid peptide p53_P27A, the residues critical for Hdm-2 binding are shown in orange. Structure numbered according to p53 sequence homology.*

The final possible location for the substitution of p53 residues for cysteines without encroaching upon the hydrophobic face of the p53 α-helix is Glu17 and Lys24. This does not interfere with any additional hydrogen bonds, although Lys24 has been implicated in salt bridge formation due to its proximity to complementary residues, although this has not been proven to contribute to p53 helix formation. The loss of a charged amino acid (Glu17) may reduce the solubility of the peptide, however attachment of the azobenzene crosslinker modified by Woolley *et al.* to enhance its water solubility by the addition of sulphonate groups to the *meta* position on the aromatic rings is proposed to offset the charge loss from the substitution of Glu17 for cysteine.[142] The sequence of the resulting peptide p53_P27A_*i,i*+7 is documented in Table 3.2.

This same principle was applied to the design of a peptide incorporating an *i,i*+11 spacing for cysteines in which a crosslinked version of the peptide would be encouraged to adopt a helical conformation when the crosslinker is in the relaxed,

dark adapted state. The *i,i*+11 spacing enables the critical amino acids for Hdm-2 binding to be contained between the cysteine residues. The only suitable location for the positioning of the cysteines is the substitution of Glu17 and Glu28. As discussed previously when designing p53_P27A_*i,i*+7 the loss of charged amino acids has a detrimental effect upon the peptide solubility, however this is counteracted by the attachment of the crosslinker as a result, the peptide p53_P27A_*i,i*+11 was synthesised and is shown in Table 3.2.

The benefit of having the crosslinker attached and in a conformation that would promote α-helix formation is believed to out-weigh the helix stabilising contribution of this hydrogen bond if it were eliminated, whilst its removal would also encourage the crosslinker-mediated disruption of the helical structure. Chapter 1.8, Table 1.1 highlights the observation that amino acids in which the side-chains are only one carbon atom in length prior to the functional group have a lesser ability to stabilise an α-helical conformation that those with two carbon atoms, most likely due to the close proximity of the side-chains to the backbone of the α-helix and their repulsive and steric effects upon one another when encouraged to be packed this tightly. Using this information, it was proposed that the modification of Asp21 for Glu and therefore the elimination of the side-chain hydrogen bond with Thr18 would improve the overall helix-forming ability of the peptide, whilst having no change to the relative quantity of charged and uncharged amino acids and thus no detrimental effect upon the solubility of the peptide.

As discussed previously we proposed that the modification of Asp21 to Glu, although enhancing the promotion of an α-helical conformation, will also disrupt the formation

of the hydrogen bond between p53 residue 21 and Thr18. Although ultimately this modification will decrease the overall helix-forming ability of the peptide through the loss of a potential stabilising interaction, it is proposed to enhance the degree of control exercised by the crosslinker. To test this hypothesis, two peptides were synthesised which were identical to p53_P27A_*i,i*+7 and p53_P27A_*i,i*+11 with the exception of Asp21 which was substituted with Glu (Table 3.2).

3.2.3 Design and Synthesis of Cysteine Containing Hdm-2 Binding Peptides Based Upon a Polyalanine Scaffold

Polyalanine forms a stable α-helix in water.[156] As previously shown (Chapter 1.8 Table 1.1), alanine has the highest helical propensity out of all the natural amino acids, hence its selection as a suitable residue for the substitution of Pro27 in the optimisation of the p53-based peptides. We decided to investigate the possibility of designing a Hdm-2 binding α-helical peptide based on a polyalanine scaffold by the incorporation of key residues critical for the p53-Hdm-2 interaction. In order to regulate the interaction between Hdm-2 and the polyalanine based peptide scaffolds it was also decided to incorporate the cysteine residues to enable the attachment of the azobenzene crosslinker.

Table 3.3: *Summary of the FAM labelled cysteine containing Hdm-2 binding peptides based on a polyalanine scaffold. Cysteine residues are highlighted in bold.*

Peptide	Sequence	Calculated	Actual m/z	% Yield
p53_Ala_*i,i*+7	EACTFADAWCALAAR	1955.8	1953.8	1.6
p53_Ala_*i,i*+11	EACTFADAWAALACR	1955.8	1954.4	1.9

Two peptides were synthesised incorporating cysteine residues in both an $i,i+7$ and

$i,i+11$ spacing (Table 3.3). These peptides were 15 amino acids in length and it was

decided to substitute all residues except for those essential for the p53-Hdm-2 binding

interaction or that provide additional helix stabilising contributions. The three amino

acids directly involved in the p53-Hdm-2 interaction, Phe19, Trp23 and Leu26 were

retained, as were Thr18 and Asp21. In order to reduce the helix dipole a positively

charged Arg residue was situated at the C-terminus of the peptide, and negatively

charged Glu residue at the N-terminus. It was noted when preparing the crude peptide

for purification that a reduction in the number of charged amino acids had a

significant effect upon the solubility of these peptides.

3.3 Synthesis of the Azobenzene Crosslinker and Attachment to Peptides

The water-soluble azobenzene crosslinker described by Zhang *et al.* was synthesised according to the published method for the synthesis (Scheme 3.2).[142]
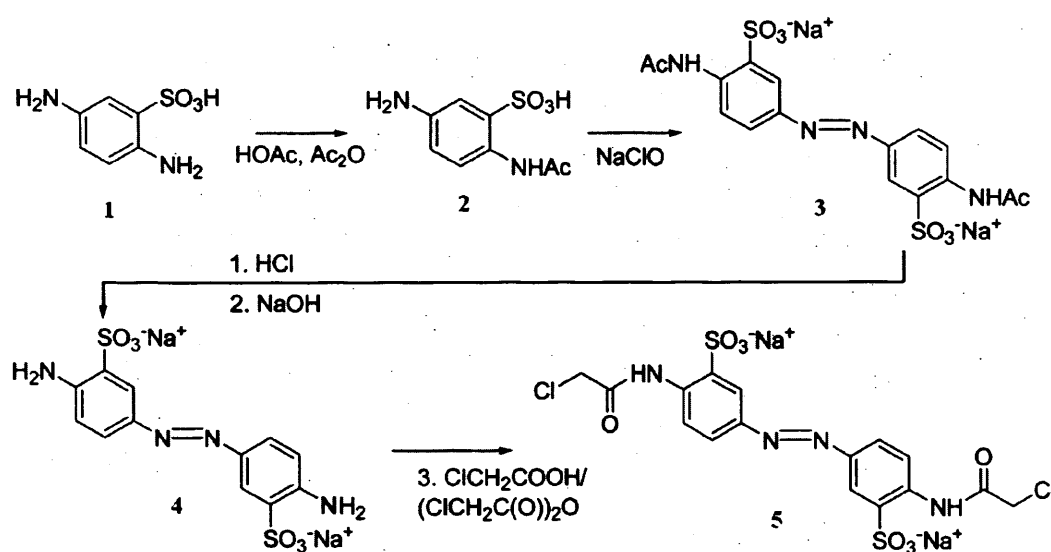
Scheme 3.2 – *Schematic representation of the key stages involved in the synthesis of the azobenzene crosslinker 3,3'-Bis(sulfo)-4,4'-bis(chloroacetamido)azobenzene.*[142]

The methodology employed to attach the crosslinker to the cysteine-containing peptides was taken from the work of Guerrero *et al.*[145] The mechanism by which the crosslinker attaches to the side-chains of the cysteine residues is thought to be a bimolecular nucleophilic substitution reaction mediated by the loss of the chlorine atoms from the terminal chloroacetamido groups of the crosslinker. It was noted that as proposed in Section 3.2 the water-solubility of the peptides upon the addition of the azobenzene crosslinker was improved, particularly in the peptides where the

optimisation for Hdm-2 binding and allocation of space for the cysteine residues had

resulted in the removal of charged amino acids. As described for the crude peptide

precipitate in Chapter 3.2, the crosslinked peptides were purified by reversed-phase

HPLC using a water-acetonitrile gradient (crosslinked peptide observed at both 210

nm and 360 nm), and each fraction verified by MALDI-TOF mass spectrometry

(Table 3.4). The crosslinked peptide was then isolated by lyophilisation of the

appropriate fraction.

Table 3.4 – *Summary of crosslinked p53-based cysteine containing modified peptides. Cysteine residues are highlighted in bold.*

Peptide	Sequence	Calculated	Actual m/z
p53_i,i+4_XL	ETF**C**DLW**C**LL	2051.4	2051.9
P53_P27A_i,i+7_XL	S**C**TFSDLW**C**LLPEN	2561.5	2560.4
p53_P27A_i,i+11_XL	S**C**TFSDLWKLLP**C**N	2537.5	2538.3
p53_D21E_i,i+7_XL	S**C**TFSELW**C**LLPEN	2552.5	2549.2
p53_D21E_i,i+11_XL	S**C**TFSELWKLLP**C**N	2551.5	2550.8

3.4 Expression and Purification of Hdm-2

The cDNA clone corresponding to the human equivalent of Mdm-2 (Hdm-2) residues

1-188 was provided by Professor Sir D. P. Lane, Dundee University, as a pGEX-2T

expression vector, cloned within the *BamH1* and *EcoR1* multiple cloning site (Figure

3.4).[72] Initial attempts to purify Hdm-2$_{1-188}$ as a GST fusion protein were unsuccessful

at the stage involving the cleavage of the GST from Hdm-2$_{1-188}$ using thrombin

protease. Upon incubation of the thrombin with GST-Hdm-2$_{1-188}$ SDS-PAGE

indicated the presence of a protein with a mass comparable to GST, however there

was only a faint indication of the presence of cleaved Hdm-2. It is proposed that upon

cleavage, the Hdm-2$_{1-188}$ forms aggregates resulting in its precipitation from solution.

Indeed previous research detailing the interaction of p53 with Hdm-2 residues 1-188

utilised predominantly the uncleaved protein GST-Hdm-2$_{1-188}$.[74,157]
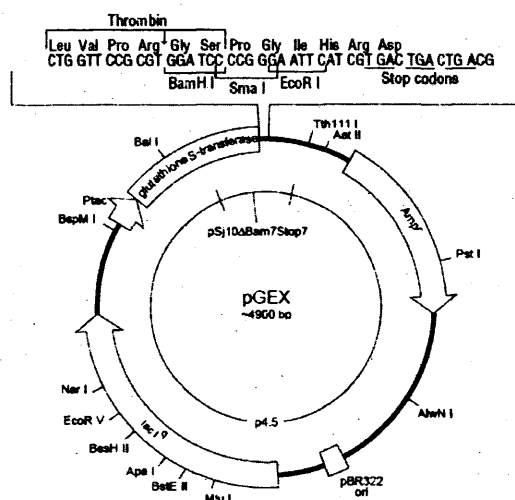
Figure 3.4: *The pGEX-2T expression vector, Hdm-2 1-188 was inserted between BamH1 and EcoR1 within the multiple cloning site.*[72]

Table 3.5 *– Primer sequences for the mutation of Hdm-2$_{1-188}$ residues 126-127 giving rise to Hdm-2$_{1-125}$.*

Primer	Oligonucleotide
Hdm-2$_{1-188}$ Wild-Type	5'-CTGTGAGTGAGAAC**AGGTGT**CA CCTTGAAGGTGGG-3'
Hdm-2$_{1-125}$ Fwd	5'-CTGTGAGTGAGAAC**TGATGA**CA CCTTGAAGGTGGG-3'
Hdm-2$_{1-125}$ Rev	5'-CCCACCTTCAAGGTG**TCATCA**G TTCTCACTCACAG-3'

```
MCNTNMSVPTDGAVTTSQIPASEQETLVRPKPLLLKLLKSVGAQKDTYT

MKEVLFYLGQYIMTKRLYDEKQQHIVYCSNDLLGDLFGVPSFSVKEHRK

IYTMIYRNLVVVNQQESSDSGTSVSEN
```

Figure 3.5: *The amino acid sequence for Hdm-2 residues 1-125 resulting from the mutation of Hdm-2$_{1-188}$ by the insertion of a double stop codon.*[70]

The work of Lane *et al.* and Fersht and co-workers involved the use of shorter GST-Hdm-2 residues 2-125 which was successfully cleaved to give a stable protein.[70,73] This initiative was followed to produce a cDNA clone corresponding to GST-Hdm-2 residues 1-125 by site-directed mutagenesis involving the modification of the initial cDNA sequence of GST-Hdm-2$_{1-188}$ at positions 126 and 127 to contain a double-stop codon (Figure 3.5).
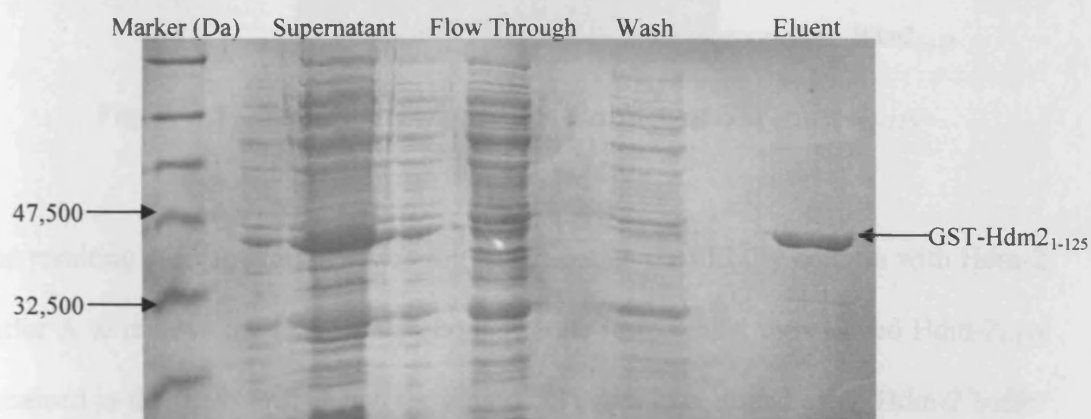
Figure 3.6 – *SDS-PAGE of affinity column fractions from step 1 of Hdm-2$_{1-125}$ purification. GST-Hdm-2$_{1-125}$ is present in the eluent.*

Once confirmed by DNA sequencing, the resulting protein Hdm-2$_{1-125}$ was expressed and successfully cleaved and purified as described by Schon *et al*. The supernatant solution from the crude cell lysate was applied to a glutathione sepharose 4B affinity column pre-equilibrated with Hdm-2 buffer A, and was washed with approximately 6 column volumes of the same buffer before eluting the GST-Hdm-2$_{1-125}$ from the column with Hdm-2 Buffer B (Figure 3.6). The affinity column eluents were combined and concentrated before incubating at 30 °C overnight in the presence of thrombin protease, (Figure 3.7).
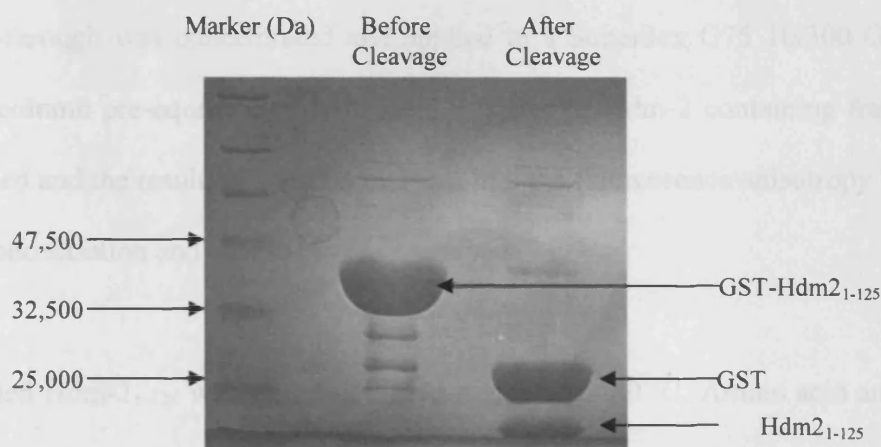
Figure 3.7 – *SDS-PAGE of thrombin cleavage of GST-Hdm-2$_{1-125}$.*

The resulting cleavage mixture was run back through the affinity column with Hdm-2 buffer A to remove the GST, which bound to the resin whilst the cleaved Hdm-2$_{1-125}$ remained in the flow-through and the bound GST was later eluted using Hdm-2 buffer B (Figure 3.8). Any residual GST remaining in the Hdm-2 solution was later removed by gel filtration chromatography.
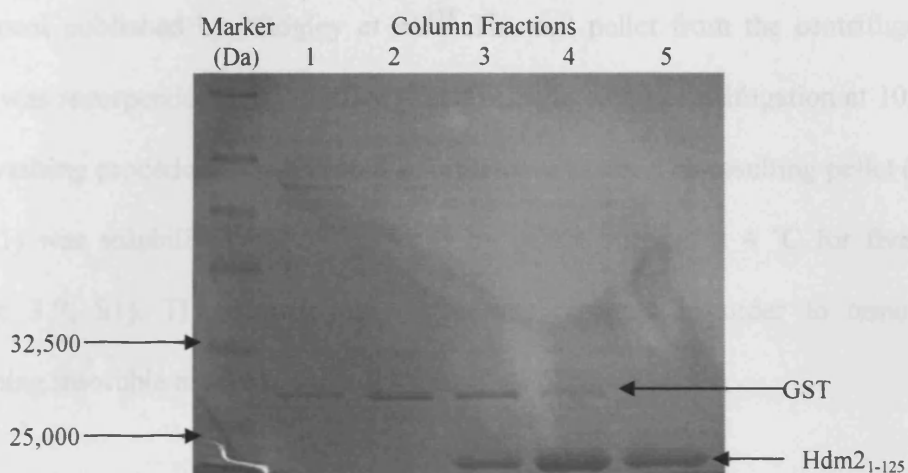
Figure 3.8 – *SDS-PAGE detailing the separation of Hdm-2$_{1-125}$ from residual GST by gel filtration chromatography.*

The flow-through was concentrated and applied to a Superdex G75 10/300 GL gel filtration column pre-equilibrated with Hdm-2 buffer A. Hdm-2 containing fractions were pooled and the resulting solution dialysed into the fluorescence anisotropy buffer prior to concentration and quantitative UV analysis.

The purified Hdm-2$_{1-125}$ was stored in 200 µl aliquots at –80 °C. Amino acid analysis of the cleaved and purified protein enabled the calculation of the molar extinction coefficient for Hdm-2$_{1-125}$, reported as 54,055 M^{-1} cm^{-1} (± 1809, see Appendix A2 for data) and provided the means to calculate the concentration of Hdm-2$_{1-125}$ in solution.

3.5 Expression and Purification of Human p53

Professor Sir D. P. Lane, Dundee University, also provided the cDNA clone corresponding to full-length human p53. The purification was undertaken according to

a protocol published by Midgley *et al.*[158] The cell pellet from the centrifuged cell lysate was resuspended in p53 buffer A and re-pelleted by centrifugation at 10,000 g. This washing procedure was repeated a further two times. The resulting pellet (Figure 3.9, P1) was solubilised in p53 buffer B by gentle stirring at 4 °C for five hours (Figure 3.9, S1). The centrifugation step was repeated in order to remove the remaining insoluble matter (Figure 3.9, P2)
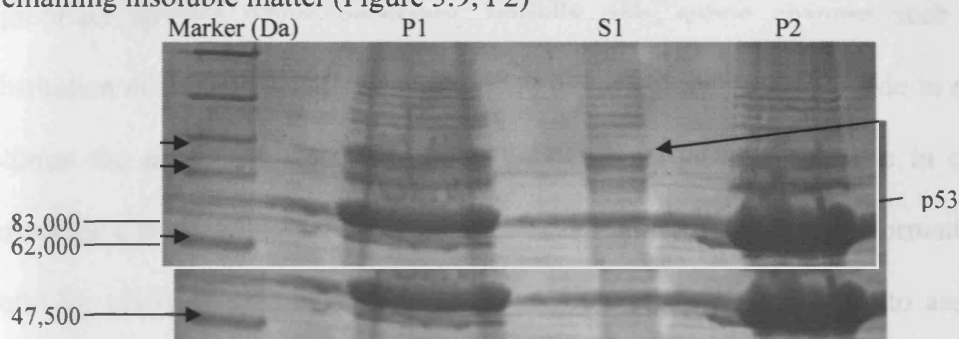
Figure 3.9 – *SDS-PAGE detailing the initial purification steps for p53.*
P = Pelleted Lysate, S1 = Solubilised pellet, P2 = Insoluble Matter

The supernatant solution was diluted in order to give a final buffer concentration equivalent to p53 buffer C. This solution was stirred for a further 18 hours at 4 °C (to aid protein refolding), dialysed against p53 buffer D and then centrifuged at 10,000 g to remove any insoluble matter. The resulting supernatant was applied to a DEAE ion exchange column where pure p53 was eluted using an NaCl gradient (0.15 M to 0.5 M) using p53 buffers E and F.

It was noted that the p53 protein was obtained in a low yield as estimated from the intensity of the band observed by SDS-PAGE, however no attempts were made to optimise this further since a sufficient quantity of the p53 protein was obtained for the initial assays.

3.6 Conclusion

Peptides have been designed taking into consideration the requirements for both p53-Hdm-2 binding and also the attachment of the azobenzene crosslinker in the appropriate spacing where necessary. Initially only subtle changes such as the substitution of Pro27 for Ala and the truncation of the peptide were made in order to optimise the natural p53 peptide amino acid sequence. This was done in order to provide data to use as a benchmark for comparative purposes. This information was useful for planning subsequent modifications of the p53 peptides and to assess the influence of the attached azobenzene crosslinker with respect to not only the relative spacing between cysteine residues but also where modifications have been undertaken to the p53 peptide such as the substitution of Asp21 for Glu, that are predicted to enhance the changes in the degree of control over the peptide helicity exhibited by the azobenzene crosslinker.

A reliable method for the expression and purification of Hdm-2 residues 1-125 has been employed based on the work of Schon *et al.*[70] This protein was produced as a consequence of problems encountered with the purification of the initial 188 amino acid protein upon cleavage from GST with thrombin. Once the purification of Hdm-2$_{1-125}$ was refined, amino acid analysis enabled the determination of the molar extinction coefficient allowing for the accurate quantification of Hdm-2 residues 1-125 in solution. This is a critical requirement in the design of an accurate, repeatable binding assay to enable the measurement of the p53-Hdm-2 interaction. The

acquisition of purified p53 enables some exploratory binding assays to be conducted

which can be used to compare the binding behaviour of some p53-based peptides with

Hdm-2$_{1-125}$ in both the presence and absence of its complementary binding protein.

CHAPTER 4:

EVALUATION OF PEPTIDE

SECONDARY STRUCTURE

4.1 Use of Circular Dichroism to Probe Peptide Secondary Structure

Chiral molecules such as amino acids and sugars interact with circularly polarised light. The extent of this interaction depends on both the direction of rotation of the polarised light and the conformation of the chiral molecule. Circular dichroism spectroscopy exposes a sample to equal amounts of left and right circularly polarised light and, depending upon the chirality of the molecules present, one of the two types of polarised light is absorbed more than the other. When the remaining unabsorbed left and right circularly polarised light are combined, the result is no longer an oscillation along a straight line but along an ellipsoid path, the direction of rotation of which depends upon which circularly polarised component retains the greatest intensity upon emerging from the sample cell, *i.e.* the component that is absorbed the least. This yields a value for the degree of ellipticity (θ), Figure 4.1.
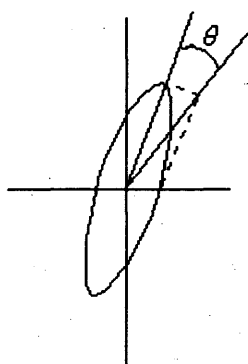
Figure 4.1: *The angle of ellipticity (θ) arises from the preferential absorption of left or right circularly polarised light.*

CD spectroscopy can be used to determine the secondary structure of proteins and peptides by observing the CD signal in the far UV region (190-250 nm), where the chromophore of interest is the peptide bond. The CD signal, hence the degree of ellipticity is dependent upon the rotation of the Phi (φ) and Psi (ψ) dihedral angles along the amino acid chain backbone (Figure 4.2).
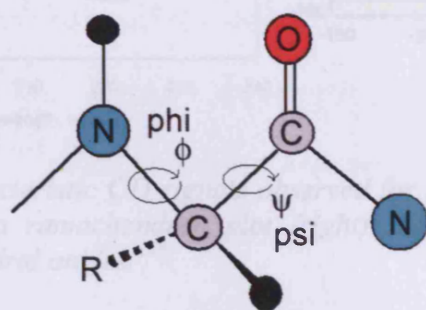
Figure 4.2: *The phi (φ) and psi (ψ) dihedral angles of an amino acid are found between the α-carbon atom and the amino nitrogen and carbonyl carbon atoms respectively.*

Secondary structure motifs exhibit specific patterns of ellipticity with respect to wavelength, and hence α-helices, β-sheets and random coil conformations give characteristic shapes and magnitudes of CD spectra (Figure 4.3), the α-helix for example exhibits a positive value for ellipticity at 192 nm, and negative at 209 nm and 222 nm. The CD signal given by a molecule reflects an average of the entire molecular population, so whilst CD spectroscopy enables the overall percentage composition of a specific structural motif to be determined, it is unable to assign the role of specific residues with respect to the conformations within the observed structure.
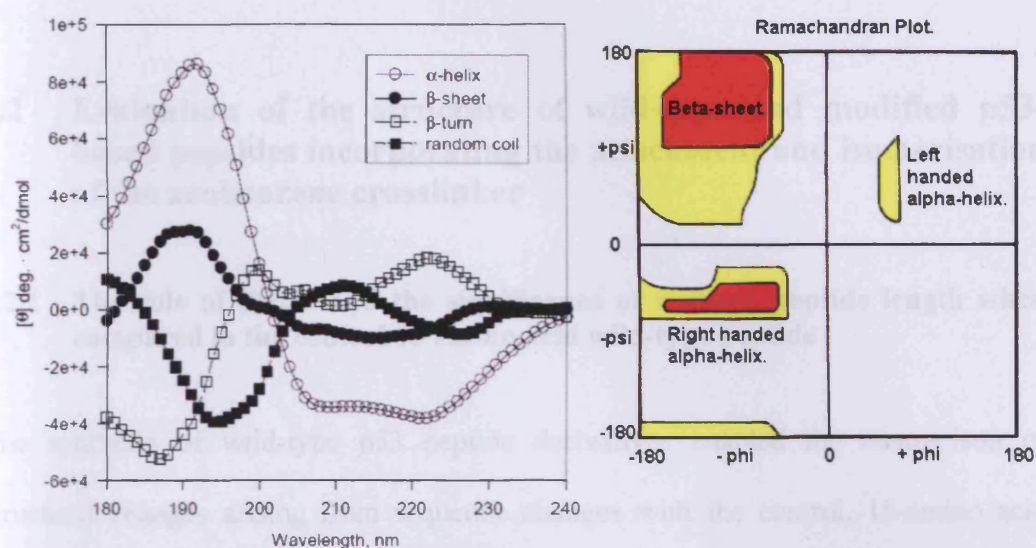
Figure 4.3: *Characteristic CD signals observed for secondary structural motifs (left) and a ramachandran plot (right) showing corresponding differences in dihedral angles.*[159]

As described previously in chapter 1.5 the p53 *N*-terminal transactivation domain has a random coil conformation when in the un-bound state and upon binding to Hdm-2 adopts an α-helical conformation. It is proposed that the transition from random coil to α-helix is dependent firstly upon the interaction of key residues of p53 such as Phe19, Trp23 and Leu26 with residues within the hydrophobic binding site of Hdm-2.[68] This is preceded by intra-molecular hydrogen bonding interactions within p53, where the proximity of the critical p53 residues facilitates the adoption of an α-helical structure to reduce steric constraints between residues.

The proposed crosslinking of p53 peptides is designed to control the proximity of key residues of p53 so as to make adoption of an α-helical conformation sterically and energetically favourable upon photo-isomerisation of the crosslinker when covalently attached to the peptide with the appropriate spacing.[142]

4.2 Evaluation of the structure of wild-type and modified p53-based peptides incorporating the attachment and isomerisation of the azobenzene crosslinker

4.2.1 The role of Pro27 and the significance of reduced peptide length when compared to the control 15 amino acid wild-type peptide

The synthesis of wild-type p53 peptide derivatives enabled the comparison of structural changes arising from sequence changes with the control, 15-amino acid wild-type peptide (p53_WT). This further allows changes in the structure and stability of the peptide to be attributed to progressive changes to the peptide sequence, be it the substitution of residues for cysteines, or the attachment of the azobenzene crosslinker and subsequent isomerism between the *cis* and *trans* isomers.

The CD signals at 197 nm, 209 nm and 222 nm corresponding to an α-helical structure will become more pronounced with increasing helicity and it can be seen from Figure 4.4 that the wild-type peptide p53_WT exhibits a predominantly random coil structure with only 9.5 % (± 1) α-helical content (calculated using equation 2.2). The substitution of Pro27 for Ala can be seen to increase peptide helicity with the mean residue ellipticity at 222 nm ($[\Theta]_{r\,222}$) increasing from -2705 deg cm^2 dmol^{-1} to -13030 deg cm^2 dmol^{-1} equating to a structure with 45.6 % helicity (± 0.9 %) relative to p53_WT. This supports the rationale for the substitution of the proline residue at position 27 within the p53 peptide sequence, whereby the proline was considered to contribute to the disruption of the formation of the p53 α-helix due to its poor helical propensity as outlined in chapter 1.8, Table 1.1.
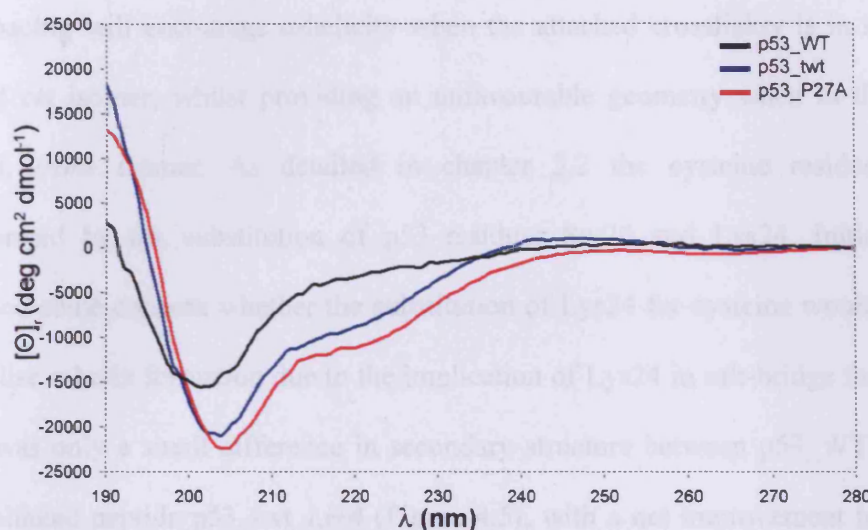
Figure 4.4: *CD MRE spectra of p53_WT, p53_twt and p53_P27A. For conditions see Section 2.3.2.*

The deletion of the *C* and *N*-terminal amino acids to yield the ten amino acid truncated peptide p53_twt results in a structure with greater α-helicity than p53_WT (33.9 % ± 1.1) but less helicity than p53_P27A (Table 4.1). The loss in α-helicity of p53_twt when compared to p53_P27A is proposed to be due to the reduction in peptide chain length, decreasing the number of supporting helix promoting residues (in addition to the loss of Pro27) and therefore the reduction in the helix stabilising backbone hydrogen bonding network.

4.2.2 A light stabilised short p53-based peptide designed to promote α-helix formation by the attachment of the azobenzene crosslinker in an i,i+4 spacing

When designing the peptide incorporating cysteine residues in an *i,i*+4 spacing we decided to use the ten amino acid truncated wild-type peptide (p53_twt) due to there being fewer residues outside the constraint of the proposed site for the azobenzene crosslinker. When crosslinked, we proposed that peptides with cysteine residues in an

i,i+4 spacing will encourage α-helicity when the attached crosslinker is in the light induced *cis* isomer, whilst providing an unfavourable geometry when in the dark-adapted, *trans* isomer. As detailed in chapter 3.2 the cysteine residues were incorporated by the substitution of p53 residues Ser20 and Lys24. Initially this generated some concern whether the substitution of Lys24 for cysteine would further destabilise α-helix formation due to the implication of Lys24 in salt-bridge formation. There was only a small difference in secondary structure between p53_WT and the uncrosslinked peptide p53_twt_*i,i*+4 (Figure 4.5), with a net improvement in p53 α-helicity from 9.5 % (± 1.0) to 21.4 % (± 0.5) being observed. Comparing the CD data for the truncated peptide, p53_twt with p53_twt_*i,i*+4 demonstrates a reduction in α-helicity, with a reduced value of $[\Theta]_{r\ 190}$ and increased value of $[\Theta]_{r\ 222}$ from -7532.6 deg cm^2 dmol^{-1} (± 243.6) to -4753.1 deg cm^2 dmol^{-1} (± 121.4). This represents a reduction in α-helicity from 33.9 % (± 1.1) to 21.4 % (± 0.5) for p53_twt and p53_twt_*i,i*+4 respectively (relative to p53_WT).
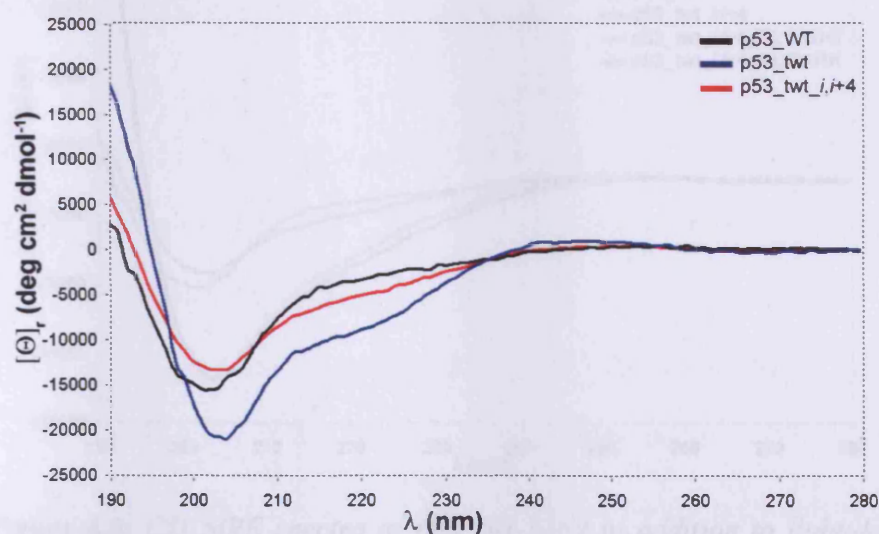
Figure 4.5: *CD MRE spectra of p53_WT, p53_twt and p53_twt_,i,i+4. For conditions see Section 2.3.2.*

This adds further evidence to the suggestion that Lys24 plays a part in stabilising an α-helical conformation besides its contribution *via* backbone hydrogen bonding. Chapter 1.8, Table 1.1 shows that aside from the issue of salt-bridge formation, lysine has a high helical propensity whereas its substitution for cysteine will reduce the relative stabilisation of the α-helical conformation. Upon crosslinking p53_twt_*i,i*+4, there is a significant increase in α-helicity when compared to the uncrosslinked peptide. However, when comparing the crosslinker in both the dark-adapted *trans* and light induced *cis* conformations, the difference in α-helicity was fairly insignificant with $[\Theta]_{r\,222}$ of -12236 deg cm^2 dmol^{-1} ($\pm$ 306.7) and -10708 deg cm^2 dmol^{-1} ($\pm$ 188.6) respectively (Figure 4.6). We have proposed that the steric constraints between the crosslinker and peptide and additionally between residues within the peptide itself may be unfavourable when the crosslinker attached in an *i,i*+4 spacing and in the *trans* conformation. As a result, the attached crosslinker may be forced to adopt a *cis* conformation, permitting the adoption of a more stable α-helical structure.
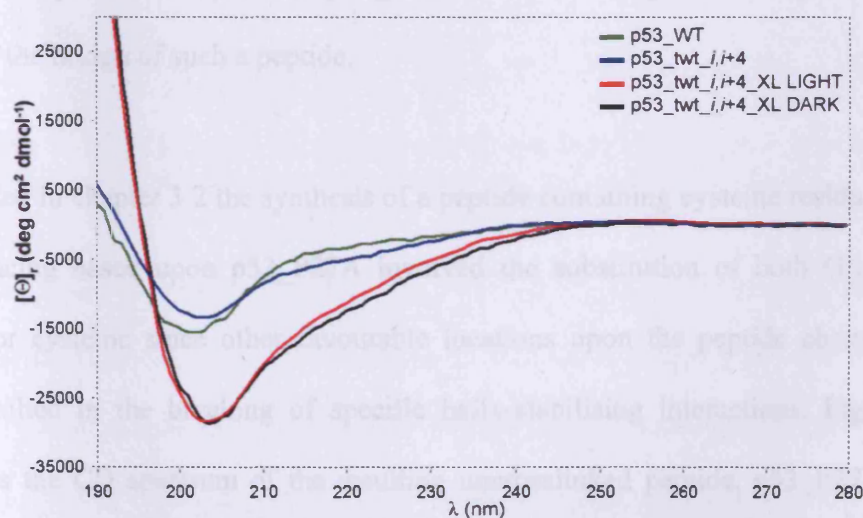
Figure 4.6: *CD MRE spectra of p53_twt_i,i+4 in addition to light/dark adapted p53_twt_i,i+4_XL and p53_WT. For conditions see Section 2.3.2.*

4.2.3 The design of α-helical light stabilised *i,i*+7 crosslinked peptides and sequence optimisation to enhance the destabilisation of the peptide α-helix upon relaxation of the crosslinker to the dark-adapted state

Like the peptides containing cysteine in an *i,i*+4 spacing, the attachment of the azobenzene crosslinker to a peptide containing cysteine residues in an *i,i*+7 spacing also favours an α-helical conformation when the crosslinker is in the *cis* isomer, with this conformation becoming unfavourable upon relaxation to the *trans* isomer. The larger spacing between the cysteine residues places more residues within the constraint of the attached crosslinker and therefore makes it favourable for a derivative of a 15 amino acid wild-type p53 peptide to be used for the basis of the design of a peptide for crosslinking where the cysteine residues are positioned in an *i,i*+7 spacing. As shown in Figure 4.4, the substitution of Pro27 for alanine in the wild-type p53 peptide p53_P27A increases the α-helicity of the resulting peptide by approximately 36 % compared to p53_WT. Therefore this provided a good starting point for the design of such a peptide.

As detailed in chapter 3.2 the synthesis of a peptide containing cysteine residues in an *i,i*+7 spacing based upon p53_P27A involved the substitution of both Glu17 and Lys24 for cysteine since other favourable locations upon the peptide chain would have resulted in the breaking of specific helix-stabilising interactions. Figure 4.7 illustrates the CD spectrum of the resulting uncrosslinked peptide, p53_P27A_*i,i*+7 overlaid against the spectra for p53_P27A and the uncrosslinked *i,i*+4 spaced peptide p53_twt_*i,i*+4. It can be seen from the spectra at $[\Theta]_{r\ 222}$ that the modification of the peptide to incorporate cysteine residues reduces the helicity of the free peptide when

compared to the wild-type P27A peptide, with values of -7583.8 deg cm^2 dmol^{-1} ($\pm$ 208.7) and -4753.1 deg cm^2 dmol^{-1} ($\pm$ 121.4) respectively corresponding to the percentage α-helix content decreasing from 45.6 % to 26.5 % relative to p53_WT. This reduction was not as significant as that of the *i,i*+4 spaced peptide (21.4 %), most likely due to the differences in relative helical stabilisations of the substituted Glu17 (-0.27 kcal mol^{-1}) of the *i,i*+7 peptide and Ser20 (-0.35 kcal mol^{-1}) of the *i,i*+4 peptide with respect to Cys (-0.23 kcal mol^{-1}).
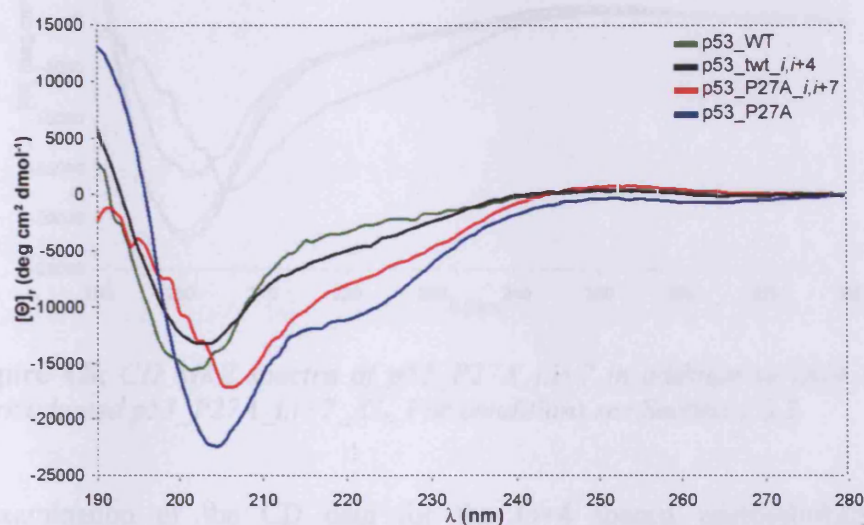
Figure 4.7: *The i,i+7 spaced peptide shows a greater degree of α-helix stability than the i,i+4 spaced peptide. For conditions see Section 2.3.2.*

The CD spectrum of the crosslinked p53_P27A_*i,i*+7_XL shows that the peptide has comparable secondary structures when the crosslinker is in the light-induced and dark adapted conformation (Figure 4.8). The $[\Theta]_{r\ 222}$ for both the light-induced and dark adapted peptide give values of 11 % α-helicity, relative to p53_WT. This is a significant decrease from the 45.6 % helicity calculated for the modified wild-type peptide p53_P27A, in addition to a reduction of approximately 15 % α-helicity when compared to the uncrosslinked peptide. This data indicates that the presence of the

attached crosslinker has only a minimal contribution to the destabilisation of the α-helicity of the peptide when in both the *cis* and *trans* isomer. We reason that the substitution of Glu17 and Lys24 for cysteines in the design of the *i,i*+7 spaced peptide significantly impairs the ability of the peptide to maintain a stable helical structure.
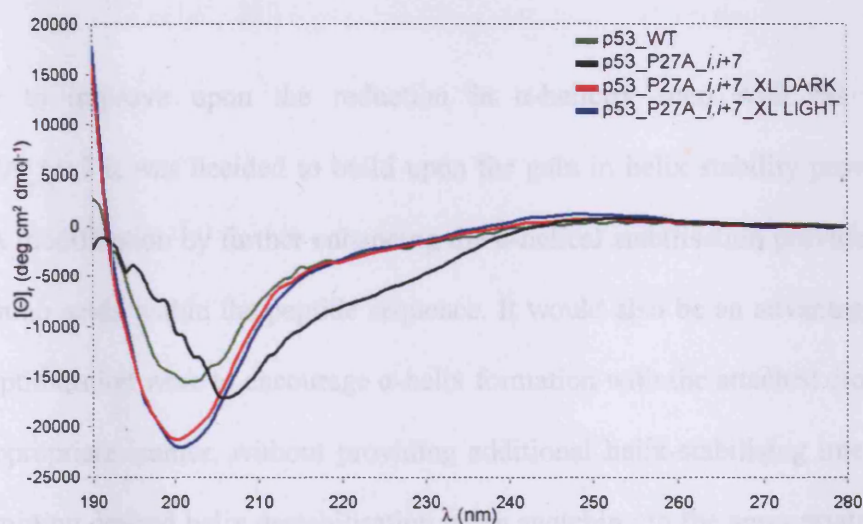
Figure 4.8: *CD MRE spectra of p53_P27A_i,i+7 in addition to light and dark adapted p53_P27A_i,i+7_XL. For conditions see Section 2.3.2.*

The examination of the CD data for the *i,i*+4 spaced uncrosslinked peptide p53_twt_*i,i*+4 showed a reduction in α-helix content by 12.5 % when compared to the template truncated wild-type peptide p53_twt (relative to p53_WT), and involved the substitution of Ser20 and Lys24 for Cys residues. Chapter 1.8, Table 1.1 shows that whilst the substitution of Ser, Lys and Glu for Cys would all result in a decrease in the relative helical stabilisation for the resulting peptide sequences, the small differences between the values of helical stabilisation given for Glu and Cys, -0.27 kcal mol^{-1} and -0.23 kcal mol^{-1} respectively suggests that the major contribution to the 19.1 % reduction in α-helicity between the peptides p53_P27A and the Cys incorporated p53_P27A_*i,i*+7 (relative to p53_WT) arises from the loss of Lys24, which has a

contribution to helical stabilisation of -0.65 kcal mol^{-1}.[99] As described previously, the decision to substitute Glu17 and Lys24 was taken since other possible locations for an $i,i+7$ spacing between Cys residues would have involved the disruption of known additional helix stabilising interactions involving residue side-chains such as the hydrogen bond between Thr18 and Asp21.

In order to improve upon the reduction in α-helicity seen with the peptide p53_P27A_$i,i+7$ it was decided to build upon the gain in helix stability provided by the P27A modification by further enhancing the α-helical stabilisation provided by all of the amino acids within the peptide sequence. It would also be an advantage if this further optimisation were to encourage α-helix formation with the attached crosslinker in the appropriate isomer, without providing additional helix-stabilising interactions thus permitting desired helix destabilisation when switching to the appropriate isomer of the crosslinker. As described in chapter 3.2, we substituted Asp21 for Glu, since this was proposed to eliminate the helix stabilising additional hydrogen bond of the Asp21 side-chain with Thr18. Chapter 1.8 Table 1.1 does not take into account side-chain interactions and so indicates that this change may also encourage an α-helical conformation since there is a net improvement in the relative helical stabilisation of the peptide upon substitution of Asp (-0.15 kcal mol^{-1}) for Glu (-0.27 kcal mol^{-1}).

The CD spectrum for the resulting peptide, p53_D21E_$i,i+7$, is shown in Figure 4.9 overlaid with its predecessor p53_P27A_$i,i+7$. The substitution of Asp21 for Glu appears to make no significant difference to the secondary structure of the peptide, although analysis of the $[\Theta]_{r\,222}$ measurements suggest an improvement in the peptide α-helix content from 26.5 % to 38.6 % respectively, relative to p53_WT. This makes

the secondary structure of the Glu21 modified peptide more comparable to that of the substituted wild-type peptide p53_P27A, with values for $[\Theta]_{r\ 222}$ of −11041 deg cm^2 dmol^{-1} and −13030 deg cm^2 dmol^{-1} respectively giving rise to a difference of only 7.8 % α-helicity between the two peptides (Figure 4.9). The secondary structure data for p53_D21E_*i,i*+7 shows that the strategy of sacrificing a helix stabilising hydrogen bond for the sake of substituting an amino acid for another which contributes to a higher degree of α-helical stabilisation was successful. An improvement in the overall α-helicity of the resulting peptide has been recorded, in this instance off-setting the loss in α-helix stability as seen with the initial *i,i*+7 substituted peptide (p53_P27A_*i,i*+7) attributed predominantly to the loss of helix stabilisation contributed by Lys24.
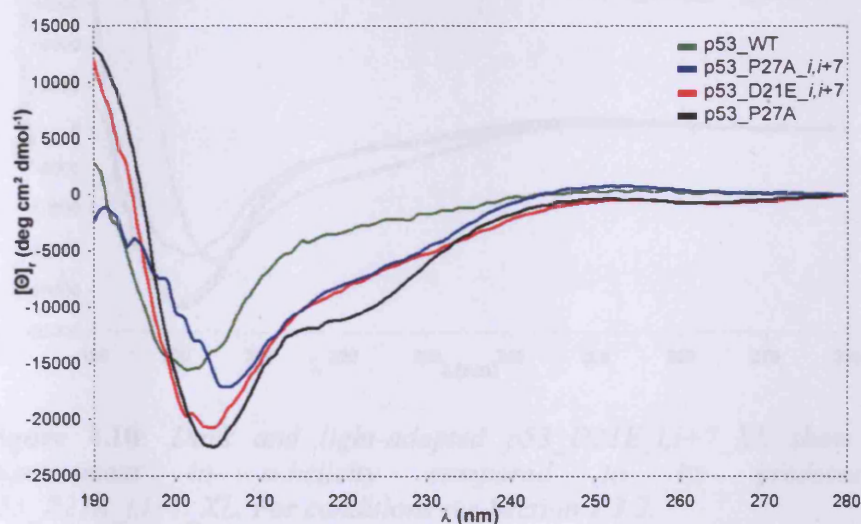
Figure 4.9: *The substitution of Asp21 for Glu compliments the P27A modification in the resulting i,i+7 spaced peptide to enhance photo-switchability of α-helicity. For conditions see Section 2.3.2.*

The crosslinked derivative of the improved *i,i*+7 Cys substituted peptide p53_D21E_*i,i*+7_XL is shown in Figure 4.10 in both the light induced and dark-

adapted states in comparison with its predecessor p53_P27A_*i,i*+7_XL. Although CD signals at 222 nm suggest p53_D21E_*i,i*+7_XL shows a greater degree of α-helicity with both the *cis* and *trans* isomers of the crosslinker than that of p53_P27A_*i,i*+7_XL, the evaluation of the line shape suggests all peptides are random. As seen previously, the isomerisation of the crosslinker appears to make an insignificant difference to the secondary structure of the peptide. This brings into question the ability of CD spectroscopy to differentiate between the structural discrepancies between the light induced and dark-adapted states of such short crosslinked peptides.
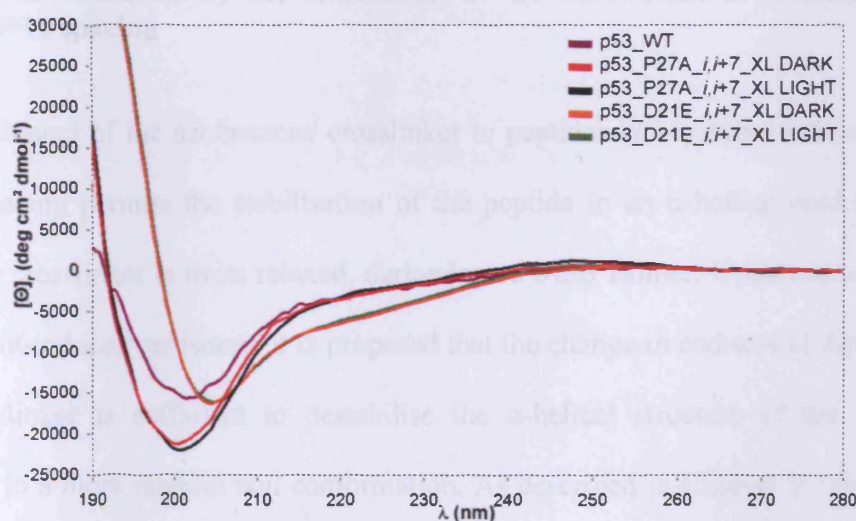
Figure 4.10: *Dark and light-adapted p53_D21E_i,i+7_XL show no improvement in α-helicity compared to its predecessor p53_P27A_i,i+7_XL. For conditions see Section 2.3.2.*

Although CD spectroscopy is able to clearly outline the differences in secondary structure characteristics between an α-helix and a truly random coil structure, it is proposed that the attachment of the crosslinker is still constraining the peptide's

structure be it in the *cis* or *trans* isomer. This may therefore contribute to difficulties

in discriminating between the ordered structure that is defined as α-helix promoting

and that which although ordered due to the constraint of the attached crosslinker is

regarded as α-helix destabilising. For example, a short crosslinked peptide in such a

conformation to destabilise α-helix formation, although potentially random in its

secondary structure, it is still effectively ordered *via* the attachment of its two cysteine

residues to the crosslinker and so potentially lacks the conformational flexibility

afforded to a truly random coil conformation.

4.2.4 Dark stabilised 15 amino acid p53-based peptides designed to promote α-helix formation by the attachment of the azobenzene crosslinker in an *i,i*+11 spacing

The attachment of the azobenzene crosslinker to peptides *via* cysteine residues in an

i,i+11 spacing permits the stabilisation of the peptide in an α-helical conformation

when the crosslinker is in its relaxed, dark-adapted *trans* isomer. Upon isomerisation

to the light-induced *cis* isomer it is proposed that the change in end-to-end distance of

the crosslinker is sufficient to destabilise the α-helical structure of the peptide,

resulting in a more random coil conformation. As described in Chapter 3.2 the *i,i*+11

spaced peptide was based on the P27A substituted wild-type peptide, due to the

improvement that this modification made to the resulting peptide secondary structure

over the wild-type 15 amino acid peptide. The only possible location for the cysteine

residues in this spacing involved the substitution of p53 Glu residues 17 and 28,

which although having a negative effect upon the solubility of the uncrosslinked

peptide, has a minimal effect upon the conformational stability of the peptide. This is

due to the relative helical stabilisation of –0.27 kcal mol^{-1} and –0.23 kcal mol^{-1} contributed by Glu and Cys respectively.[99]
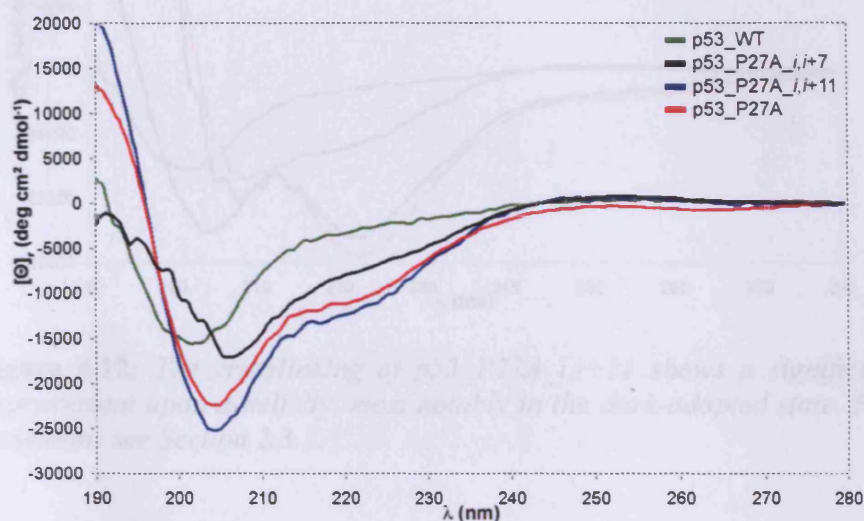
Figure 4.11: *The positioning of cysteine residues in an i,i+11 spacing shows a significant improvement in peptide α-helicity over their positioning in an i,i+7 spacing. For conditions see Section 2.3.2.*

Figure 4.11 shows the CD spectrum of the resulting peptide p53_P27A_*i,i*+11 overlaid with the equivalent *i,i*+7 peptide and the modified wild-type peptide p53_P27A. It is clear that there is a significant difference in secondary structure between the *i,i*+11 spaced peptide compared to the *i,i*+7 spaced peptide, which according to MRE data at 222 nm equates to an increase in the α-helix content from 26.5 % to 40.0 %. The CD spectra for the resulting crosslinked peptide p53_P27A_*i,i*+11_XL, for both the *cis* and *trans* isomer of the crosslinker, displaying a clear [Θ] minimum at 222 nm indicative of an α-helical structure, Figure 4.12.
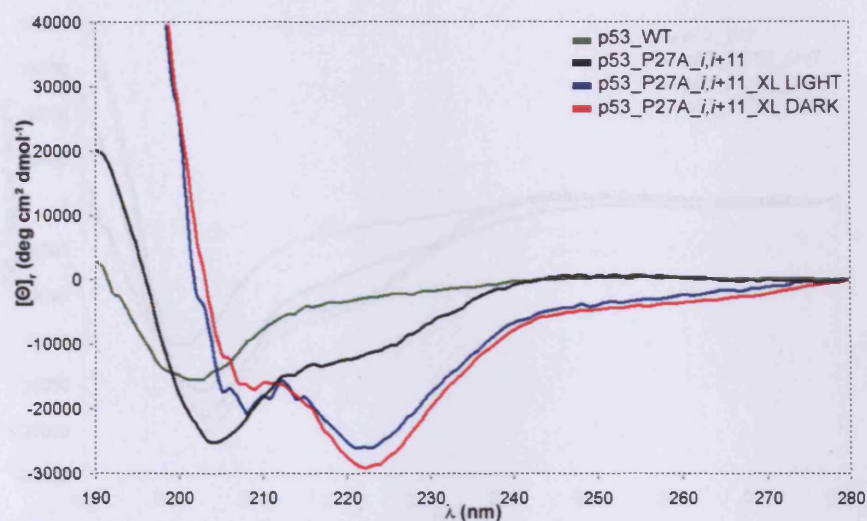
Figure 4.12: *The crosslinking of p53_P27A_i,i+11 shows a significant improvement upon α-helicity, most notably in the dark-adapted state. For conditions see Section 2.3.2.*

The crosslinked peptide shows a significant improvement in α-helicity over the uncrosslinked *i,i*+11 spaced peptide, with an α-helix content of 70.7 % and 56.8 % with respect to p53_WT for the dark-adapted and light induced conformations respectively. Although clearly demonstrating the ability of the azobenzene crosslinker to influence the secondary structure of a peptide, the desired degree of secondary structure switching that arises from the isomerism of the attached crosslinker is still lacking in significance. We therefore employed the same modification as used for the *i,i*+7 spaced peptide and made the Asp21Glu mutation which was proposed to increase the influence of the crosslinker over the peptide secondary structure.
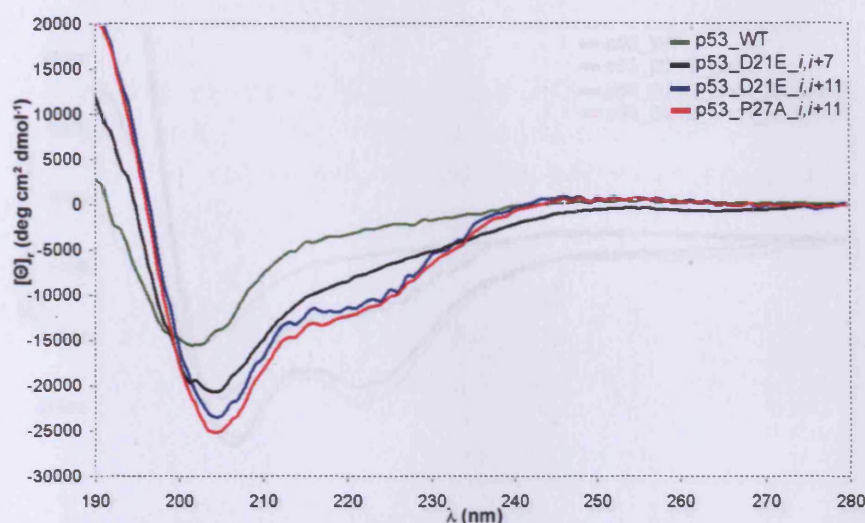
Figure 4.13: *The substitution of Asp21 for Glu in the peptide p53_D21E_ i,i+11 shows comparable secondary structure to its predecessor p53_P27A_ i,i+11. For conditions see Section 2.3.2.*

Substitution of Asp21 for Glu causes a loss of α-helicity in comparison with the Asp21 containing peptide p53_P27A_*i,i*+11 (Figure 4.13) as expected, since the loss of the additional stabilisation provided by Asp21 would destabilise the free peptide. Figure 4.14 highlights the differences between the peptide secondary structures when the crosslinker is in its respective isomers. Although there is clearly a greater helical structure in the dark-adapted state (86.6 %) when compared to the light-induced state (75 %), there is only an 11.6 % difference in α-helicity between the *cis* and *trans* isomers compared to the 13.9 % difference observed between the isomers of the peptide p53_P27A_*i,i*+11_XL. This shows that whilst the substitution of Asp21 for Glu reduced α-helicity, there is no observed improvement in the secondary structure switching abilities for the respective crosslinker conformation required to initiate α-helix destabilisation.
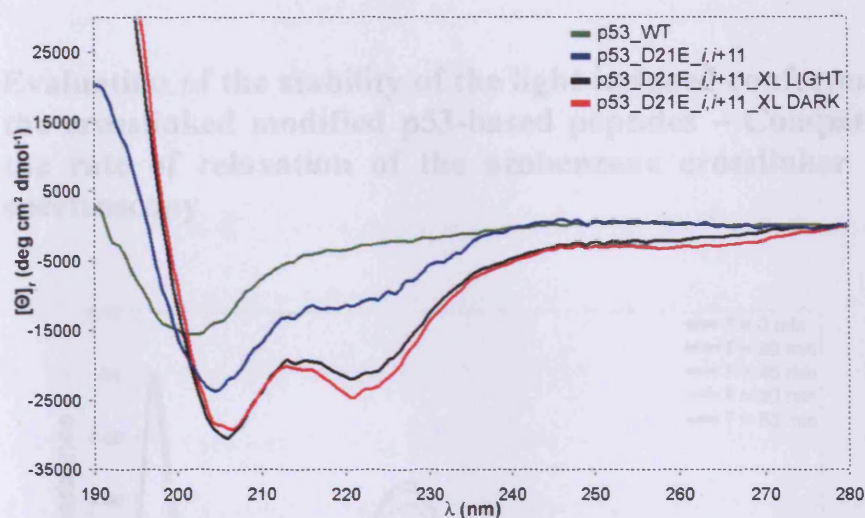
Figure 4.14: *The crosslinking of p53_D21E_i,i+11 shows a significant improvement upon α-helicity, most notably in the dark-adapted state. For conditions see Section 2.3.2.*

4.3 Evaluation of the stability of the light-induced conformation of the crosslinked modified p53-based peptides – Comparison of the rate of relaxation of the azobenzene crosslinker by UV spectroscopy
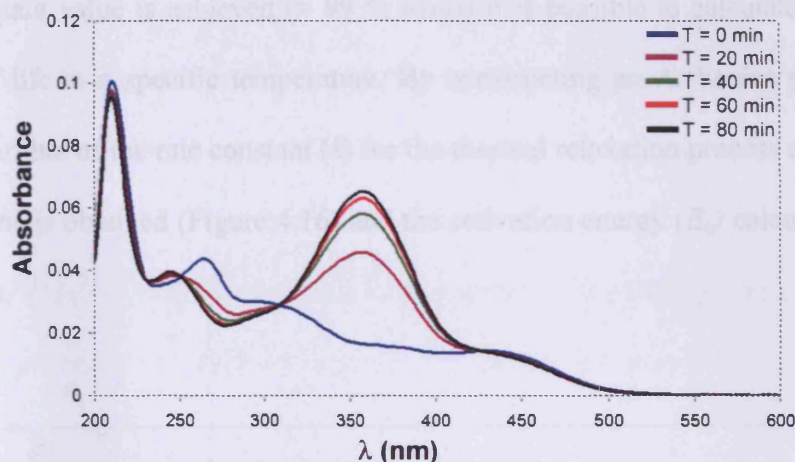
Figure 4.15: *The UV spectrum of the azobenzene crosslinker shows relaxation from the cis to trans isomer, recovering its maxima at 360 nm. T = 20 °C in CD buffer.*

The UV absorbance spectrum for the dark-adapted, *trans* isomer of the azobenzene crosslinker shows an absorbance maximum at 360 nm. Upon isomerisation to the *cis* form, the absorbance of the crosslinker at 360 nm is significantly reduced. As detailed in chapter 1.9 due to the continuous relaxation of the *cis* isomer to the *trans* form only 70-90% *cis* is obtained, and therefore by taking this value of UV absorbance as representative of the total possible conversion of the crosslinker to the *cis* isomer it is possible to monitor the relaxation of the crosslinker towards the dark-adapted, *trans* isomer. This relaxation can be achieved over time and in a temperature dependant manner with a yield > 99 % of the *trans* isomer, thus permitting the crosslinker relaxation to be monitored by the use of UV spectroscopy. Figure 4.15 shows UV spectra for the azobenzene crosslinker in a light induced state in addition to UV scans

taken at intervals of 20 minutes at 20 °C demonstrating the recovery of the 360 nm

absorbance maxima upon relaxation to the dark-adapted *trans* isomer.

By monitoring the increase in absorbance of the light-induced crosslinker over time

until a constant value is achieved (> 99 % *trans*) it is possible to calculate the value

for the half-life at a specific temperature. By constructing an Arrhenius plot of the

natural logarithm of the rate constant (*k*) for the thermal relaxation process against 1/T

a straight line is obtained (Figure 4.16) and the activation energy (E_a) calculated from

the gradient.
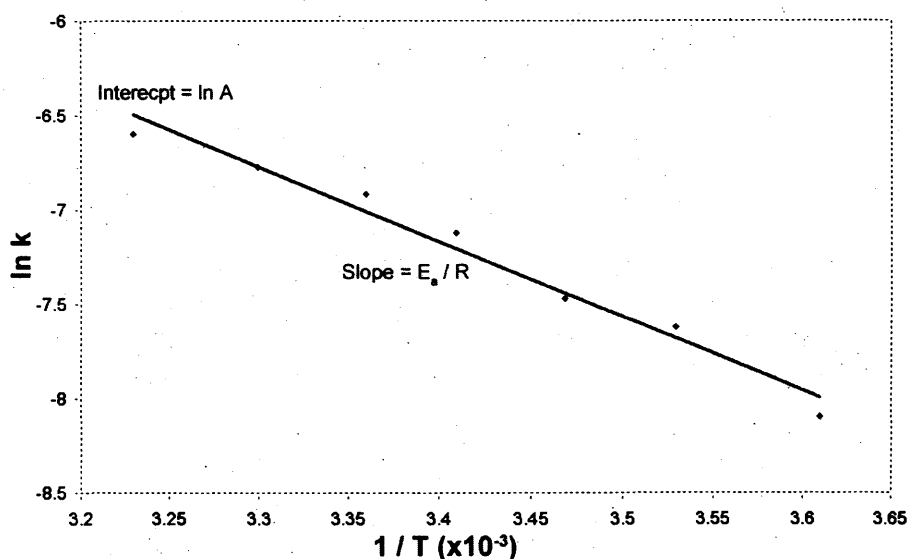
Figure 4.16: *Plotting the rate constant (k) against temperature (1/T) enables the calculation of the activation energy (E_a) for the relaxation of the crosslinked peptides.*

The results for the half-lives of all crosslinked peptides based on UV relaxation

measurements at different temperatures are given in Appendix A3, and the data based

on the Arrhenius plots for these peptides is summarised in Table 4.1. The free

azobenzene crosslinker has the fastest relaxation half-lives when compared to the

crosslinked peptides at different temperatures, but it also has the highest activation energy, and is thus proposed to undergo faster relaxation due to it being free in solution as opposed to the constraint of the crosslinker when attached at each end to the respective peptide. Almost all crosslinked peptides posses similar activation energies since they all constrain the crosslinker in the same way, however p53_D21E_*i,i*+7_XL has an activation energy approximately 10 kJ mol^{-1} lower than the other crosslinked peptides. This further highlights the importance of the role of Asp21 in stabilising the p53 α-helix and shows how the formation of a stable peptide α-helix contributes to the increased half-lives seen with the crosslinked peptides, this is because a greater helical stability opposes relaxation of the attached crosslinker.

Table 4.1: *Summary of the UV relaxation data for the crosslinked p53-based peptides and comparison with the free crosslinker.*

	Slope = $-E_a/RT$	E_a (kJ mol^{-1})	Arrhenius Parameter (s^{-1})
Crosslinker	-3890.9 ± 289.6	32.35 ± 2.41	428.76
P53_twt_*i,i*+4_XL	-2992.3 ± 229.7	24.88 ± 1.91	6.30
P53_P27A_*i,i*+7_XL	-3101.7 ± 291.0	25.79 ± 2.42	6.05
P53_D21E_*i,i*+7_XL	-1876.3 ± 155.4	15.60 ± 1.29	0.09
P53_P27A_*i,i*+11_XL	-3030.2 ± 352.9	25.19 ± 2.93	3.77
P53_D21E_*i,i*+11_XL	-3237.2 ± 413.3	26.91 ± 3.44	8.54

4.4 Investigating the secondary structure of cysteine containing peptides based upon a polyalanine scaffold incorporating residues critical for Hdm-2 binding

The synthesis of p53_Ala_*i,i*+7 and p53_Ala_*i,i*+11 was intended to demonstrate the use of a stabilised polyalanine scaffold incorporating only the residues critical for

p53-Hdm-2 binding in addition to those known to stabilise the p53 α-helix. As noted previously, the increase in the number of alanine residues within the 15-amino acid peptides had a clear effect upon the solubility of the peptides, despite the inclusion of charged terminal capping residues whose function was predominantly to stabilise the helix dipole.
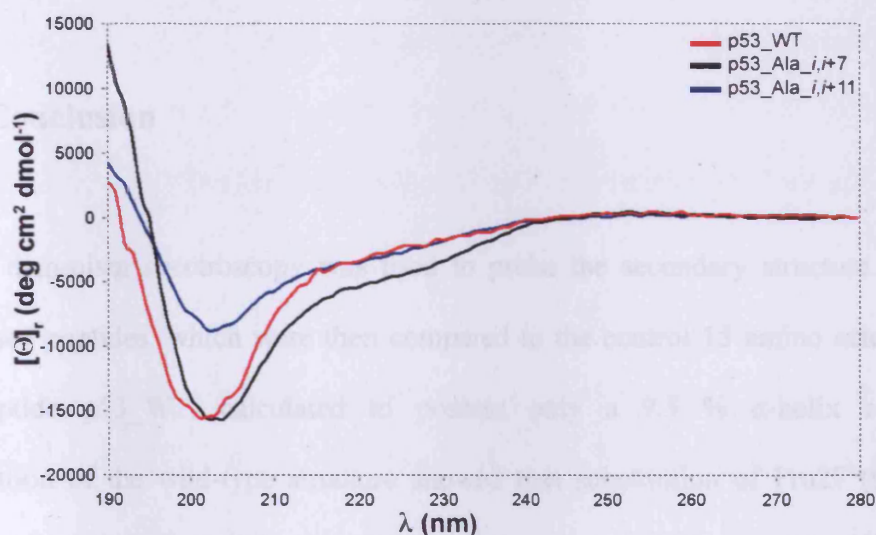
Figure 4.17: *The i,i+7 spaced Ala scaffold peptide showed improved α-helicity when compared to the wild-type peptide p53_WT.*

The CD spectra of these peptides are shown in Figure 4.17, where it is apparent that the secondary structure is not truly α-helical for either peptides. The CD spectrum of the *i,i*+7 spaced peptide p53_Ala_*i,i*+7 shows a structure with an increased α-helix character at 222 nm compared to the control, wild-type peptide p53_WT, with a total α-helix content of approximately 17.8 % and 9.5 % respectively. There is however, a greater resemblance to a random conformation for p53_Ala_*i,i*+11 which is more comparable to p53_WT. Although identical with respect to the critical amino acids and number of alanine residues, both the *i,i*+7 and *i,i*+11 spaced peptides contain a

single cysteine residue in differing positions and this is proposed as the reason for the significant difference in α-helicity between the two peptides. In the *i,i*+7 spaced peptide, the cysteine is positioned as residue 24 within the middle of the peptide sequence, whereas it corresponds to residue 28 for the *i,i*+11 spaced peptide, the penultimate amino acid from the peptide *C*-terminus.

4.5   Conclusion

Circular dichroism spectroscopy was used to probe the secondary structure of the synthesised peptides, which were then compared to the control 15 amino acid wild-type peptide p53_WT, calculated to possess only a 9.5 % α-helix content. Optimisation of the wild-type structure showed that substitution of Pro27 (to give p53_P27A) increased α-helicity to 45.6 % (relative to p53_WT) as predicted due to the disruption proline contributes to an α-helical structure. Reducing the peptide length (p53_twt) also increases the α-helicity with respect to the initial peptide p53_WT. However, the low α-helicity of the wild-type peptide has been attributed to the presence of Pro27 so when compared to p53_P27A the truncated ten amino acid peptide shows a net reduction of 11.7 % α-helicity.

Comparison of the secondary structures of the peptides designed to incorporate cysteine residues at defined spacings revealed key information regarding the involvement of specific amino acids in the stabilisation of the p53 α-helix. The *i,i*+4 spaced peptide was based on the ten amino acid peptide p53_twt, and the subsequent

peptide (p53_twt_*i,i*+4) although still more α-helical than the 15 amino acid wild-type peptide showed a reduction of 12.5 % α-helicity when compared to the peptide p53_twt. This is expected since the reduction in the length of the peptide chain results in a decrease in the number of potential α-helix stabilising hydrogen bonds, however it also highlighted the contribution of Lys24 in terms of increasing the overall α-helix propensity of the peptide sequence. The addition of the azobenzene crosslinker improves the α-helicity of both the dark-adapted and the light induced structures (55.0 % and 48.2 % respectively), which is surprising since although it was intended to induce a helical conformation when in the light induced state; this increase is also seen for the dark-adapted structure.

The distribution of cysteines in an *i,i*+7 spacing supported the results of the *i,i*+4 spaced peptide in which the significance of the helical propensity of Lys (–0.65) becomes evident. The peptide p53_P27A_*i,i*+7 showed a 19.1 % reduction in α-helicity since incorporation of Cys required the substitution of Lys24, although upon crosslinking, both the *cis* and *trans* isomers showed an 11 % increase in α-helicity over the uncrosslinked peptide. Like the peptide p53_twt_*i,i*+4_XL, we proposed that the addition of the crosslinker whether in the *cis* or *trans* isomer adds some degree of order to the peptide. When comparing the crosslinked to the uncrosslinked peptide, it is thought that the uncrosslinked peptide has greater mobility in such a way as the movement of one Cys residue when not attached to the crosslinker is independent of the other.

In order to compensate for the loss of Lys24 when designing the *i,i*+7 spaced peptide, in addition to giving more control of the peptide secondary structure to the isomerism

of the crosslinker, it was decided to substitute Asp21 for Glu. The loss of Lys24 was

unavoidable in the design of the *i,i+7* spaced peptide since other favourable locations

for cysteine residues would have disrupted known helix stabilising interactions. This

modified uncrosslinked peptide (p53_D21E_*i,i+7*) shows a 12.1 % increase in the α-

helix content when compared to its predecessor p53_P27A_*i,i+7* giving an α-helix

content comparable to the wild-type peptide p53_P27A. Again the resulting

crosslinked peptide showed an increase in α-helicity, however there was no further

evidence of the regulation of the peptide secondary structure by the isomerism of the

crosslinker.

The principle of the design for the *i,i+11* spaced peptides was to yield dark-adapted,

trans stabilised α-helices which become destabilised upon isomerism of the

crosslinker from *trans* to *cis*. The *i,i+11* spaced peptides allow for Lys24 to remain

included within the peptide sequence and as a result the uncrosslinked peptide shows

an increase in α-helicity over p53_P27A_*i,i+7* by 13.5 %. Upon crosslinking, the α-

helix content was significantly increased again for both the dark-adapted and light-

induced peptides, however there was 13.9 % greater α-helicity observed for the dark-

adapted, *trans* isomer. The designed Hdm-2 binding peptides based upon a

polyalanine α-helix incorporating cysteine residues show a defined secondary

structure, with the *i,i+11* spaced peptide more helical than the *i,i+7* spaced peptide

which is comparable to that of the peptide p53_WT. This further highlights the

importance of the positioning of the cysteine residues with respect to the resulting

secondary structure since in both cases alanine is substituted for cysteine.

Examination of the UV relaxation of the crosslinked peptides showed a temperature dependant decrease in the half-life of the *cis* isomer of the azobenzene crosslinker as observed with the crosslinker in a free un-bound state. The calculation of the half-life for the crosslinker enables the determination of the activation energy for this process and interestingly, the free crosslinker has the highest value, 32.35 kJ mol^{-1}. All of the crosslinked peptides have similar values for E_a, with the exception of p53_D21E_*i*,i+7_XL which is approximately 10 kJ mol^{-1} lower, supporting the evidence for the D21E mutation promoting the disruption of α-helicity in the dark-adapted state when attached in an *i*,*i*+7 spacing.

This work has yielded peptides able to be crosslinked in addition to presenting key residues required for interaction with Hdm-2. Although the addition of the crosslinker using cysteine residues incorporated within the sequence in an *i*,*i*+4 and *i*,*i*+7 spacing proved unsuccessful for the regulation of the peptide secondary structure there is potential for further optimisation of this sequence to gain further α-helical preference and enhance the effect of photoswitching on peptide conformation. UV spectroscopy has been successfully used to monitor the relaxation of the crosslinker, this has shown as proposed that the half-life of the *cis* isomer is significantly affected by attachment to a peptide, the extent of which provides a good guide to the stability of the peptide conformation induced from the photoisomerisation of the crosslinker.

CHAPTER 5:

EVALUATION OF THE

BINDING INTERACTION

BETWEEN p53 AND HDM-2

5.1　Measuring Peptide-Protein Interactions

The importance of the interaction between p53 and Mdm-2 for the regulation of apoptosis has been highlighted in chapter 1.4. Further investigation into this interaction has revealed a 1:1 relationship between the binding of these two proteins (Equation 5.1). Therefore the dissociation constant (K_D) can be defined as the relationship between the free protein ([P]) and ligand ([L]) with respect to the bound protein-ligand complex ([PL]), Equation 5.2.
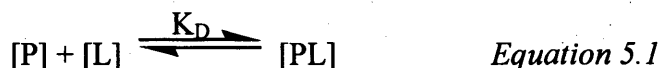
$$[P] + [L] \xrightleftharpoons{\quad K_D \quad} [PL] \qquad\qquad Equation\ 5.1$$

$$K_D = \frac{[P]\,[L]}{[PL]} \qquad\qquad Equation\ 5.2$$

Previous investigations of the interaction between p53 and Mdm-2 have been conducted using a variety of techniques including enzyme-linked immunosorbent assay (ELISA),[74] isothermal titration calorimetry (ITC)[70] and also fluorescence-based techniques.[50,75,77] Schon *et al.* investigated the mechanism of p53-Mdm-2 binding by examining the binding of a set of peptides derived from the *N*-terminus of wild-type p53.[70] Their experiments showed how phosphorylation of p53 Ser15 and Ser20 did not affect p53-Mdm-2 binding, however the phosphorylation of Thr18 resulted in the reduction in binding affinity for Mdm-2 by an order of magnitude. NMR studies carried out by Schon and co-workers revealed how upon binding Mdm-2 undergoes a conformational change that is not limited to the hydrophobic cleft. The ITC data

reported by Schon *et al.* gave a K_D of 580 nM (± 19 nM) for a 15 amino acid peptide representing p53 residues 15-29. This result was comparable with the work of Fersht *et al.* who also used ITC to measure the binding of full-length p53 to Hdm-2 residues 2-125.[50] They measured a K_D of 340 nM (± 10 nM), an improvement over the 15 amino acid peptide of Schon *et al.*[70] The crystal structure of the p53-Mdm-2 complex reveals the terminal ends of the p53 α-helix to be in an extended conformation, less ordered when compared to the residues actively involved in Mdm-2 binding.[68] As a result, these may contribute to the destabilisation of the p53 α-helix whereas in full-length p53 these same residues are somewhat constrained between other secondary structural motifs of p53 reducing the flexibility in the extended conformation of these residues.

5.2   Evaluation of the binding of p53-based peptides with Hdm-2

Due to steric constraints, the functionality of the crosslinker requires a clear path between the two cysteine residues where it forms its covalent attachments to the peptide. Consequently the attachment of a fluorophore to any part of the p53 peptide other than the *N* or *C*-terminus would not only restrict the possible combination of locations for the attachment of the crosslinker but also may interfere with and contribute to the inhibition of p53-Hdm-2 binding. Attachment of the fluorophore to either the flexible *N*- or *C*- terminus means the change in anisotropy observed upon complexation may be reduced.

Table 5.1: *Binding data for the wild-type p53-based peptides.*

Peptide	K_D (nM)
p53_WT (15-29)	268 ± 49
p53_P27A	22 ± 3
p53_twt	11 ± 1
p53 (15-29) Schon *et al.*[70]	580 ± 19
p53 protein	340 ± 10

Fluorescence anisotropy binding assays were carried out by titrating Hdm-2 of a pre-determined concentration into a 1 cm fluorescence cuvette containing a 1 ml solution of a specific concentration of peptide (typically 10 nM), anisotropy values were recorded two minutes after each addition of protein. The binding data for the wild-type p53-based peptides is summarised in Table 5.1, and demonstrate the effectiveness of the optimised fluorescence anisotropy binding assay since the 15 amino acid control peptide p53_WT, yields Hdm-2 binding results comparable to values previously reported for this peptide without the amidated *C*-terminus.[70]
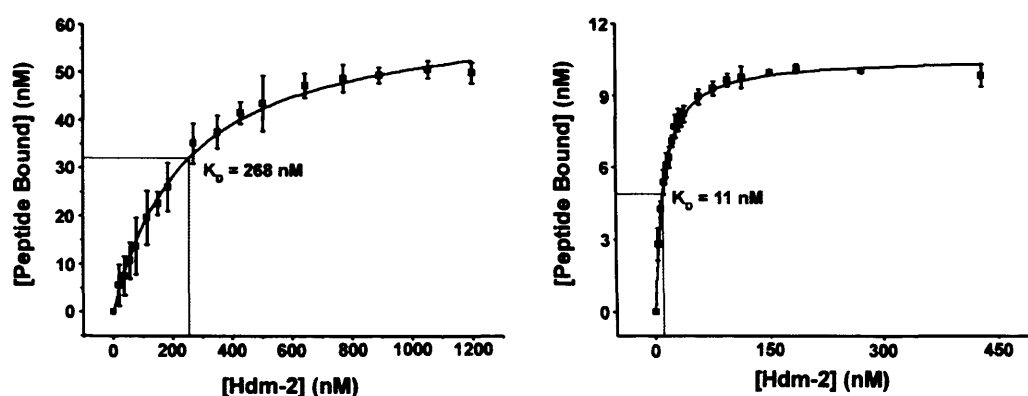
Figure 5.1: *Fluorescence anisotropy binding curves for a 1:1 binding model. p53_WT (left, K_D = 268 nM ± 49) and p53_twt (right, K_D = 11 nM ± 1).*

Figure 5.1 highlights the difference between a binding curve for a weakly binding peptide (p53_WT) when compared to a tightly binding peptide (p53_twt). Table 5.1

shows that there is a significant improvement in the binding affinity for the modified

wild-type peptides over the control, 15 amino acid wild-type peptide p53_WT. This

binding affinity is marginally stronger than the values given by previous researchers,

possibly due to the additional stabilisation provided by the amidation at the *C*-

terminus of the peptides.[50,70]

The modification of the wild-type peptide by the substitution of Pro27 for Ala

improved the binding affinity of the peptide for $Hdm-2_{1-125}$ by an order of magnitude,

supporting the proposal for the *N*-terminus of the p53 α-helix being in an extended

conformation resulting in α-helix destabilisation,[68] since α-helix instability would

have a negative effect upon p53-Hdm-2 binding. The substitution of the proline

residue in position 27 for a more helix promoting amino acid reduced the extent of

helix destabilisation resulting in a higher $p53 - Hdm-2_{1-125}$ binding affinity. This is

supported by the CD data of Chapter 4 where the α-helix content increases by

approximately four times its value for p53_WT. The two orders of magnitude increase

in Hdm-2 binding for the truncated peptide p53_twt also correlates with the CD

secondary structure data, since the free peptide is shown to have a more highly

ordered α-helical structure compared to p53_WT, 33.9 % and 9.7 % α-helicity

respectively (Chapter 4.2, Figure 4.4). We propose the shorter α-helix is potentially

able to fit deeper within the hydrophobic cleft of Hdm-2 therefore increasing the

binding affinity. Additionally, we believe the shorter peptide has less of an extended

conformation, and is therefore a more stable helical structure than the longer, 15

amino acid peptides.

The truncated ten amino acid peptide was used as the template for the design of the $i,i+4$ spaced cysteine containing peptides, and the binding data is given in Table 5.2. The incorporation of the cysteine residues appears to have had only a slightly negative effect upon the binding affinity of the uncrosslinked $i,i+4$ spaced peptide when compared to the wild-type peptide p53_twt, supporting the CD data where approximately a one-third reduction in the peptide α-helicity is observed. Upon crosslinking, a further reduction in Hdm-2 binding affinity occurs to approximately half that of the initial truncated wild-type peptide. There also appears to be some functionality introduced between the binding affinity of the light-induced and dark-adapted structures, with tighter binding in favour of the light-adapted structure as desired. However, upon closer examination of the error values, for these assays it is apparent that these binding affinities are essentially identical. Interestingly, whilst the CD data shows a significant improvement upon the α-helix content of the $i,i+4$ spaced peptides upon crosslinking, the binding affinity is reduced implying that the proposed increase in penetration of the truncated peptide within the hydrophobic cleft of Hdm-2 is in some way inhibited by the presence of the crosslinker however this is unlikely since the binding affinity data is still significantly more improved than the wild-type. It is proposed that the interaction of the conserved peptide residues from the p53 sequence with their respective residues of Hdm-2 are strong enough to overcome the constraints imposed by the crosslinker, hence both the *cis* and *trans* isomers have no impact upon the binding interaction of this particular peptide.

Table 5.2: *Binding data for the i,i+4 spaced p53-based peptides.*

Peptide	K_D (nM)
p53_twt_*i*,*i*+4	19 ± 2
P53_twt_*i*,i+4_XL Dark	27 ± 4
P53_twt_*i*,*i*+4_XL Light	21 ± 2

It was therefore decided to investigate the competition between the p53 protein and a selection of p53 peptides for the binding to Hdm-2_{1-125}. The results show that for the truncated wild-type peptide p53_twt there is no change in the binding affinity of the peptide for Hdm-2_{1-125} when in the presence of the p53 protein (Table 5.3).

Table 5.3: *Binding data for peptides in the presence of full-length human p53.*

Peptide	K_D (nM)
p53_twt_*i*,*i*+4	20 ± 2
p53_twt_*i*,i+4_XL Dark	20 ± 3
p53_twt_*i*,i+4_XL Light	12 ± 2

When this experiment was repeated using a crosslinked peptide (p53_twt_*i*,*i*+4_XL) , no change in the binding affinity of the *trans*, dark-adapted peptide was observed. However, upon isomerisation to the *cis*, light-induced state the binding affinity was twice the strength of the same peptide in the absence of the p53 protein. Since the other peptides show no change in their binding affinities when p53 is present in the assay mixture, it is proposed that this additional increase in α-helicity arises due to experimental error.

The binding data for the uncrosslinked and crosslinked *i*,*i*+7 spaced peptides is shown in Table 5.4, where in general it can be seen that the change from the distribution of

the cysteines from an $i,i+4$ to an $i,i+7$ spacing has a negative effect upon Hdm-2 binding. This is contrary to the calculated increase in α-helicity observed by CD spectroscopy, and it is proposed that substitution of Glu17 as observed by Schon *et al.* is a contributing factor,[70] in addition to the difference in peptide length as previously described when discussing the significant binding increase observed for the truncated wild-type peptide, p53_twt. The substitution of a charged residue (Glu17Cys) and the reduction in hydrophilicity (Lys24Cys) are proposed to influence the behaviour of the p53 peptide within the hydrophobic cleft of Hdm-2.

Upon crosslinking, the binding affinity for Hdm-2_{1-125} of both the P27A and D21E modified $i,i+7$ spaced peptides is marginally increased in the light-induced conformation. Indeed, to achieve binding affinities in this conformation comparable to the uncrosslinked peptide is in-line with the data for the same conformer of p53_twt_$i,i+4$. However this contradicts the CD data in which upon crosslinking a decrease in helicity is observed for both the P27A and D21E modified peptides in the *trans* and *cis* conformations, and again highlights the role of the Hdm-2 hydrophobic cleft in the alignment and orientation of p53 *N*-terminal residues. The substitution of Asp21 for Glu, proposed to assist in destabilising the p53 α-helix, appears to actually stabilise the *trans* isomer of the crosslinked peptide, a contradiction to the intention for its design. As previously discussed, according to the work of Degrado *et al.* the substitution of Asp21 for Glu results in the incorporation of a more helix promoting residue.[105] Although this modification has not had a negative effect upon Hdm-2 binding, it has not achieved its desired effect of enhancing the degree of control over peptide secondary structure exerted by the crosslinker.

Table 5.4: *Binding data for the i,i+7 spaced p53-based peptides.*

Peptide	K_D (nM)
p53_P27A_*i,i*+7	42 ± 6
p53_P27A_*i,i*+7_XL Dark	80 ± 9
p53_P27A_*i,i*+7_XL Light	37 ± 4
p53_D21E_*i,i*+7	24 ± 2
p53_D21E_*i,i*+7_XL Dark	23 ± 5
p53_D21E_*i,i*+7_XL Light	16 ± 5

The objective for the design of the *i,i*+11 spaced p53-based peptides was to obtain dark-stabilised α-helical peptides, the structures of which become disrupted upon the application of 360 nm UV light and subsequent isomerism of the crosslinker from *trans* to *cis*. The Hdm-2$_{1-125}$ binding data for these peptides is summarised in Table 5.5, where it can be seen that the peptide p53_P27A_*i,i*+11 has 15 nM improvement over the *i*,i+7 spaced equivalent. Since the crosslinking of this peptide showed no significant loss or gain in Hdm-2 binding despite the observed > 46 % increase in α-helicity, we decided to test the D21E *i,i*+11 spaced modified peptide. This gave a binding affinity comparable to the P27A equivalent peptide in accordance with the CD data, however upon crosslinking no significant difference in binding affinities were observed between the light and dark-adapted peptides.

Table 5.5: *Binding data for the i,i+11 spaced p53-based peptides.*

Peptide	K_D (nM)
p53_P27A_*i,i*+11	27 ± 2
p53_P27A_*i,i*+11_XL Light	25 ± 5
p53_P27A_*i,i*+11_XL Dark	22 ± 3
p53_D21E_*i,i*+11	24 ± 1
p53_D21E_*i,i*+11_XL Light	27 ± 3
p53_D21E_*i,i*+11_XL Dark	18 ± 2

Previously, the designed polyalanine-based peptide scaffolds incorporating only the key residues required to facilitate the p53-Hdm-2 interaction and enable the addition of the crosslinker had shown CD spectra indicating the presence of a helical structure comparable to that of the wild-type peptide p53_WT. Further investigation into the binding behaviour of these peptides in the presence of Hdm-2$_{1-125}$ revealed that an interaction was occurring (Figure 5.2) The strength of their binding with Hdm-2$_{1-125}$ is summarised in Table 5.6, and it can be seen that the alanine scaffold peptides display binding affinities with Hdm-2$_{1-125}$, which although not as high as those observed for the optimised p53-based peptides, are still comparable to the K_D obtained for the 15 amino acid wild-type peptide p53_WT (268 nM ± 49).[70]
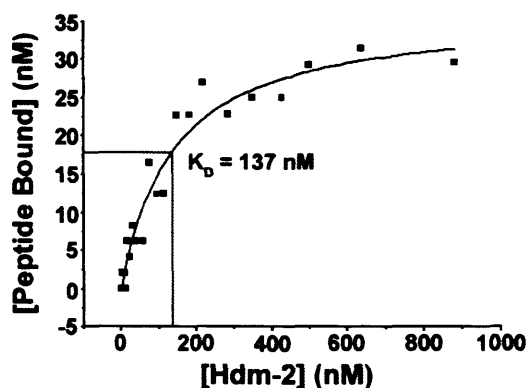
Figure 5.2: *A fluorescence anisotropy binding curve for the alanine scaffold peptide p53_Ala_i,i+11 (K_D = 137 nM ± 26).*

Table 5.6: *Binding data for the designed polyalanine-based Hdm-2 binding peptides.*

	K_D (nM)	Error (1σ)
p53_Ala_*i,i*+7	283	120
p53_Ala_*i,i*+11	137	26

The data suggests that there is definitely an interaction taking place, between the polyalanine scaffold peptides and Hdm-2$_{1-125}$, although the more structured $i,i+7$ peptide has the weaker binding affinity. We proposed that these results represent a good starting point for the use of a stable polyalanine scaffold, much like the previously described work of Schepartz *et al.* where the stability of the aPP α-helix was exploited.[122] Throughout the design of the $i,i+11$ spaced p53-based peptides all of the data has reinforced the significance of the relocation of a single cysteine residue from the central region of the peptide near to the *C*-terminus, thus increasing the α-helicity of the crosslinked peptide in the appropriate conformation. This has also been observed for the polyalanine scaffold peptides despite as discussed when examining the CD data, the presence of Ala in positions 24 and 28 in the $i,i+11$ and $i,i+7$ peptides respectively. In short, the amino acid composition of each of the $i,i+11$ and $i,i+7$ alanine scaffold peptides remain the same with the exception of the positioning of this one cysteine residue, yet differences in their affinities for Hdm-2$_{1-125}$ was observed. Further experimentation is required to determine the effect of crosslinking on the secondary structure of the polyalanine-based peptides.

5.3   Conclusion

The binding affinities of modified and (where applicable) crosslinked p53 peptides with Hdm-2$_{1-125}$ were examined by fluorescence anisotropy measurements. The binding data for the control, 15-amino acid wild-type peptide (p53_WT) validated the assay by producing values for the K_D between p53_WT and Hdm-2$_{1-125}$ slightly lower

than previously published data, which has been proposed to arise from the additional stability gained from the amidation of the peptide at the C-terminus.[50,70] The 246 nM (tenfold) improvement of the binding affinity of the wild-type peptide in which Pro27 was substituted for Ala has supported the hypothesis of the increased stability of the α-helix resulting in an improvement in the Hdm-2 binding affinity. This too has been highlighted by the repetition of the work of Schon *et al.* which has been used as the basis for the design of an *i,i*+4 crosslinked peptide.

Analysis of the binding interaction between the crosslinked peptides and Hdm-2$_{1-125}$ has generally yielded data supported by the degree of α-helicity calculated from the CD data. Experiments with full-length human p53 have indicated that the presence of p53 has no effect upon the binding affinity of the p53-based peptides for Hdm-2$_{1-125}$. The significantly low binding affinities of the modified p53-based peptides are unlikely to be affected by the weakly binding full-length p53, however this is not conclusive evidence suggesting that they function as inhibitors of the p53-Hdm-2 interaction.

Overall, the addition of the azobenzene crosslinker has failed to introduce any specific isomeric control over the binding of the peptides to Hdm-2$_{1-125}$, with the exception of the dark-stabilised peptide p53_D21E_*i,i*+11_XL which loses 33 % of its binding affinity upon isomerisation of the crosslinker to the *cis* conformation. This supports the reasoning for the substitution of Asp21 for Glu, as increased functionality has been assigned to the photoswitching of the crosslinker due to the loss of a helix stabilising hydrogen bond between p53 amino acid side-chains. The polyalanine scaffold-based peptides have been shown to exhibit an interaction with Hdm-2$_{1-125}$,

and there is potential for the optimisation of these peptides by further substitutions, although as shown in Table 5.6 the assay requires further repetition in order to reduce the error values and improve the accuracy of the dissociation constants.

CHAPTER 6:

EXPRESSION OF HDM-2

MUTANTS DESIGNED FOR

LOW AFFINITY P53 BINDING

6.1 The Significance of p53 Phe19 in Hdm-2 Binding and α-Helix Initiation

The crystal structure of the p53-Mdm-2 complex reveals the key interactions between critical residues of both p53 and Mdm-2 that enable binding to occur.[68] Previous mutational analysis has identified the presence of Phe19 and Trp23 as important for p53-Hdm-2 binding, since a double alanine mutation of both residues resulted in a complete loss of p53 binding.[64] The substitution of p53 residue Asp21 for Ala also showed a significant reduction in p53-Hdm-2 binding,[65] destabilising the p53 α-helix by the same mechanism as mentioned in chapter 5.1 where phosphorylation of Thr18 prevents the formation of a helix-stabilising hydrogen bond between the side-chain hydroxyl group of Thr18 and the backbone amine and side-chain carboxyl groups of Asp21. The crystal structure of the p53 – Mdm2 interaction shows that p53 Phe19 forms van der Waals contacts with Gly58 and Ile61 of Mdm-2, as does p53 Trp23.[68] Hydrogen bonding was also reported between the backbone amide of Phe19 and the amide side-chain of Mdm-2 Gln72 (Figure 6.1) in addition to the indole group of p53 Trp23 and the backbone carbonyl of Mdm-2 Leu54.
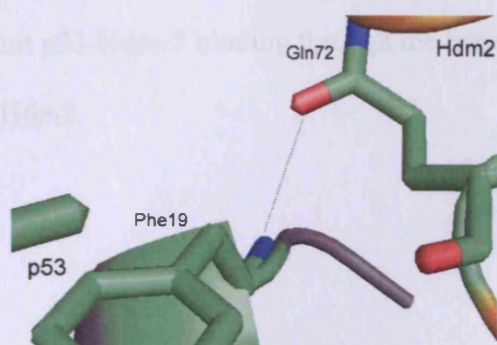
Figure 6.1: *The backbone amide of p53 Phe19 forms a hydrogen bond with the amide side-chain of Hdm-2 Gln72.*

The critical role of p53 Phe19 in the p53-Hdm-2 interaction supports the mechanism

of p53-Hdm-2 binding in which it is proposed that the interaction of this residue with

key functional groups of Hdm-2 amino acids initiates the formation of an α-helical

conformation for the p53 *N*-terminal chain. The interaction of p53 residues Trp23 and

Leu26 with the hydrophobic binding cleft of Hdm-2 further stabilises the p53 α-

helical conformation due to the steric constraints imposed by their binding. The p53-

Hdm-2 interaction and the subsequent formation of the p53 *N*-terminal α-helix are

proposed to propagate from the interaction of Phe19 with the p53-binding site of

Hdm-2.

By modifying the hydrophobic p53-binding cleft of Hdm-2 to reduce its ability to

form interactions with Phe19 of p53 we tested the hypothesis that the binding

interaction between p53 and Hdm-2 will be reduced (increase K_D) for p53-based

peptides that are structurally disordered. For peptides in the unbound state where they

are in a more highly-ordered α-helical conformation, for example, an *i,i*+7 crosslinked

peptide in a light induced conformation, we predict that although the binding when

compared to the wild-type Hdm-2 would be reduced, the ordered structure of the p53

peptide would still permit p53-Hdm-2 binding through the interactions of p53 residues

Trp23 and Leu26 with Hdm2.

6.2   Design and Purification of Mutant Hdm-2

The aim of the mutation of Hdm-2_{1-125} as discussed in section 6.1 was to reduce the binding interaction between Hdm-2 and the structurally disordered p53-based peptides in order to increase the specificity of the p53-binding site for the induced α-helical conformation arising from the appropriately positioned crosslinker. The interactions of p53 Phe19 with Hdm-2 are critical to the nucleation of the p53 α-helix and subsequent Hdm-2 binding, thus by examining the interactions of this residue with Hdm-2 it is apparent to focus on its van der Waals contact with Ile61 and the hydrogen bond between the Phe19 backbone amide and the amide side-chain of Hdm-2 Gln72 (Figure 6.2).
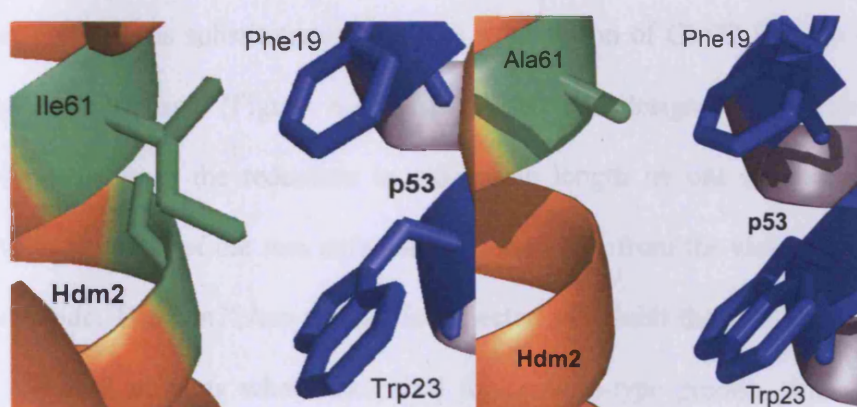
Figure 6.2: *Ile61 of wild-type Hdm-2 (left) was mutated to Ala (right).*

The presence of Ile in position 61 of Hdm-2, a hydrophobic amino acid with a reasonably large side-chain appears to be present to provide hydrophobic bulk to the binding site and mutation to Leu, Val and Ala were considered. Examination of

molecular models of the mutated proteins derived from the p53-Hdm-2 crystal structure suggest the most effective mutation of Ile61 is Ala since Leu and Val provide almost as much hydrophobic bulk as Ile and so may have a lesser impact upon minimising the interaction with Phe19 of p53.[68] Mutation of Ile61 to Ala for Hdm-2$_{1-125}$ was achieved by site-directed mutagenesis (Table 2.1) using the conditions outlined in section 2.2.2, confirmation was achieved by DNA sequencing. The resulting protein was expressed and purified as previously described for wild-type Hdm-2$_{1-125}$.

The role of Hdm-2 residue Gln72 was highlighted from the crystal structure data that showed a hydrogen bond with Phe19.[68] When considering the possible mutations of Hdm-2 Gln72 to eliminate this hydrogen bond it is important to maintain the structural integrity of the Hdm-2 hydrophobic cleft. Residues without large side-chains are favoured as substitutes to Gln, the substitution of Gln72 for Asn and Leu was therefore proposed (Figure 6.3). Gln72Asn was designed to eliminate the hydrogen bond due to the reduction in side-chain length by one carbon atom and subsequent orientation of the Asn side-chain amide away from the vicinity of the Phe backbone amide. The Gln72Asn mutant is expected to exhibit the smallest difference out of all Hdm-2 mutants when compared to the wild-type protein, this is due to Gln72Asn differing from wild-type Hdm-2$_{1-125}$ by a side-chain shorter by one carbon atom in position 72.
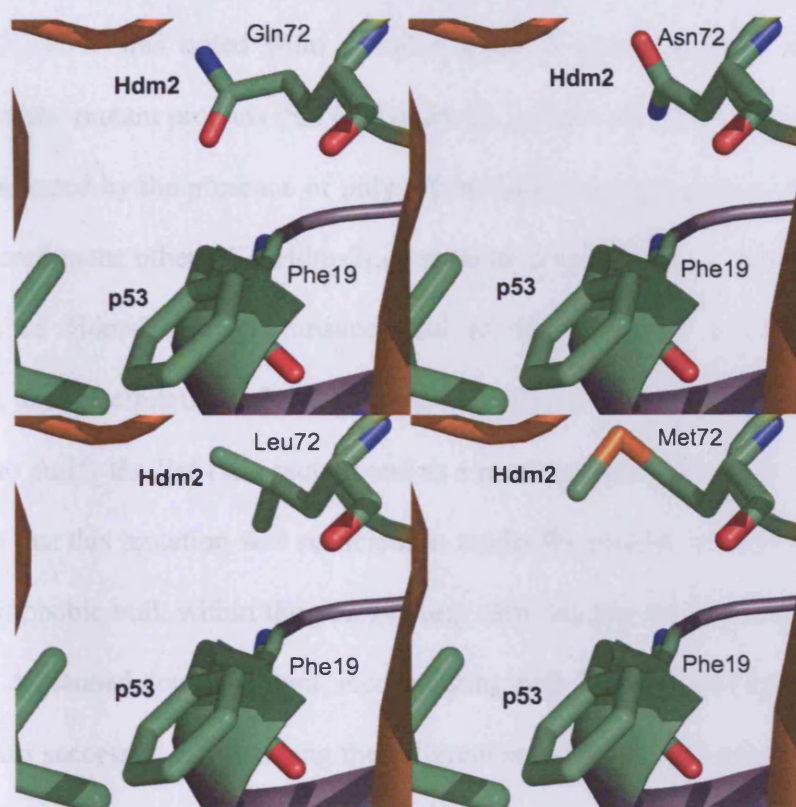
Figure 6.3: *Proposed mutants of Hdm-2$_{1-125}$ (top left), Hdm-2Gln72Asn (top right) and Gln72Leu (bottom left) and Gln72Met (bottom right)*

The Hdm-2 mutant Gln72Leu was expected to eliminate the hydrogen bond by the removal of charged functional groups from residue 72 side-chain, whilst maintaining approximately the same steric bulk as Gln. The substitution of Hdm-2 Gln72 with Met was also considered since Met possesses a bulky side-chain, thus occupying a similar space to Gln72 within the hydrophobic binding cleft of Hdm-2. However Met in position 72 is proposed to not be capable of forming a hydrogen bond with the p53 Phe19 backbone amide (Figure 6.3).

The Hdm-2 position 72 mutants were obtained by site-directed mutagenesis using the PCR procedure outlined in section 2.2.2 (Table 2.2). Expression and purification of mutant GST-Hdm-2$_{1-125}$ was carried out as previously described for the wild-type

GST-Hdm-2$_{1-125}$. It was noted from samples taken at timed intervals during the expression of the mutant proteins that GST-Hdm-2$_{1-125}$ Ile61Ala was expressed at low levels, as indicated by the presence of only a faint band corresponding to this mutant when compared to the other GST-Hdm-2$_{1-125}$ mutants. As described in chapter 3.4, the purification of Hdm-2$_{1-188}$ was unsuccessful at the thrombin cleavage due to aggregation and precipitation of the cleaved Hdm-2$_{1-188}$. This also occurred when attempting to purify the Ile61Ala mutant and as a result no pure protein was obtained. We propose that this mutation was sufficient to render the protein unstable due to the loss of hydrophobic bulk within the p53 binding cleft, leading to the precipitation of the protein. A planned double mutant, incorporating both Ile61Ala and the residue 72 mutation most successful at enhancing the differences in binding affinities of the light and dark-adapted crosslinked peptides was proposed, however the poor yield of the Hdm-2 mutant Ile61Ala led us to the conclusion that this additional mutagenesis would not be constructive.

6.3 Determination of the extent of p53 peptide binding with modified Hdm-2 proteins

The fluorescence anisotropy binding assay used for the p53-based peptides with wild-type Hdm-2$_{1-125}$ was employed firstly with the control peptide p53_WT. The dissociation constants for the Hdm-2 mutants are summarised in Table 6.1. No binding was detected for the Hdm-2 mutants with the control, wild-type peptide p53_WT. This implies that the Hdm-2 mutations were effective enough to result in the complete loss in wild-type p53 binding, and that the p53_WT peptide was not α-

helical enough to induce binding through the interactions of Trp23 and Leu26 in the absence of the interactions with Phe19. We therefore decided to compare the binding of the *i,i*+4 spaced peptides, since the proposed mechanism of binding involving the positioning of the peptide deeper within the hydrophobic cleft of Hdm-2 was proposed to promote the optimal geometry for binding interactions to occur.

Table 6.1: *Binding data for the modified Hdm-2 proteins with selected peptides compared with wild-type Hdm-2 1-125.*

Hdm-2 Mutant	Peptide	K_D (nM)
Gln72	p53_WT	268 ± 49
	p53_twt	11 ± 1
	p53_twt_*i,i*+4_XL LIGHT	27 ± 4
	p53_twt_*i,i*+4_XL DARK	21 ± 2
Gln72Met	p53_WT	NO BINDING
	p53_twt	54 ± 9
	p53_twt_*i,i*+4_XL LIGHT	27 ± 8
	p53_twt_*i,i*+4_XL DARK	57 ± 27
Gln72Asn	p53_WT	NO BINDING
	p53_twt	26 ± 5
	p53_twt_*i,i*+4_XL LIGHT	17 ± 1
	p53_twt_*i,i*+4_XL DARK	33 ± 15
Gln72Leu	p53_WT	NO BINDING
	p53_twt	NO BINDING
	p53_twt_*i,i*+4_XL LIGHT	NO BINDING
	p53_twt_*i,i*+4_XL DARK	NO BINDING

The Gln72Leu mutant showed no binding with any of the peptides indicating that whilst the approximate volume occupied by the replaced Gln side-chain was sufficiently compensated for, the loss in charge and subsequent placement of a hydrophobic residue resulted in an unfavourable environment for the positioning of Phe19 of p53. The binding of the mutant Hdm-2 proteins with the truncated wild-type peptide p53_twt was examined, which binds the wild-type Hdm-2 residues 1-125 with

a K_D of 11 nM (± 1). Whilst p53_twt was able to bind both the Gln72Met and Gln72Asn Hdm-2 mutants, there was an approximate five and two-fold reduction respectively in the p53_twt binding affinity when compared to the wild-type protein (Table 6.1). The Hdm-2 mutant that least affected the binding of p53_twt was Gln72Asn, as previously predicted, since the only change is the reduction in the side-chain length of residue 72 by one carbon atom, and the subsequent change in the orientation of its amide group.

The binding data of the p53-based peptides demonstrates a clear preference for the presence of a hydrophilic residue at position 72 of the Hdm-2 protein. However, table 6.1 shows that binding between this peptide and the hydrophobic mutant Gln72Met is still favoured. We believe that the increase in hydrophobicity is not as great as that experienced with the Hdm-2 mutant Gln72Leu. This tolerance of the p53 *N*-terminal transactivation domain to moderate increases in hydrophobicity enables the positioning of the p53 Phe19 residue within the hydrophobic cleft of Hdm-2 in such a conformation so as to permit the interaction of p53 key residues Trp23 and Leu26 with Hdm-2.

Upon examination of the crosslinked *i,i*+4 spaced peptides, we propose that the reduction in attractive forces of the Hdm-2 mutants for p53 residue Phe19 had permitted a greater degree of control to be exerted over the binding interaction by altering the crosslinker conformation. Indeed, the preference for an α-helical structure when the crosslinker is in the light-induced, *cis* conformation within an *i,i*+4 spaced peptide is highlighted in Table 6.1, where the binding is marginally improved upon the uncrosslinked peptide. It was also found that upon relaxation to the dark-adapted

trans conformation, the binding to both the Gln72Met and Gln72Asn Hdm-2 mutants

was reduced by approximately 50 %.

6.4   Conclusion

The involvement of the p53 residues critical for Hdm-2 binding, in particular Phe19

have been highlighted by the development of Hdm-2 mutant proteins 125 amino acids

in length. These show how the removal or reduction in the ability of Hdm-2 to interact

with p53 residue Phe19, influences the ability of p53 to bind to Hdm-2. The

underlying principle employed in the design of these mutants was that the binding of

p53 to Hdm-2 relies upon the p53 *N*-terminus adopting an α-helical conformation, and

that the deletion of p53 Phe19 has been reported to eliminate p53-Hdm-2 binding.[64]

Based on these findings it was proposed that the inhibition of p53 α-helix formation

arises from the positioning of p53 residue Phe19 within the Hdm-2 hydrophobic cleft

where it then becomes entropically favourable for p53 to adopt an α-helical

conformation. Upon initiation of the formation of the p53 α-helix, p53 residues Trp23

and Leu26 become oriented in such a position so as to form additional helix

stabilising interactions.

By modifying Hdm-2 in such a way it was intended to enhance the difference between

the stabilised and destabilised conformations of the crosslinked peptides. From the

crystal structure of the p53-Mdm-2 complex, interactions were highlighted between

Phe19 of p53 and Hdm-2 residues Gly58, Ile61 (van der Waals), and Gln72 (hydrogen

bonding).[68] We proposed that the simplicity of the Gly58 side-chain, *i.e.* the presence

of a single methyl group, meant that any modifications to Hdm-2 residue 58 would

most likely be too disruptive to the Hdm-2 hydrophobic cleft. This, if not by the

introduction of charged groups, or the change in hydrophobicity, would almost

certainly be due to the increased bulk of other amino acid side-chains with the

exception of Gly. As a result, we decided to focus on Hdm-2$_{1-125}$ residues 61 and 72

since the mutation of residues in these positions offered more flexibility and tolerance

for different amino acid side chains. Four mutants were proposed, firstly mutation of

Ile61 to Ala, and also mutation of Gln72 to Asn, Met and Leu. These were all

successfully generated from the wild-type cDNA and expressed. Upon purification it

was found that while the three Hdm-2 variants with mutation at site 72 all expressed

well, yielding soluble protein in quantities comparable to wild-type Hdm-2$_{1-125}$, the

Hdm-2 Ile61Ala mutant however, precipitated and so further work on this mutant was

discontinued.

We found that all of the Hdm-2 mutants showed no measurable binding affinity to the

wild-type peptide. p53_WT was demonstrated to display a weaker binding affinity to

the wild-type protein than all of the modified p53-based peptides synthesised (K_D =

268 nM ± 49), and it is proposed that the reduction in affinity of the Hdm-2 mutants

for p53 Phe19 prevented the initiation of an α-helix from a predominantly random coil

structure. The decision to then use the most potent wild-type p53-based peptide

(p53_twt) revealed a trend where an increase in hydrophobicity in Hdm-2 residue 72

beyond a certain limit resulted in a reduction in binding affinity. This led to there

being no binding detected between the peptide p53_twt and the Leu72 mutant of

Hdm-2$_{1-125}$.

There are several possible reasons for the loss of binding observed between p53_twt and Hdm-2$_{1-125}$ Gln72Leu. Firstly, the increase in hydrophobicity results in there being no interaction with p53 Phe19 and so no initiation of the α-helix from the free conformation of the peptide. This is unlikely, since the peptide has approximately 34 % α-helicity (calculated from the CD data). It is also possible that the mutation of Gln72 to Leu within Hdm-2$_{1-125}$ results in a change in the conformation of the hydrophobic p53 binding site of the protein, thus preventing the binding of p53 to the Gln72Leu mutant protein. Although this is supported by the fact that no binding was observed for any peptides with the Gln72Leu mutant protein, the suggested conformational change in the structure of Hdm-2$_{1-125}$ Gln72Leu may affect the stability of the protein. As previously discussed, the mutant Hdm-2 protein Gln72Leu was obtained in a yield comparable to the wild-type parent protein, and as a result a conformational change is unlikely. We propose instead that the increase in hydrophobicity arising from the Gln72Leu mutant makes the orientation of p53 residue Phe19 within the Hdm-2 hydrophobic cleft unfavourable promoting additional helix stabilising interactions, such as those involving p53 residues Trp23 and Leu26. This consequently inhibits the adoption of an α-helical structure, preventing p53 binding.

The effect of the Hdm-2 modifications was examined using a crosslinked peptide in both its dark-adapted and light-induced states, where it was found that the binding affinity for the Hdm-2 mutants differed between the peptide conformations. This was much like the result initially intended when designing the D21E modified p53 peptides, however whereas these peptides showed only a slight difference in binding affinities for wild-type Hdm-2$_{1-125}$ when comparing the light and dark-adapted

conformations, the Hdm-2 mutant proteins yielded a greater reduction in their binding affinities for p53_twt_*i,i*+4_XL by approximately 50% when switching to the conformation favouring α-helix destabilisation. These results demonstrate the importance of the flexibility of the p53 peptide structure, where with the wild-type Hdm-2 protein there are sufficient interactions stabilising p53 to permit a less ordered α-helical conformation such as that exhibited by a crosslinked peptide in a destabilised conformation. The improvement in the degree of mutant Hdm-2 binding observed with the helix stabilised crosslinked peptides over the uncrosslinked peptides reinforces the previous hypothesis whereby an induced, increased α-helical structure compensates for the reduced stabilisation of the peptide Phe19 residue, through the improved alignment of residues Trp23 and Leu26. These results reinforce the potential functionality afforded by the attachment of the crosslinker to an appropriately designed peptide. In circumstances in which a binding interaction is facilitated by the adoption of an α-helical structure, the application of a crosslinker to the α-helical motif reduces the significance of the interaction of a particular residue within the peptide required initially to propagate the formation of an α-helical structure.

Whilst the interaction of p53 residue Phe19 with Hdm-2$_{1-125}$ *N*-terminal residues 58, 61 and 72 has been previously reported to induce α-helix formation of the p53 *N*-terminus.[68] This work highlights that a reduction in the interaction of p53 Phe19 with Hdm-2 and the associated reduction in the peptide binding affinity can be compensated for by the introduction of a crosslinker to the p53 peptide in a conformation such that the other key Hdm-2 binding residues of p53 become pre-ordered to permit their additional interactions with the Hdm-2 binding site, even if

this induced conformation is not a true α-helix. This principle supports the results

obtained for the crosslinked peptides involving wild-type Hdm-2$_{1-125}$ whereby there

was little difference in Hdm-2 binding observed between peptides in the light and

dark-adapted conformations. We propose the strength of the interaction of p53 Phe19

with the wild-type Hdm-2 protein brings the additional p53 residues Trp23 and Leu26

required for Hdm-2 binding within a suitable proximity of the p53 binding site of

Hdm-2 to facilitate a binding interaction, regardless of the conformation of the

crosslinker. In effect, the conformation of the crosslinker does not influence the initial

binding behaviour of p53 Phe19 with Hdm-2, leading to the previously described

behaviour of its associated residues resulting in Hdm-2 binding.

CHAPTER 7:

CONCLUSIONS &

FUTURE WORK

The aim of this work was the design of short α-helical peptides based upon the *N*-terminus of the p53 tumour suppressor which function as inhibitors or antagonists of the interaction of p53 with its repressor Hdm-2. Such peptides are only likely to have therapeutic potential if there is an in-built mechanism to control the functionality of the molecules, allowing targeting of only cells with defective apoptosis signalling pathways. Upon reviewing methods of exercising control over peptide secondary structure such as the introduction of side chain constraints and the use of metal clips, it was decided to build upon the work of Zhang *et al.* with the incorporation of a water-soluble photoisomerisable azobenzene crosslinker *via* attachment to the thiol groups of cysteine residues.[141,143,144] By the attachment of the crosslinker to cysteine residues of the appropriate spacing, it was proposed that the secondary structure of the modified p53-based peptides could be switched between a random coil and α-helical conformation by the application of 360 nm UV light.[142]

The α-helix content of the synthesised peptides was monitored using circular dichroism spectroscopy, while the binding between the peptides and $Hdm-2_{1-125}$ was monitored using a fluorescence anisotropy binding assay. A 15 amino acid peptide based on p53 *N*-terminal residues 15-29 showed comparable Hdm-2 affinity to that seen in previous work using this same control peptide, its slight improvement was concluded to be due to the amidation of the *C*-terminus of the peptide providing additional stabilisation. This demonstrated not only the effectiveness of the binding assay, but also that the presence of the 5,6-carboxyfluorescein fluorophore upon the *N*-terminus of the peptides does not negatively impact upon Hdm-2 binding. Using CD spectroscopy it was determined that the free peptide had a low α-helix content, implying that a significant conformational change was required upon binding to Hdm-

2. A variety of other wild-type peptides were synthesised, including a peptide modified by the substitution of the helix destabilising Pro27 for Ala, which showed a four-fold improvement in α-helicity and a significant improvement in Hdm-2 binding. Truncation of the control peptide results in the production of a ten amino acid peptide with a binding affinity 20 times more potent than the 15 amino acid control peptide. Although the truncated peptide showed less α-helicity when compared to the Pro27Ala modified peptide it is proposed that the reduced peptide length enables deeper penetration of the peptide within the Hdm-2 hydrophobic cleft. The lower α-helix content of the free peptide is likely a direct consequence of the reduced length of the truncated wild-type peptide, which would result in a less stable conformation when free in solution.

The incorporation of Cys residues within the modified p53 peptides was based on their inclusion within the peptide sequences in 3 possible spacings. The *i,i*+4 and *i,i*+7 spacing was employed to permit the stabilisation of an α-helical conformation with the attached crosslinker in a light-induced *cis* conformation. The *i,i*+11 spacing was employed to stabilise an α-helical conformation with the crosslinker in a dark-adapted *trans* conformation. The Cys-containing modified uncrosslinked peptides possessed a lower percentage α-helicity and reduced binding affinity for Hdm-2 when compared to the parent wild-type peptides. This is due to the substitution of more helix promoting residues with Cys.

The crosslinking of the cysteine containing peptides resulted in no observed improvement in the peptide secondary structures as observed by CD spectroscopy. Also, little difference in secondary structure was observed for the crosslinked peptides

when comparing the light and dark-adapted conformations. The only exception being the dark-stabilised *i,i*+11 spaced peptides where upon isomerism from *trans* to *cis* there was a 10-15 % reduction in α-helicity. The crosslinked peptides show a clear trend, where the crosslinker conformation favouring α-helix formation shows an increased affinity for Hdm-2 binding over the helix destabilised conformation. This indicates that the peptide is constrained in such a way to be under the influence of the crosslinker despite the lack of observed change in α-helicity. However, the peptide sequence itself gave a greater effect on binding affinity, and so the predicted trend, whereby a general increase in α-helicity results in improved Hdm-2 binding, was not observed. As α-helicity is measured for the free peptide in solution, the attachment of the crosslinker may enforce a constraint upon the peptide regardless of its conformation. Consequently, for such short peptides the dark and light-adapted peptides show little difference in α-helicity. It is worth noting that since the p53 *N*-terminus only adopts an α-helical structure upon binding with Hdm-2 it may therefore be difficult to directly relate the secondary structure of peptides when free in solution with their binding affinities for Hdm-2.

The reason behind the small change in binding affinity on photoswitching was further investigated by the mutation of Hdm-2 in order to weaken the interaction between Hdm-2 and the helix inducing p53 Phe19. As the hydrophobicity of the residue in position 72 of Hdm-2 increased, the binding affinity for p53 peptides was reduced, to the point where Gln72Leu resulted in no binding being detected. We noted that reducing the affinity of Hdm-2 for p53 Phe19 led to an improvement in the degree of photocontrol over the binding affinity of the crosslinked peptides. This provides further evidence for the crosslinker providing a slight yet meaningful change to the

peptide secondary structure, since a reduction in the ability of the Hdm-2 mutants to interact with p53 Phe19 permits a greater binding interaction with residues oriented in the most appropriate conformation. This supports the initial proposal where in peptides with a pre-organised α-helical conformation Trp23 and Leu26 of p53 are able to interact without re-organisation arising from the interaction of p53 Phe19. Indeed, the organisation of p53 Trp23 and Leu26 into an α-helical conformation prior to Hdm-2 binding may achieve the reverse of the initiation of wild-type p53-Hdm-2 binding, whereby it is the interaction between p53 residues Trp23 and Leu26 that facilitates the interaction of Phe19 with Hdm-2.

Since polyalanine forms a stable α-helix, peptides were also synthesised using this as the basis of a helical scaffold for the incorporation of only the amino acids critical for Hdm-2 binding in addition to cysteine residues to enable the attachment of the azobenzene crosslinker. The resulting polyalanine p53 scaffolds showed Hdm-2 binding affinities comparable to the 15 amino acid wild-type p53 peptide. This provides a sound proof-of-principle demonstration for the use of such a scaffold to provide the backbone for an α-helical peptide when the residues involved in the binding interaction are clearly defined. We found that there may be issues with solubility, in particular with longer poly-alanine chains, however there are also advantages associated with structures predominantly containing alanine residues. The simplicity of alanine in addition to there being no need for the protection of the side-chain, means that from a manufacturing perspective costs are reduced when compared to the more complex amino acids. Also from a therapeutic perspective, the stability of the peptides may be improved in the body due to a reduction in the number of protease cleavage sites.

Previous research has shown that the substitution of Trp23 within p53 for chloro-tryptophan (Cl-Trp) significantly increases p53-Hdm-2 binding affinity.[160] Cl-Trp23 was proposed to occupy hydrophobic regions within the Hdm-2 hydrophobic cleft previously exposed when binding to wild-type p53. Further investigation may be conducted with crosslinked peptides analogous to those synthesised in this research, however incorporating Cl-Trp at position 23. The binding affinities for these peptides with the mutant Hdm-2 proteins could be compared with those of the parent peptides to provide supporting data for the significance of the pre-organisation of Trp23 with respect to the binding affinity of p53-based peptides with weakened binding *via* Phe19.

Interestingly, it is proposed that the better inhibitor need not have the strongest affinity for Hdm-2 in circumstances in which a controllable crosslinker is employed. Indeed, if a crosslinked peptide in a helix stabilising conformation were to have a binding affinity comparable to the wild-type peptide, yet the affinity of the helix destabilising conformation was significantly reduced, the gain in increased functionality with respect to the crosslinker is worth more than the loss in binding affinity. An increased binding affinity reduces the degree of control the crosslinker has over the peptide conformation, since a stronger interaction with Hdm-2 can exert a greater influence over the peptide secondary structure than the crosslinker, which may be conflicting. An example of such is when the crosslinker is in a helix destabilising conformation, yet high Hdm-2 binding affinities are still observed. There is potential for further optimisation of the peptide sequences to enhance Hdm-2 binding, or perhaps engineer instability when the crosslinker is attached and in the appropriate helix destabilising conformation. This is a novel approach well worth

considering since the difference in Hdm-2 binding affinity between light and dark-adapted crosslinked peptides was found to increase as the affinity was reduced.

Enhancing the effect of photoswitching a crosslinked peptide may be further investigated by the development of peptides containing cysteine residues in alternative spacings. Woolley *et al.* reported the use of an $i,i+5$ and $i,i+10$ spacing to be theoretically as effective as the $i,i+4$ and $i,i+11$ spacing respectively, however chose not to pursue this further.[141] This is worth examining further since the effectiveness of the spacing of the cysteine residues may depend upon the individual peptide sequences.[141] This method of research is complementary to that mentioned in the previous paragraph, where it was suggested that α-helix instability be engineered within the peptide sequences. However, there are opportunities to explore novel cysteine spacings within the peptides already described in this work that may also result in new orientations of the crosslinker within the p53 binding site of Hdm-2, possibly enhancing also the extent of peptide binding with respect to the conformation of the crosslinked peptide.

This research has yielded short Hdm-2 binding peptides with affinities an order of magnitude greater than a peptide based on wild-type p53. Although the attachment of an azobenzene-based crosslinker has not significantly influenced the peptide secondary structure, its presence is notable when examining the fluorescence anisotropy binding data where the helix stabilising conformation results in a slightly increased affinity of the peptide for Hdm-2$_{1-125}$. Mutation of Hdm-2 has provided supporting evidence for previous work where the initiation of the formation of the p53 α-helix was proposed to commence from the interaction of p53 Phe19 with Hdm-2,

and has yielded information on the reduced degree of photocontrol observed. There is the potential for the future development of Hdm-2 mutants that would enable a more precise degree of tolerance of the Hdm-2 binding site to be calculated with respect to hydrophobicity. Future investigation should also be focussed on the use of polyalanine scaffolds in addition to exploring the impact of optimising the residue at position 19 within the p53 peptides that is occupied by Phe in the wild-type sequence. This is worthwhile since weakening the interaction of the previously reported p53 residue critical for Hdm-2 binding (p53 Phe19) has been shown to only impact slightly upon the p53-Hdm-2 binding interaction in cases where an increased secondary structure with respect to Trp23 and Leu26 is observed. The development of the polyalanine scaffold peptides provides a blank canvas for the optimisation of specific positions within the sequence. This has the potential to provide template for the design of an optimised peptide sequence incorporating the azobenzene crosslinker at specific spacings, where specific residues may be substituted to introduce functionality as opposed to taking a functional sequence and optimising this for improved structure.

APPENDICES

A1 Spectrosopic Characterisation of the Synthesised Azobenzene Crosslinker
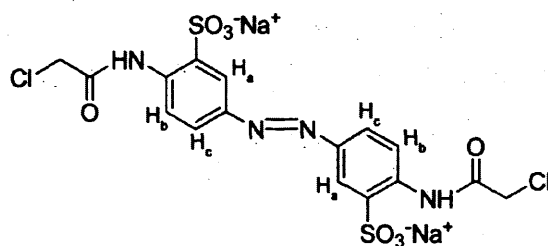
Figure A1.1 – Schematic representation of the crosslinker showing proton assignments used for NMR characterisation.

Synthesis of Compound 2 – 2-Acetylamino-5-aminobenzenesulfonic acid

$C_8H_{10}N_2O_4S$: MW_{calc} = 230.0361, MW_{obs} = 230.2, Yield = 55 %

^1H NMR (500 MHz, DMSO-d_6): CH_3 (2.10 ppm, s, 1H), H_c (7.30 ppm, dd, J = 2.7, 8.7 Hz, 1H), H_a (7.70 ppm, d, J = 2.7 Hz, 1H), H_b (8.40 ppm, d, J = 8.7 Hz, 1H), NH (10.35 ppm, s, 1H).

^{13}C NMR (125 MHz, DMSO-d_6): CH_3 (25 ppm), CH_b (122 ppm), CH_a (123 ppm), CH_c (125 ppm), C_{NH2} (126 ppm), C_{SO3} (135 ppm), $C_{acetamido}$ (136 ppm), C(O) (168 ppm).

Synthesis of Compound 3 – Sodium 3,3'-Bis(sulfonato)-4,4'-bis-(acetamido) azobenzene

$C_{16}H_{15}N_4O_8S_2^-$: MW_{calc} = 455.0366, MW_{obs} = 455.1, Yield = 27 %

^{1}H NMR (500 MHz, D$_2$O): CH$_3$ (2.10 ppm, s, 6H), H$_c$ (7.80 ppm, dd, J = 2.2, 8.4 Hz, 2H), H$_b$ (7.95 ppm, d, J = 8.4 Hz, 2H), H$_a$ (8.12 ppm, d, J = 2.2 Hz, 2H).

^{13}C NMR (125 MHz, D$_2$O): CH$_3$ (25 ppm), CH$_b$ (124 ppm), CH$_a$ (122 ppm), CH$_c$ (126 ppm), C$_{azo}$ (147 ppm), C$_{SO3}$ (136 ppm), C$_{acetamido}$ (134 ppm), C(O) (173 ppm).
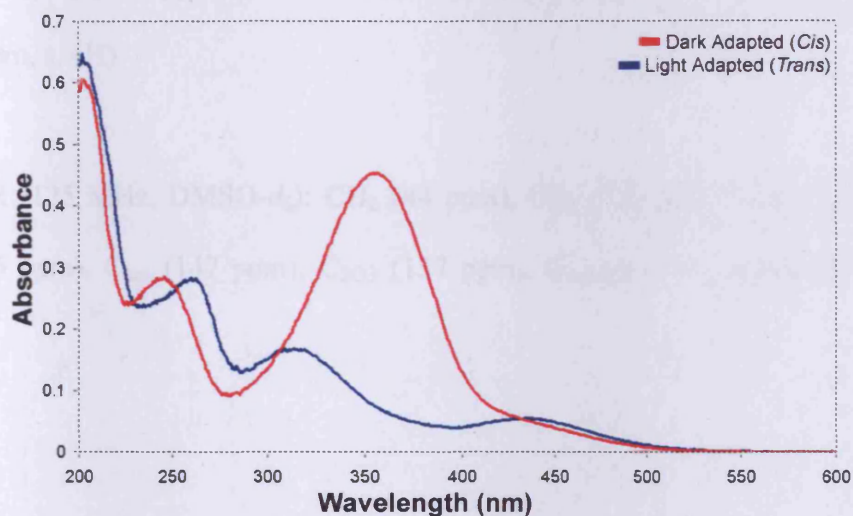
Figure A1.2 – *Azobenzene formation confirmed by UV spectroscopy; irradiation with 360 nm UV light resulted in isomerism from trans (red) to cis (blue)*

Synthesis of Compound 4 – Sodium 3,3'-Bis(sulfonato)-4,4'-bis-(amino) azobenzene

C$_{12}$H$_{11}$N$_4$O$_6$S$_2^-$: MW$_{calc}$ = 371.0125, MW$_{obs}$ = 371.3, Yield = 82 %

^{1}H NMR (500 MHz, DMSO-d_6): H$_c$ (7.55 ppm, dd, J = 2.4, 8.6 Hz, 2H), H$_b$ (6.70 ppm, d, J = 8.6 Hz, 2H), H$_a$ (7.95 ppm, d, J = 2.4 Hz, 2H), NH$_2$ (6.20 ppm, 4H).

^{13}C NMR (125 MHz, DMSO-d_6): CH$_b$ (115 ppm), CH$_a$ (122 ppm), CH$_c$ (125 ppm), C$_{azo}$ (142 ppm), C$_{SO3}$ (148 ppm), C$_{NH2}$ (130 ppm).

Synthesis of Compound 5 – 3,3'-Bis(sulfo)-4,4'-bis-(chloroacetamido) azobenzene

$C_{16}H_{13}N_4O_8S_2Cl_2^-$: MW_{calc} = 522.9557, MW_{obs} = 522.4, Yield = 11 %

^{1}H NMR (500 MHz, DMSO-d_6): CH_2 (4.45 ppm, s, 4H), H_c (8.00 ppm, dd, J = 2.4, 8.8 Hz, 2H), H_b (8.60 ppm, d, J = 8.8 Hz, 2H), H_a (8.20 ppm, d, J = 2.4 Hz, 2H), NH (11.20 ppm, s, 4H).

^{13}C NMR (125 MHz, DMSO-d_6): CH_2 (44 ppm), CH_b (121 ppm), CH_a (120 ppm), CH_c (126 ppm), C_{azo} (147 ppm), C_{SO3} (137 ppm), $C_{acetamido}$ (137 ppm), C(O) (165 ppm).

A2   Hdm-2$_{1-125}$ Amino Acid Analysis Data

Amino Acid	nmol ml^{-1}	µg ml^{-1}
Aspartic acid	73.200	8.43
Threonine	58.100	5.87
Serine	77.100	6.72
Glutamic acid	96.400	12.40
Proline	29.100	2.83
Glycine	49.700	2.84
Alanine	22.800	1.62
Cysteine	2.0300	0.45
Valine	67.000	6.64
Methionine	4.580	0.60
Isoleucine	25.000	2.83
Leucine	75.400	8.54
Tyrosine	34.700	5.66
Phenylalanine	17.100	2.52
Histidine	43.600	5.98
Tryptophan	-	-
Lysine	52.600	6.74
Arginine	21.700	3.39
TOTAL	750.000	84.10

Notes:

Asn and Gln are converted to Asp and Glu during acid hydrolysis of the protein

Values for Thr and Ser are corrected for hydrolysis losses of 5 % and 10 % respectively

Trp suffers complete loss during hydrolysis and is therefore not quantified

A3 Determination Of The Half-Lives Of The *Cis* Isomer Of Crosslinked Peptides

Azobenzene Crosslinker

Temp (K)	k	$t_{1/2}$ (min)
277	3.04×10^{-4}	36.91
283	4.90×10^{-4}	23.58
288	5.71×10^{-4}	20.24
293	8.06×10^{-4}	14.33
298	9.91×10^{-4}	11.65
303	11.4×10^{-4}	10.91
310	13.6×10^{-4}	8.76

p53_twt_*i*,i+4_XL

Temp (K)	k	$t_{1/2}$ (min)
277	1.32×10^{-4}	87.63
283	1.52×10^{-4}	72.96
288	1.79×10^{-4}	64.60
293	2.50×10^{-4}	46.18
298	3.02×10^{-4}	38.23
303	3.17×10^{-4}	36.39
310	3.85×10^{-4}	29.97

p53_P27A_*i*,i+7_XL

Temp (K)	k	$t_{1/2}$ (min)
277	8.86×10^{-5}	141.17
283	9.53×10^{-5}	121.18
288	1.20×10^{-4}	96.4
293	1.58×10^{-4}	73.35
298	2.12×10^{-4}	57.81
303	2.04×10^{-4}	56.68
310	2.67×10^{-4}	43.19

p53_D21E_*i*,i+7_XL

Temp (K)	k	$t_{1/2}$ (min)
277	1.06×10^{-4}	109.33
283	1.28×10^{-4}	97.35
288	1.30×10^{-4}	89.09
293	1.48×10^{-4}	78.06
298	1.82×10^{-4}	63.36
303	1.96×10^{-4}	58.94
310	2.11×10^{-4}	54.88

p53_D21E_*i*,i+7_XL 10 % TFE

Temp (K)	k	$t_{1/2}$ (min)
277	7.98×10^{-5}	144.71
283	1.02×10^{-4}	112.71
288	1.11×10^{-4}	104.23
293	1.25×10^{-4}	92.17
298	1.31×10^{-4}	83.51
303	1.58×10^{-4}	73.27
310	2.18×10^{-4}	53.03

p53_D21E_*i*,i+7_XL 20 % TFE

Temp (K)	k	$t_{1/2}$ (min)
277	6.02×10^{-5}	222.16
283	7.91×10^{-5}	146.23
288	8.42×10^{-5}	137.26
293	8.52×10^{-5}	135.65
298	9.71×10^{-5}	119.10
303	1.14×10^{-4}	101.04
310	2.35×10^{-4}	56.68

p53_D21E_*i*,i+7_XL 30 % TFE

Temp (K)	k	$t_{1/2}$ (min)
277	6.46×10^{-5}	178.65
283	7.39×10^{-5}	156.11
293	7.76×10^{-5}	148.74
298	8.07×10^{-5}	143.21
303	8.83×10^{-5}	130.78
310	1.08×10^{-4}	106.97

p53_P27A_*i*,i+11_XL

Temp (K)	k	$t_{1/2}$ (min)
277	7.71×10^{-5}	150.03
283	8.06×10^{-5}	143.51
288	8.33×10^{-5}	138.63
293	1.25×10^{-4}	92.30
298	1.49×10^{-4}	77.71
303	1.68×10^{-4}	68.83
310	2.28×10^{-4}	50.78

p53_D21E_*i*,i+11_XL

Temp (K)	k	$t_{1/2}$ (min)
277	8.05×10^{-5}	143.51
283	9.07×10^{-5}	127.42
288	1.13×10^{-4}	101.93
293	1.23×10^{-4}	94.31
298	1.33×10^{-4}	86.75
303	2.03×10^{-4}	56.82
310	2.91×10^{-4}	39.70

REFERENCES

(1)   Lockshin, R. A. Williams, C. M. Programmed cell death. II. Endocrine potentiation of the breakdown of the intersegmental muscles of silkmoths *J. Insect Physiol* **1964**, *10*, 643-649.

(2)   Kerr, J. F. Wyllie, A. H. Currie, A. R. Apoptosis: A basic biological phenomenon with wide-ranging implications in tissue kinetics *Br. J. Cancer* **1972**, *26*, 239-257.

(3)   Vaux, D. L. Korsmeyer, S. J. Cell Death in Development *Cell* **1999**, *96*, 245-254.

(4)   Zuzarte-Luis, V. Hurle, J. M. Programmed cell death in the developing limb *Int. J. Dev. Biol* **2002**, *46*, 871-876.

(5)   Rathmell, J. C. Thompson, C. B. Pathways of apoptosis in lymphocyte development, homeostasis and disease. *Cell* **2002**, *109(Suppl)*, S97-107.

(6)   Saraste, A. Pulkki, K. Morphologic and biochemical hallmarks of apoptosis *Cardiovasc. Res.* **2000**, *45*, 528-537.

(7)   Leist, M. Jaattela, M. Four deaths and a funeral: from caspases to alternative mechanisms *Nat. Rev. Mol. Cell Biol.* **2001**, *2*, 589-598.

(8)   Reed, J. C. Apoptosis-based therapies *Nat. Rev. Drug Discov* **2002**, *1*, 111-121.

(9)   Müllauer, L. Gruber, P. Sebinger, D. Buch, J. Wohlfart, S. Chott, A. Mutations in apoptosis genes: a pathogenetic factor for human disease *Mutation Research* **2001**, *488*, 211-231.

(10)   Vousden, K. H. Lu, X. Live or Let Die: The Cell's Response to p53 *Nat. Rev. Cancer* **2002**, *2*, 594-604.

(11)   Gewies, A. Introduction to Apoptosis *ApoReview* **2003**, 1-26.

(12)   Hirsch, T. Marchetti, P. Susin, S. A. Dallaporta, B. Zamzami, N. Marzo, I. Geuskens, M. Kroemer, G. The apoptosis-necrosis paradox. Apoptogenic proteases activated after mitochondrial permeability transition determine the mode of cell death. *Oncogene* **1997**, *15*, 1573-1581.

(13)   Woo, M. Hakem, R. Soengas, M. S. Duncan, G. S. Shahinian, A. Kagi, D.
         Hakem, A. McCurrach, M. Khoo, W. Kaufman, S. A. Senaldi, G. Howard, T.
         Lowe, S. W. Mak, T. W. Essential contribution of caspase 3/CPP32 to
         apoptosis and its associated nuclear changes *Genes & Dev.* **1998**, *12*, 806-819.

(14)   Janicke, R. U. Sprengart, M. L. Wati, M. R. Porter, A. G. Caspase-3 Is
         Required for DNA Fragmentation and Morphological Changes Associated
         with Apoptosis *J. Biol. Chem.* **1998**, *273*, 9357-9360.

(15)   Bratton, S. B. Macfarlane., M. Cain, K. Cohen, G. M. Protein complexes
         activate distinct caspase cascades in death receptor and stress-induced
         apoptosis *Exp. Cell Res.* **2000**, *256*, 27-33.

(16)   Denault, J. B. Salvesen, G. S. Caspases: keys in the ignition of cell death
         Chem. Rev. **2002**, *102*, 4489-4500.

(17)   Lazebnik, Y. A. Cole, S. Cooke, C. A. Nelson, W. G. Earnshaw, W. C.
         Nuclear Events of Apoptosis In Vitro in Cell-free Mitotic Extracts: A Model
         System for Analysis of the Active Phase of Apoptosis *J. Cell Biol.* **1993**, *123*,
         7-22.

(18)   Solary, E. Bertrand, R. Kohn, K. W. Pommier, Y. Differential Induction of
         Apoptosis in Undifferentiated and Differentiated HL-60 Cells by DNA
         Topoisomerase I and II Inhibitors *Blood* **1993**, *81*, 1359-1368.

(19)   Sartorius, U. Schmitz, I. Krammer, P. H. Molecular mechanisms of death-
         receptor-mediated apoptosis *Chembiochem* **2001**, *2*, 20-29.

(20)   Scaffidi, C. Fulda, S. Srinivasan, A. Friesen, C. Li, F. Tomaselli, K. J.
         Debatin, K. M. Krammer, P. H. Peter, M. E. Two CD95 (APO-1/Fas)
         signaling pathways *Embo J.* **1998**, *17*, 1675-1687.

(21)   Kaufmann, S. H. Earnshaw, W. C. Induction of Apoptosis by Cancer
         Chemotherapy *Exp. Cell Res.* **2000**, *256*, 42-49.

(22)   Li, H. Zhu, H. Xu, C. Yuan, J. Cleavage of BID by Caspase 8 Mediates the
         Mitochondrial Damage in the Fas Pathway of Apoptosis *Cell* **1998**, *94*, 491-
         501.

(23)   Strasser, A. O'Connor, L. Dixit, V. M. Apoptosis signalling *Annu. Rev.
         Biochem.* **2000**, *69*, 217-245.

(24)   Susin, S. A. Lorenzo, H. K. Zamzami, N. Marzo, I. Snow, B. E. Brothers, G.
M. Mangion, J. Jacotot, E. Costantini, P. Loeffler, M. Larochette, N. Goodlett,
D. R. Aebersold, R. Siderovski, D. P. Penninger, J. M. Kroemer, G. Molecular
characterization of mitochondrial apoptosis-inducing factor. *Nature* **1999**, *397*,
441-446.

(25)   Green, D. R. Reed, J. C. Mitochondria and Apoptosis *Science* **1998**, *281*,
1309-1312.

(26)   Kroemer, G. Zamzami, N. Susin, S. A. Mitochondrial control of apoptosis
Immunol. Today **1997**, *18*, 44-51.

(27)   Dinsdale, D. Zhuang, J. Cohen, G. M. Redistribution of Cytochrome c
Precedes the Caspase-Dependent Formation of Ultracondensed Mitochondria,
with a Reduced Inner Membrane Potential, in Apoptotic Monocytes *Am. J.
Pathol* **1999**, *155*, 607-618.

(28)   Kroemer, G. Petit, P. Zamzami, N. Vayssiere, J. L. Mignotte, B. The
Biochemistry of Programmed Cell Death *FASEB. J.* **1995**, *9*, 1277-1287.

(29)   Loeffler, M. Kroemer, G. The Mitochondrion in Cell Death Control:
Certainties and Incognita *Exp. Cell Res.* **2000**, *256*, 19-26.

(30)   Salvesen, G. S. Renatus, M. Apoptosome: the seven-spoken death machine
Dev. Cell **2002**, *2*, 256-257.

(31)   Acehan, D. Jiang, X. Morgan, D. G. Heuser, J. E. Wang, X. Akey, C. W.
Three-dimensional structure of the apoptosome: implications for assembly,
procaspase-9 binding, and activation. *Mol. Cell* **2002**, *9*, 423-432.

(32)   Xiang, J. Chao, D. T. Korsmeyer, S. J. BAX-induced cell death may not
require interleukin 1b-converting enzyme-like proteases *93* **1996**, *25*, 44559-
44563.

(33)   McCarthy, N. J. Whyte, M. K. B. Gilbert, C. S. Evan G. I. Inhibition of Ced-
3/ICE-related Proteases Does Not Prevent Cell Death Induced by Oncogenes,
DNA Damage, or the Bcl-2 Homologue Bak *J. Cell Biol.* **1997**, *136*, 215-227.

(34)   Brunet, C. L. Gunby, R. H. Benson, R. S. P. Hickman, J. A. Watson, A. J. M.
        Brady, G. Commitment to cell death measured by loss of clonogenicity is
        separable from the appearance of apoptotic markers *Cell Death & Differen.*
        1998, *5*, 107-115.

(35)   Amarante-Mendes, G. P. Finucane, D. M. Martin, S. J. Cotter, T. G. Salvesen,
        G. S. Green, D. R. Anti-apoptotic oncogenes prevent caspase-dependent and
        independent commitment for cell death *Cell Death & Differen.* **1998**, *5*, 298-
        306.

(36)   Hengartner, M. O. The biochemistry of apoptosis. *Nature* **2000**, *407*, 770-776.

(37)   Nicotera, P. Leist, M. Manzo, L. Neuronal cell death: a demise with different
        shapes *Trends Pharmacol Sci* **1999**, *20*, 46-51.

(38)   Ameisen, J. C. On the origin, evolution, and nature of programmed cell death:
        a timeline of four billion years *Cell Death & Differen.* **2002**, *9*, 367-393.

(39)   Vaux, D. L. Cory, S. Adams, J. M. Bcl-2 gene promotes haemopoietic cell
        survival and cooperates with c-*myc* to immortalize pre-B cells *Nature* **1988**,
        335, 440-442.

(40)   Hockenbery, D. Nunez, G. Millman, C. Schreiber, R. D. Korsmeyer, S. J. Bcl-
        2 is an inner mitochondrial membrane protein that blocks programmed cell
        death *Nature* **1990**, *348*, 334-336.

(41)   Borner, C. The Bcl-2 protein family: sensors and checkpoints for life-or-death
        decisions *Molecular Immunology* **2003**, *39*, 615-647.

(42)   Huang, D. C. Strasser, A. BH3-only proteins - essential initiators of apoptotic
        cell death. *Cell* **2000**, *103*, 839-842.

(43)   Antonsson, B. Montessuit, S. Sanchez, B. Martinou, J. C. Bax is present as a
        high molecular weight oligomer/complex in the mitochondrial membrane of
        apoptotic cells. *J. Biol. Chem.* **2001**, *276*, 11615-11623.

(44)   Lane, D. P. p53, guardian of the genome *Nature* **1992**, *358*, 15-16.

(45)   Wu, Y. Mehew, J. W. Heckman, C. A. Arcinas, M. Boxer, L. M. Negative regulation of bcl-2 expression by p53 in hematopoietic cells *Oncogene* **2001**, *20*, 240-251.

(46)   Mihara, M. Erster, S. Zaika, A. Petrenko, O. Chittenden, T. Pancoska, P. Moll, U. M. p53 Has a Direct Apoptogenic Role at the Mitochondria *Mol. Cell* **2003**, *11*, 577-590.

(47)   Chène, P. Inhibiting The p53–Mdm2 Interaction: An Important Target For Cancer Therapy *Nat. Rev. Cancer* **2003**, *3*, 102-109.

(48)   Tidow, H. Melero, R. Mylonas, E. Freund, S. M. Grossmann, J. G. Carazo, J. M. Svergun, D. I. Valle, M. Fersht, A. R. Quaternary structures of tumor suppressor p53 and a specific p53–DNA complex *PNAS* **2007**, *104*, 12324-12329.

(49)   Olivier, M. Eeles, R. Hollstein, M. Khan, M. A. Harris, C. C. Hainaut, P. The IARC TP53 database: new online mutation analysis and recommendations to users *Hum. Mutat.* **2002**, *19*, 607-614.

(50)   Yu, G. W. Rudiger, S. Veprintsev, D. Freund, S. Fernandez-Fernandez, M. R. Fersht, A. R. The central region of HDM2 provides a second binding site for p53 *PNAS* **2006**, *103*, 1227-1232.

(51)   Banin, S. Moyal, L. Shieh, S. Taya, Y. Anderson, C. W. Chessa, L. Smorodinsky, N. I. Prives, C. Reiss, Y. Shiloh, Y. Ziv, Y. Enhanced phosphorylation of p53 by ATM in response to DNA damage *Science* **1998**, *281*, 1674-1677.

(52)   Shieh, S. Y. Ikeda, M. Taya, Y. Prives, C. DNA damage-induced phosphorylation of p53 alleviates inhibition by MDM2 *Cell* **1997**, *91*, 325-334.

(53)   Sakamuro, D. Sabbatini, P. White, E. Prendergast, G. C. The polyproline region of p53 is required to activate apoptosis but not growth arrest. *Oncogene* **1997**, *15*, 887-898.

(54)   Chen, X. Ko, L. J. Jayaraman, L. Prives, C. p53 levels, functional domains, and DNA damage determine the extent of the apoptotic response of tumor cells *Genes & Dev.* **1996**, *10*, 2438-2451.

(55)   Montes de Oca Luna, R. Wagner, D. S. Lozano, G. Rescue of early embryonic
        lethality in mdm2-deficient mice by deletion of p53 *Nature* **1995**, *378*, 203-
        206.

(56)   Ginsberg, D. E2F1 pathways to apoptosis *FEBS Letters* **2002**, *529*, 122-125.

(57)   Marchetti, A. Buttitta, F. Girlando, S. Palma, P. D. Pellegrini, S. Fina, P.
        Doglioni, C. Bevilacqua, G. Barbareschi, M. mdm2 gene alterations and
        mdm2 protein expression in breast carcinomas *J. Pathol* **1995**, *175*, 31-38.

(58)   Bueso-Ramos, C. E. deLeon, Y. Y. E. McCowm, P. Stass, S. Albitar, M. The
        human MDM-2 oncogene is overexpressed in leukemias *Blood* **1993**, *82*,
        2617-2623.

(59)   Oliner, J. D. Kinzler, K. W. Meltzer, P. S. Vogelstein, G. B. Amplification of
        a gene encoding a p53-associated protein in human sarcomas *Nature* **1992**,
        358, 80-83.

(60)   Leach, F. S. Tokino, T. Meltzer, P. Burrell, M. Oliner, J. D. Smith, S. Hill, D.
        E. Sidransky, D. Kinzler, K. W. Vogelstein, B. p53 Mutation and MDM2
        Amplification in Human Soft Tissue Sarcomas1 *Cancer Res* **1993**, *53*, 2231-
        2234.

(61)   Fang, S. Jensen, J. P. Ludwig, R. L. Vousden, K. H. Weissman, A. M. Mdm2
        is a RING finger-dependent ubiquitin protein ligase for itself and p53 *J. Biol.
        Chem.* **2000**, *275*, 8945-8951.

(62)   Hay, T. J. Meek, D. W. Multiple sites of in vivo phosphorylation in the
        MDM2 oncoprotein cluster within two important functional domains *FEBS
        Letters* **2000**, *478*, 183-186.

(63)   Meek, D. W. Knippschild, U. Posttranslational modification of MDM2 *Mol.
        Cancer Res.* **2003**, *1*, 1017-1026.

(64)   Lin, J. Chen, J. Elenbaas, B. Levine, A. J. Several hydrophobic amino acids in
        the p53 amino-terminal domain are required for transcriptional activation,
        binding to mdm-2 and the adenovirus 5 E1B 55-kD protein *Genes & Dev.*
        1994, *8*, 1235-1246.

(65)   Picksley, S. M. Vojtesek, B. Sparks, A. Lane, D. P. Immunochemical analysis of the interaction of p53 with MDM2;--fine mapping of the MDM2 binding site on p53 using synthetic peptides *Oncogene* **1994**, *9*, 2523-2529.

(66)   Oliner, J. D. Pietenpol, J. A. Thiagalingam, S. Gyuris, J. Kinzler, K. W. Vogelstein, B. Oncoprotein MDM2 conceals the activation domain of tumour suppressor p53 *Nature* **1993**, *362*, 857-860.

(67)   Chen, J. Marechal, V. Levine, A. J. Mapping of the p53 and mdm-2 interaction domains *Mol. Cell* **1993**, *13*, 4107-4114.

(68)   Kussie, P. H. Gorina, S. Marechal, V. Elenbaas, B. Moreau, J. Levine, A. J. Pavletich, N. P. Structure of the MDM2 Oncoprotein Bound to the p53 Tumour Suppressor Transactivation Domain *Science* **1996**, *274*, 948-953.

(69)   Uhrinova, S. Uhrin, D. Powers, H. Watt, K. Zheleva, D. Fischer, P. McInnes, C. Barlow, P. N. Structure of Free MDM2 N-terminal Domain Reveals Conformational Adjustments that Accompany p53-binding *J. Mol Biol* **2005**, *350*, 587-598.

(70)   Schon, O. Friedler, A. Bycroft, M. Freund, S. M. V. Fersht, A. R. Molecular Mechanism of the Interaction between MDM2 and p53 *J. Mol Biol* **2002**, *323*, 491-501.

(71)   Schon, O. Friedler, A. Freund, S. Fersht, A. R. Binding of p53-derived Ligands to MDM2 Induces a Variety of Long Range Conformational Changes *J. Mol Biol* **2004**, *336*, 197-202.

(72)   Bottger, V. Bottger, A. Howard, S. F. Picksley, S. M. Chene, P. Echeverria, C. G. Hochkeppel, H. K. Lane, D. P. Identification of novel mdm2 binding peptides by phage display *Oncogene* **1996**, *13*, 2141-2147.

(73)   Liu, W. L. Midgley, C. Stephen, C. Saville, M. Lane, D. P. Biological Significance of a Small Highly Conserved Region in the N Terminus of the p53 Tumour Suppressor Protein *J. Mol Biol* **2001**, *313*, 711-731.

(74)   Bottger, A. Bottger, V. Echeverria, C. G. Chene, P. Hochkeppel, H. K. Sampson, W. Ang, K. Howard, S. F. Picksley, S. M. Lane, D. P. Molecular Characterization of the hdm2-p53 Interaction *J. Mol Biol* **1997**, *269*, 744-756.

(75) Lai, Z. Auger, K. R. Manubay, C. M. Copeland, R. A. Thermodynamics of p53 Binding to hdm2(1-126): Effects of Phosphorylation and p53 Peptide Length *Archives of Biochemistry and Biophysics* **2000**, *381*, 278-284.

(76) Lu, H. Levine, A. J. Human TAF1131 protein is a transcriptional coactivator of the p53 protein *PNAS* **1995**, *92*, 5154-5158.

(77) Sakaguchi, K. Saito, S. Higashimoto, Y. Roy, S. Anderson, C. W. Appella, E. Damage-mediated Phosphorylation of Human p53 Threonine 18 through a Cascade Mediated by a Casein 1-like Kinase *J. Biol. Chem.* **2000**, *275*, 9278-9283.

(78) Bargonetti, J. Manfredi, J. J. Multiple roles of the tumour suppressor p53 *Curr. Opinion in Oncology* **2002**, *14*, 86-91.

(79) Oren, M. Regulation of the p53 Tumor Suppressor Protein *J. Biol. Chem.* **1999**, *274*, 36031-36034.

(80) Vassilev, L. T. Vu, B. T. Graves, B. Carvajal, D. Podlaski, F. Filipovic, Z. Kong, N. Kammlott, U. Lukacs, C. Klein, C. Fotouhi, N. Liu, E. A. In Vivo Activation of the p53 Pathway by Small-Molecule Antagonists of MDM2 *Science* **2004**, *303*, 844-848.

(81) Stoll, R. Renner, C. Hansen, S. Palme, S. Klein, C. Belling, A. Zeslawski, W. Kamionka, M. Rehm, T. Mühlhahn, P. Schumacher, R. Hesse, F. Kaluza, B. Voelter, W. Engh, R. A. Holak, T. A. Chalcone Derivatives Antagonize Interactions between the Human Oncoprotein MDM2 and p53 *Biochemistry* **2001**, *40*, 336-344.

(82) Garcia-Echeverria, C. Chene, P. Blommers, M.J.J. Furet, P. Discovery of potent antagonists of the interaction between human double minute 2 and tumor suppressor p53 *J. Med. Chem* **2000**, *43*, 3205-3208.

(83) Myers, M. C. Wang, J. Iera, J. A. Bang, J. Hara, T. Saito, S. Zambetti, G. P. Appella, D. H. A New Family of Small Molecules To Probe the Reactivation of Mutant p53 *J. Am. Chem. Soc* **2005**, *127*, 6152-6153.

(84) Wang, H. Yu, D. Agrawal, S. Zhang, R. Experimental Therapy of Human Prostate Cencer by Inhibiting MDM2 Expression With Novel Mixed-Backbone Antisense Oligonucleotides: In Vitro and In Vivo Activities and Mechanisms *The Prostate* **2003**, *54*, 194-205.

(85)   Kutzki, O. Park, H. S. Ernst, J. T. Orner, B. P. Yin, H. Hamilton, A. D. Development of Potent Bcl-x_L Antagonist Based on α-Helix Mimicry *J. Am. Chem. Soc* **2002**, *124*, 11838-11839.

(86)   Yin, H. Hamilton, A. D. Terephthalamide derivatives as mimetics of the helical region of Bak peptide target Bcl-xL protein *Bioorg. Med. Chem. Lett.* **2004**, *14*, 1375-1379.

(87)   Ernst, J. T. Becerril, J. Park, H. S. Yin, H. Hamilton, A. D. Design and Application of an α-Helix-Mimetic Scaffold Based on an Oligoamide-Foldamer Strategy: Antagonism of the Bak BH3/Bcl-x_L Complex *Angew. Chem. Int. Ed.* **2003**, *42*, 535-539.

(88)   Orner, B. P. Ernst, J. T. Hamilton, A. D. Toward Proteomimetics: Terphenyl Derivatives as Structural and Functional Mimics of Extended Regions of an α-Helix *J. Am. Chem. Soc* **2001**, *123*, 5382-5383.

(89)   Yin, H. Lee, G. Park, H. S. Payne, G. A. Rodriguez, J. M. Sebti, S. M. Hamilton, A. D. Terphenyl-Based Helical Mimetics That Disrupt the p53/HDM2 Interaction *Angew. Chem* **2005**, *117*, 2764-2767.

(90)   Chin, J. W. Schepartz, A. Design and Evolution of a Miniature Bcl-2 Binding Protein *Angew. Chem. Int. Ed.* **2001**, *40*, 3806-3809.

(91)   Böttger, A. Bottger, V. Sparks, A. Liu, W. L. Howard, S. F. Lane, D. P. Design of a synthetic Mdm2-binding mini protein that activates the p53 response in vivo *Curr. Biology* **1997**, *7*, 860-869.

(92)   Wasylyk, C. Salvi, R. Argentini, M. Dureuil, C. Delumeau, I. Abecassis, J. Debussche, L. Wasylyk, B. p53 mediated death of cells overexpressing MDM2 by an inhibitor of MDM2 interaction with p53 *Oncogene* **1999**, *18*, 1921-1934.

(93)   Chene, P. Fuchs, J. Bohn, J. GarcôÂa-EcheverrôÂa, C. Furet, P. Fabbro, D. A Small Synthetic Peptide, which Inhibits the p53-hdm2 Interaction, Stimulates the p53 Pathway in Tumour Cell Lines *J. Mol Biol* **2000**, *299*, 245-253.

(94)   Hara, T. Durell, S. R. Myers, M. C. Appella, D. H. Probing the Structural Requirements of Peptoids That Inhibit Hdm-2-p53 interactions *J. Am. Chem. Soc* **2006**, *128*, 1995-2004.

(95) Miller, S. M. Simon, R. J. Simon, N. G. Zuckermann, R. N. Kerr, J. M. Moos, W. H. Comparison of the proteolytic susceptibilities of homologous L-amino acid, D-amino acid, and N-substituted glycine peptide and peptoid oligomers *Drug Dev Res* **1995**, *35*, 20-32.

(96) Armand, P. Kirschenbaum, K. Falicov, A. Dunbrack, R. L. Dill, K. A. Zuckermann, R. N. Cohen, F. E. Chiral N-substituted glycines can form stable helical conformations *Folding & Design* **1997**, *2*, 369-375.

(97) Sadowsky, J. D. Fairlie, W. D. Hadley, E. B. Lee, H. S. Umezawa, N. Coleska, Z. N. Wang, S. Huang, D. C. S. Tomita, Y. Gellman, S. H. (α/β+α)-Peptide Antagonists of BH3 Domain/Bcl-x$_L$ Recognition: Toward General Strategies for Foldamer-Based Inhibition of Protein-Protein Interactions *J. Am. Chem. Soc* **2007**, *129*, 139-154.

(98) Ramachandran, G. N. Ramakrishnan, C. Sasisekharan, V. Stereochemistry of polypeptide chain configurations *J. Mol Biol* **1963**, *7*, 95-99.

(99) Fersht, A. *Structure and mechanism in protein science: A guide to enzyme catalysis and protein folding*; W. H. Freeman and Company: NY, **1998**.

(100) Scholz, A. Baldwin, R. L. The Mechanism of α-Helix Formation by Peptides *Annu. Rev. BioPhys. and Biomol. Structure* **1992**, *21*, 95-118.

(101) Chou, P. Y. Fasman, G. D. Prediction of protein conformation *Biochemistry* **1974**, *13*, 222-245.

(102) Chou, P. Y. Fasman, G. D. Empirical predictions of protein conformation *Annu. Rev. Biochem.* **1978**, *47*, 251-276.

(103) Chou, P. Y. Fasman, G. D. Prediction of the secondary structure of proteins from their amino acid sequence *Adv. Enzymol. Relat. Areas Mol. Biol.* **1978**, *47*, 145-148.

(104) Garnier, J. Osguthorpe, D. J. Robson, B. Analysis of the accuracy and implications of simple methods for predicting the secondary structure of globular proteins *J. Mol Biol* **1978**, *120*, 97-120.

(105) O'Niel, K. T. Degrado, W. F. A Thermodynamic Scale for the Helix-Forming Tendencies of the Commonly Occuring Amino Acids *Science* **1990**, *250*, 646-651.

(106) Miller, J. S. Kennedy, R. J. Kemp, D. S. Short, Solubilizing Polyalanines Are Conformational Chameleons: Exceptionally Helical If N- and C- Capped with Helix Stabilizers, Weakly to Moderately Helical if Capped with Rigid Spacers *Biochemistry* **2001**, *40*, 305-309.

(107) Beyer, R. L. Hoang, H. N. Appleton, T. G. Fairlie, D. P. Metal Clips Induce Folding of a Short Unstructured Peptide into an α-Helix via Turn Conformations in Water. Kinetic versus Thermodynamic Products *J. Am. Chem. Soc* **2004**, *126*, 15096-15105.

(108) Callewaert, G. L. Shipolini, R. Veron, C. A. The Disulphide Bridges of Apamin *FEBS Letters* **1968**, *1*, 111-113.

(109) Miroshnikov, A. I. Elyakova, E. G. Kudelin, A. B. Senyavina, L. B. A Study of the Physiochemical Characteristics of the Neurotoxin Apamin from the Venom of the Honeybee *Apis Mellifica* **1978**, *4*, 1022-1028.

(110) Pease, J. H. B. Wemmer, D. E. Solution Structure of Apamin Determined by Nuclear Magnetic Resonance and Distance Geometry *Biochemistry* **1988**, *27*, 8491-8498.

(111) Nicoll, A. J. Miller, D. J. Fütterer, K. Ravelli, R. Allemann, R. K. Designed High Affinity Cu^{2+}-Binding α-Helical Foldamer *J. Am. Chem. Soc* **2006**, *128*, 9187-9193.

(112) Cureton, C. H. Weston, C. J. Allemann, R. K. Smart, O. S. De Novo Design and Characterization of a Peptide with a Disulfide-Stabilized *N*-Terminal α-Helix *Biophys. J.* **2003**, *84*, 311A-A.

(113) Seltzer, S. Hamilton, G. A. Westheimer, F. H. Isotope Effects in the Enzymatic Decarboxylation of Oxalacetic Acid *J. Am. Chem. Soc* **1959**, *81*, 4018-4124.

(114) Westheimer, F. H. Coincidences, Decarboxylation and Electrostatic Effects *Tetrahedron* **1995**, *51*, 3-20.

(115) Johnsson, K. Allemann, R. K. Widmer, H. Benner, S. A. Synthesis, Structure and Activity of Artificial, Rationally Designed Catalytic Polypeptides *Nature* **1993**, *365*, 530-532.

(116) Taylor, S. E. Rutherford, T. J. Allemann, R. K. Design, Synthesis and Characterisation of a Peptide with Oxaloacetate Decarboxylase Activity *Bioorg. Med. Chem. Lett.* **2001**, *11*, 2631-2635.

(117) Blundell, T. L. Pitts, J. E. Tickle, I. J. Wood, S. P. Wu, C. W. X-Ray Analysis (1.4Å Resolution) of Avian Pancreatic Polypeptide - Small Globular Protein Hormone *PNAS* **1981**, *78*, 4175-4179.

(118) Taylor, S. E. Rutherford, T. J. Allemann, R. K. Design of a Folded, Conformationally Stable Oxaloacetate Decarboxylase *J. Chem. Soc. - Perkin Trans.* **2002**, *2*, 751-755.

(119) Li, X. Sutcliffe, M. J. Schwartz, T. W. Dobson, C. M. Sequence-Specific H-1-NMR Assignments and Solution Structure of Bovine Pancreatic Polypeptide *Biochemistry* **1992**, *31*, 1245-1253.

(120) Zondlo, N. J. Schepartz, A. Highly Specific DNA Recognition by a Designed Miniature Protein *J. Am. Chem. Soc* **1999**, *121*, 6938-6939.

(121) Montclare, J. K. Schepartz, A. Miniature Homeodomains: High Specificity without an N-Terminal Arm *J. Am. Chem. Soc* **2003**, *125*, 3416-3417.

(122) Kritzer, J. A. Zutshi, R. Cheah, M. Ran, F. A. Webman, R. Wongjirad, T. M. Schepartz, A. Miniature Protein Inhibitors of the p53-hDM2 Interaction *Chembiochem* **2006**, *7*, 29-31.

(123) Appella, D. H. Christianson, L. H. Klein, D. A. Powell, D. R. Huang, X. Barchi, J. R. Gellman, S. H. Residue-based control of helix shape in bold beta-peptide oligomers *Nature* **1997**, *387*, 381-384.

(124) Kritzer, J. A. Lear, J. D. Hodsdon, M. E. Schepartz, A. Helical β-Peptide Inhibitors of the p53-hDM2 Interaction *J. Am. Chem. Soc* **2004**, *126*, 9468-9469.

(125) Lyu, P. C. Sherman, J. C. Chen, A. Kallenbach, N. R. Alpha-helix stabilisation by natural and unnatural amino acids with alkyl side chains *PNAS* **1991**, *88*, 5317-5320.

(126) Lee, K. H. Lee, H. Y. Slutsky, M. M. Anderson, J. T. Neil, E. Marsh, G. Fluorous Effect in Proteins: De Novo Design and Characterization of a Four-?-Helix Bundle Protein Containing Hexafluoroleucine *Biochemistry* **2004**, *43*, 16277-16284.

(127) Chiu, H. P. Suzuki, Y. Gullickson, D. Ahmad, R. Kokona, B. Fairman, R. Cheng, R. P. Helix Propensity of Highly Fluorinated Amino Acids *J. Am. Chem. Soc* **2006**, *128*, 15556-15557.

(128) Shepherd, N. E. Abbenante, G. Fairlie, D. P. Consecutive Cyclic Pentapeptide Modules Form Short α-Helices that are Very Stable to Water and Denaturants *Angew. Chem* **2004**, *116*, 2741-2744.

(129) Cabezas, E. Satterthwait, A. C. The Hydrogen Bond Mimic Approach: Solid-Phase Synthesis of a Peptide Stabilized as an -Helix with a Hydrazone Link *J. Am. Chem. Soc* **1999**, *121*, 3862.

(130) Jackson, D. Y. King, D. S. Chmielewski, J. Singh, S, Schulz, P. G General Approach to the Synthesis of Short α-Helical Peptides *J. Am. Chem. Soc* **1991**, *113*, 9391-9392.

(131) Iqbalsyah, T. M. Doig, A. J. Anticooperativity in a Glu-Lys-Glu Salt Bridge Triplet in an Isolated α-Helical Peptide *Biochemistry* **2005**, *44*, 10449-10456.

(132) Turner, E. C. Cureton, C. H. Weston, C. J. Smart, O. S. Allemann, R. K. Controlling the DNA Binding Specificity of bHLH Proteins through Intramolecular Interactions *Chemistry & Biology* **2004**, *11*, 69-77.

(133) Wachtveitl, J. Nagele, T. Puell, B. Zinth, W. Kruger, M. RudolphBohner, S. Oesterhelt, D. Moroder, L. Ultrafast photoisomerisation of azobenzene compounds *J. Photochem. Photobiol.* **1997**, *105*, 283-288.

(134) Renner, C. Behrendt, R. Heim, N. Moroder, L. Photomodulation of Conformational States. III. Water-Soluble Bis-Cysteinyl- Peptides with (4-Aminomethyl) phenylazobenzoic Acid as Backbone Constituent *Biopolymers* **2002**, *63*, 382-393.

(135) Schutt, M. Krupka, S. S. Milbradt, A. G. Deindl, S. Sinner, E. K. Oesterhelt, D. Renner, C. Moroder, L. Photocontrol of Cell Adhesion Processes: Model Studies with Cyclic Azobenzene-RGD Peptides *Chemistry & Biology* **2003**, *10*, 487-490.

(136) Dong, S. L. Loweneck, M. Schrader, T. E. Schreier, W. J. Zinth, W. Moroder, L. Renner, C. A Photocontrolled β-Hairpin Peptide *Chem. Eur. J.* **2006**, *12*, 1114-1120.

(137) Aemissegger, A. Krautler, V. van Gunsteren, W. F. Hilvert, D. A Photoinducible β-Hairpin *J. Am. Chem. Soc* **2005**, *127*, 2929-2936.

(138) Jurt, S. Aemissegger, A. Guntert, P. Zerbe, O. Hilvert, D. A Photoswitchable Miniprotein Based on the Sequence of Avian Pancreatic Polypeptide *Angew. Chem. Int. Ed.* **2006**, *45*, 6297-6300.

(139) Liu, D. Karanicolas, J. Yu, C. Zhang, Z. Woolley, G. A. Site-specific incorporation of photoisomerizable azobenzene groups into ribonuclease S *Bioorg. Med. Chem. Lett.* **1997**, *7*, 2677-2680.

(140) Kumita, J. R. Flint, D. G. Woolley, G. A. Smart, O. S. Achieving photo-control of protein conformation and activity: producing a photo-controlled leucine zipper *Faraday Discuss.* **2002**, *122*, 89-103.

(141) Flint, D. G. Kumita, J. R. Smart, O. S. Woolley, G. A. Using an Azobenzene Cross-Linker to Either Increase or Decrease Peptide Helix Content upon *Trans*-to-*Cis* Photoisomerization *Chemistry & Biology* **2002**, *9*, 391-397.

(142) Zhang, Z. Burns, D. C. Kumita, J. R. Smart, O. S. Woolley, G. A. A Water-Soluble Azobenzene Cross-Linker for Photocontrol of Peptide Conformation *Bioconjugate Chem* **2003**, *14*, 824-829.

(143) Kumita, J. R. Smart, O. S. Woolley, G. A. Photo-control of helix content in a short peptide *PNAS* **2000**, *97*, 3803-3808.

(144) Woolley, G. A. Jaikaran, A. S. I. Berezovski, M. Calarco, J. P. Krylov, S. N. Smart, O. S. Kumita, J. R. Reversible Photocontrol of DNA Binding by a Designed GCN4-bZIP Protein *Biochemistry* **2006**, *45*, 6075-6084.

(145) Guerrero, L. Smart, O. S. Woolley, G. A. Allemann, R. K. Photocontrol of DNA Binding Specificity of a Miniature Engrailed Homeodomain *J. Am. Chem. Soc* **2005**, *127*, 15624-15629.

(146) Sambrook, J. Fritsch, E. F. Maniatis, T. *Molecular Cloning - A Laboratory Manual*; 2 ed.; Cold Spring Harbour Laboratory Press: NY, **1989**.

(147) Jones, J. *Amino Acid and Peptide Synthesis*; Oxford University Press: Oxford, **1992**.

(148) Birnboim, H. C. Doly, J. A Rapid Alkaline Extraction Procedure for Screening Recombinant Plasmid DNA *Nucleic Acids Res.* **1979**, *7*, 1513-1523.

(149) Ish-Horowicz, D. Burke, J. P. Rapid and Efficient Cosmid Cloning *Nucleic Acids Res.* **1981**, *9*, 2989-2998.

(150) Vardevanyan, P. O. Antonyan, A. P. Parsadanyan, M. A. Davtyan, H. G. Karapetyan, A. T. The Binding of Ethidium Bromide with DNA: Interaction with Single- and Double-Stranded Structures *Experimental and Molecular Medicine* **2003**, *35*, 527-533.

(151) Laemmli, U. K. Cleavage of Structural Proteins During the Assembly of the Head of Bacteriophage T4 *Nature* **1970**, *227*, 680-685.

(152) Kallenbach, N. R. Spek, E. J. Modified amino acids as probes of helix stability *Methods Enzymol* **1998**, *295*, 26-41.

(153) Lakowicz, J. R. *Principles of Fluorescence Spectroscopy*; Plenum Press: NY, **1999**.

(154) Heyduk, T. Ma, Y. Tang, H. Ebright, R. H. Fluorescence Anisotropy: Rapid quantitative assay for protein-DNA and protein-protein interaction *Methods Enzymol* **1996**, *274*, 492-503.

(155) Merrifield, R. B. Solid Phase Peptide Synthesis. I. The Synthesis of a Tetrapeptide *J. Am. Chem. Soc* **1963**, *85*, 2149-2154.

(156) Peng, Y. Hansmann, U. H. E. Solvation Model Dependency of Helix-Coil Transition in Polyalanine *Biophys. J.* **2002**, *82*, 3269-3276.

(157) Bottger, V. Bottger, A. Echeverria, C. G. Ramos, Y. F. M.; van der Eb, A. J. Jochemsen, A. G. Lane, D. P. Comparative study of the p53-mdm2 and p53-MDMX interfaces *Oncogene* **1999**, *18*, 189-199.

(158) Midgley, C. A. Fisher, C. J. Bartek, J. Vojtesek, B. Lane, D. Barnes, D. M. Analysis of p53 expression in human tumours: an antibody raised against human p53 expressed in *Escherichia coli J. Cell Science* **1992**, *101*, 183-189.

(159) Yang, J. T. Wu, C. S. Martinez, H. M. Calculation of protein conformation from circular dichroism *Methods Enzymol* **1986**, *130*, 208-269.

(160) Chene, P. Inhibition of the p53-MDM2 Interaction: Targeting a Protein-Protein Interface *Mol. Cancer Res.* **2004**, *2*, 20-28.